Neurotrophin-3 signalling in neurons derived from human embryonic stem cells

Sarah Ateaque

A thesis submitted to Cardiff University with the requirements for the degree of Doctor of Philosophy in the discipline of Neuroscience

School of Biosciences

Cardiff University

March 2022

For Nadia, Layla and Zahra

Acknowledgements

I would first like to thank my supervisor, Professor Yves-Alain Barde for his constant enthusiasm, support, and advice throughout my PhD. I have really valued our partnership and have learnt so much during our discussions over the past few years. I also want to thank my co-supervisor, Professor Nick Allen for always providing support and for kindly sharing his expertise on growing stem cells and CRISPR-Cas9. Also thank you to Kim Jones and Bridget Allen for their useful technical advice and for lending me reagents when there were delivery delays! I want to thank Dr. Stéphane Baudouin, Dr. Isabel Martinez Garay, Dr. David Petrik and all the past and present members of these labs for being the best colleagues one could ask for! A special thank you also to Dr. Xinsheng Nan for generously sharing his outstanding troubleshooting skills and helping me optimise my experiments, to Dr. Spyros Merkouris for his expertise and help with the RNAseq analysis and to Dr. Sean Wyatt for performing the RT-qPCR experiments. I want to thank Professor Neil McDonald and Dr. David Briggs for kindly sharing their TrkB constructs and thank you to Dr. Jia Xie for sharing the HEK283 and CHO Trk overexpressing cell lines. I want to further thank the NMHRI for helping to sponsor this PhD, and give a huge thank you to Dr. Ron Lindsay and Dr. Pete DiStefano of Zebra Biologics for being outstanding collaborators and for their generous funding throughout the project. Without it, this work would not have been possible. A special thanks also goes to: Dr. Laura Cassels for her constant kindness and willingness to offer advice, to Dr. Hayley Dingsdale for teaching me so many techniques and for encouraging me to undertake this PhD, and to Dr. Erin Wosnitzka – thank you for the support, laughs and for always being there.

I want to thank my partner George for being by my side throughout this journey and for supporting me unconditionally through both the happy and the stressful times – I am so lucky to have you and thank you for always believing in me. Thank you to my parents, Asif and Katie for inspiring me to never stop asking questions and to pursue science ‘for the joy of finding things out’. You have both taught me so much and I truly owe you everything. Finally, I want to thank my amazing sisters, Nadia, Layla and Zahra. Thank you for being the best friends anyone could ask for, I am so proud of all 3 of you.

Summary

The objective of this Thesis was to analyse TrkC-mediated signalling in human neurons following activation of this receptor tyrosine kinase by its ligand neurotrophin-3 (NT3). Neurons were generated from human embryonic stem cells and found to express the brain-derived neurotrophic factor (BDNF) receptor TrkB at higher levels than TrkC. Whilst this dual expression reflects the situation in the mammalian CNS where most neurons express both receptors, it significantly complicates the analysis of NT3-mediated TrkC signalling as NT3 also readily activates TrkB. As a result, very little is known about TrkC activation by NT3 in neurons. To gain mechanistic insights about the impact of selective TrkC activation, human embryonic stem cells were engineered to eliminate ligand-activated forms of TrkB using the CRISPR/Cas9 system. Neurons generated from these engineered cells were found to express unchanged levels of TrkC and gene expression was analysed by RNAseq following TrkC activation by NT3. The transcriptional changes turned out to closely resemble those previously observed following TrkB activation. They include a number of genes associated with neuronal activity and synaptic plasticity, including a rapid increase in the levels of Arc/Arg3.1, a post-synaptic protein extensively studied in the context of synaptic plasticity. The overall conclusion is that TrkC can be activated in human neurons by picomolar concentrations of NT3, lower than the concentrations of BDNF required to activate TrkB, and that TrkC activation leads to changes relevant to synaptic plasticity. The selectivity of NT3/TrkC signalling in neurons co-expressing TrkB is suggested to be determined by the availability of the ligand, not by the downstream consequences of Trk activation. This notion is in line with previous results indicating that the expression of *BDNF* and *NTF3* in neurons is regulated by different mechanisms.

Abbreviations

°C	degrees Celsius
AA	amino acid(s)
AD	anti-depressants
AMP	adenosine monophosphate
Arc/Arg3.1	activity-regulated cytoskeleton-associated protein
ARC	activity-regulated cytoskeleton-associated protein (gene)
Aβ	amyloid beta
BCA	bicinchoninic assay
BDNF	brain-derived neurotrophic factor
BDNF	brain-derived neurotrophic factor (human gene)
bdnf	Brain-derived neurotrophic factor (mouse gene)
BMP	bone morphogenetic protein(s)
bp	base pair(s)
BSA	bovine serum albumin
$CaCl_2$	calcium chloride
Cas9	CRISPR-associated protein 9
CCI	cysteine-rich cluster I
CCII	cysteine-rich cluster II
CD271	low affinity nerve growth factor receptor
cDNA	complementary DNA

CHO	Chinese hamster ovary cell
cm	centimetre(s)
CNS	central nervous system
Cre	cyclic recombinase
CREB	cAMP-response element binding protein
CRISPR	clustered regularly interspaced short palindormic repeats
crRNA	CRISPR RNA
CTIP2	chicken ovalbumin upstream promotor transcription factor-Interacting protein 2
Da	Daltons
DAPI	4',6-diamidino-2-phenylindole
DARPP-32	dopamine- and cAMP-regulated neuronal phosphoprotein
ddH_20	double distilled water
DIV	days *in vitro*
DMEM	Dulbecco's modified eagle medium
DMEM/F12	Dulbecco's modified eagle medium/nutrient mixture F12
DNA	deoxyribonucleic acid
DNT1	drosophila neurotrophin-1
DNT2	drosophila neurotrophin-2
dNTP	deoxynucleotide triphosphates
DPBS	Dulbecco's phosphate-buffered saline
DTT	dithiothreitol
EC_{50}	half maximal effective concentration

ECL	enhanced chemiluminescence
ECD	extracellular domain
EDTA	ethylenediaminetetraacetic acid
EtBr	ethidium bromide
FACS	fluorescence-activated cell sorting
FBS	foetal bovine serum
FC	fold change
fg	femtogram
FGF	fibroblast growth factor(s)
FOXP1	forkhead box protein P1
FOXP2	forkhead box protein P2
FPKM	fragments per kilobase of transcript per million mapped reads
GABA	gaba-aminobutyric acid
GABRQ	gamma-aminobutyric acid type A receptor subunit theta
GAD1	glutamate decarboxylase 1
GAD2	glutamate decarboxylase 2
GAD65	glutamate decarboxylase (65 kDa)
GAD67	glutamate decarboxylase (67 kDa)
GRch38	Genome Reference Consortium human build 38
gRNA	guide RNA
h	hour(s)
HCl	hydrochloric acid

HEK293	human embryonic kidney 293 cells
hESC	human embryonic stem cell(s)
HRP	horseradish peroxidase
hTrkA	human TrkA
hTrkB	human TrkB
hTrkC	human TrkC
IDT	Integrated DNA Technologies
IEG	immediate early gene
IgI	Immunoglobulin-like domain I
IgII	Immunoglobulin-like domain II
INSIG1	insulin induced gene 1
KCl	potassium chloride
kDa	kilodaltons
KIFC1	kinesin family member C1
KLF10	kruppel like factor 10
KLF9	kruppel like factor 9
LDLR	low density lipoprotein receptor
LDS	lithium dodecyl sulfate
LGE	lateral ganglionic eminence
LIMA1	LIM domain and actin binding protein 1
LRM	leucine-rich motif
LTP	long-term potentiation

M	molar
mAB	monoclonal antibody
MES	2-(n-morpholino) ethane sulfonic acid
mESCs	mouse embryonic stem cells
min	minute(s)
ml	millilitre(s)
mM	millimolar
mRNA	messenger RNA
MSN	medium spiny neuron(s)
MW	molecular weight
n.s	not significant
NaCl	sodium chloride
NFKBIZ	nuclear factor kappa-B inhibitor zeta
ng	nanogram(s)
NGF	nerve growth factor
nM	nanomolar
NPAS4	neuronal PAS domain protein 4
NPTX1	neuronal pentraxin 1
NR4A2	nuclear receptor subfamily 4 group A member 2
NR4A3	nuclear receptor subfamily 4 group A member 3
NT3	neurotrophin-3
NT4	neurotrophin-4

NTF3	neurotrophin-3 (human gene)
Ntf3	neurotrophin-3 (mouse gene)
NTF4	neurotrophin-4 (human gene)
Ntf4	neurotrophin-4 (mouse gene)
NTRK1	neurotrophin receptor tyrosine kinase 1
NTRK2	neurotrophin receptor tyrosine kinase 2
NTRK3	neurotrophin receptor tyrosine kinase 3
P-Trk	phosphorylated Trk
p75	p75 neurotrophin receptor
pAB	polyclonal antibody
padj	adjusted p value
PBS	phosphate-buffered saline
PC12	pheochromocytoma cell line 12
PCA	principal component analysis
PCR	polymerase chain reaction
PCSK1	proprotein convertase subtilisin/kexin type 1
PFA	paraformaldehyde
pH	potential of hydrogen
pM	picomolar
PNS	peripheral nervous system
PTPσ	dual domain receptor type protein tyrosine phosphatase
RIPA	radioimmunoprecipitation assay

RNA	ribonucleic acid
RNAseq	RNA sequencing
RNP	ribonucleoprotein
rpm	revolutions per minute
rRNA	ribosomal RNA
RT-qPCR	real-time quantitative PCR
RTK	receptor tyrosine kinase
SDS-PAGE	sodium dodecyl-sulfate polyacrylamide gel electrophoresis
s	second(s)
SEM	standard error of the mean
SIK1B	salt inducible kinase 1B
SJA	Synaptojuice A
SJB	Synaptojuice B
SNP	single nucleotide polymorphism
SP	signal peptide
TBS	tris-buffered saline
TBS-T	tris-buffered saline with 0.1% Tween-20
TGF- β	transforming growth factor beta
TK	tyrosine kinase
TM	transmembrane
TNFRSF	tumour necrosis factor receptor superfamily
tracrRNA	trans-activating CRISPR RNA

TRIB1	tribbles pseudokinase 1
Tris	tris-aminomethane
TrkA	tropomyosin receptor kinase A
TrkB	tropomyosin receptor kinase B
TrkC	tropomyosin receptor kinase C
Tuj1	neuron-specific class III beta-tubulin
UBALD1	ubiquitin-associated-like domain-containing protein 1
Wnt	wingless-related integration site
WT	wild-type
ZNF331	zinc finger protein 331
µg	microgram(s)
µl	microlitre (s)
µM	nanomolar
Mm	millimolar

Contents

Figures

Chapter 1 - General Introduction

1.1. Growth factors in the nervous system

Growth factors are proteins that are either secreted by conventional or by unconventional pathways from the cells synthesising them (Nickel 2010). They allow short-range communication with other cells in close proximity. In the nervous system, growth factors play critical roles from the earliest stages of development (for review, see Wilson and Edlund 2001). For example, bone morphogenetic proteins (BMPs), fibroblast growth factors (FGFs) and Wingless-and-Int-1s (Wnts) and their pathways are involved in neural induction.

1.1.1. Discovery of Nerve Growth Factor

Whilst forward genetics with model systems such as *Drosophila melanogaster* was key to the discovery and the delineation of the signalling pathways of many growth factors, neurotrophins and their tyrosine kinase receptors were discovered following a series of observations made with developing vertebrate embryos (for review, see Hamburger 1993). These observations included experimental manipulations such as limb removals and it was found that somehow, the presence or the absence of a limb to be innervated plays a role in the size of the neural structure innervating them (Shorey 1909; Hamburger 1934). Subsequently, Elmer Bueker (Bueker 1948) and Rita Levi-Montalcini then went on to show that transplantation of mouse tumour cells onto developing chick embryos resulted in the growth of both sensory and sympathetic neurons in the direction of the tumour cells. It was then realised that the tumour cells used secreted a diffusible growth factor (Levi-Montalcini and Hamburger 1951), later purified from the adult male mouse submandibular gland and named Nerve Growth Factor (NGF, Cohen and Levi-Montalcini 1957). Moreover, it was shown that an antiserum blocking the biological activity of NGF eliminated most of the peripheral sympathetic nervous system when administered to new-born rodents (Cohen 1960; Levi-Montalcini and Booker 1960). These experiments had thus proven both the existence of the first nerve growth factor as well as its *in vivo* biological relevance.

1.1.2. Discovery of Brain-derived neurotrophic factor

It then took around 2 decades for the field to realise that NGF was actually the first member of a small family of closely related proteins to have been characterised (Bothwell 2014) and a growth factor with characteristics similar to NGF was reported in the early 1980's (Barde et al. 1982). As it was purified from brain tissue, it was named brain-derived neurotrophic factor (BDNF) and its properties include the prevention of the death of embryonic neurons during

development (Hofer and Barde 1988). Given the impact of forward genetics in the discovery of most growth factors and their receptors it is worth noting that this approach actually played no role in the neurotrophin field. This however raises the question as to whether the corresponding neurotrophin genes exist in the type of short-lived organisms typically used by geneticists such as *Drosophila melanogaster* and *Caenorhabditis elegans*. Whilst the genome of the latter organism is known to not comprise of genes involved in neurotrophin signalling, such is not the case in *Drosophila melanogaster* where neurotrophin-like genes have been identified (Zhu et al. 2008). This was not the result of a classical genetic screen based on particular phenotypes but of detailed structural comparisons with the crystal structure of the *Spaetzle*-related horseshoe crab gene *Coagulogen*. The 3-dimensional structure of coagulogen forms a neurotrophin fold (Bergner et al. 1996) first described for NGF (McDonald et al. 1991). Interestingly, Spaetzle use Toll-like receptors to signal and so do the Drosophila neurotrophins, namely DNT1 and DNT2 (Zhu et al. 2008). Moreover, more recent work indicates that DNTs bind to Toll-like receptors and are involved in synaptic plasticity (Li and Hidalgo 2021).

1.1.3. Discovery of NT3 and NT4

Following the realisation that the amino acid sequence of BDNF shares similarities with NGF (Leibrock et al. 1989), a search for related genes was initiated using cloning by homology. This approach rapidly led to the identification of neurotrophin-3 (NT3, Ernfors et al. 1990; Hohn et al. 1990; Jones and Reichardt 1990; Kaisho et al. 1990; Maisonpierre et al. 1990; Rosenthal et al. 1990). Neurotrophin-4 was subsequently identified, initially in *Xenopus Laevis* (Hallbook et al. 1991) and later in mammals (Ip et al. 1992). Neurotrophin-4 (NT4) binds to the same receptor as BDNF, namely TrkB (see below). NT4 seems to have been a relatively late addition during the course of evolution and the deletion of its gene in the mouse only causes a mild phenotype, unlike is the case with the other 3 neurotrophins that are all lethal within a few weeks after birth (see below).

1.2. The neurotrophin family

1.2.1. Expression and regulation of neurotrophins

All neurotrophin genes encode secretory proteins that are translated as pre-pro-protein precursors (for reviews, see Huang and Reichardt 2001; Bothwell 2014). These precursors can be subsequently cleaved to form mature neurotrophins (Figure 1.1). Neurotrophins are primarily expressed in the brain and also in many peripheral tissues where their secretion plays crucial roles both during development and in the adult. Neurotrophins and especially BDNF now receive a great deal of attention because of multiple links with crucial functions of the nervous system including virtually all aspects of synaptic plasticity including memory-related mechanisms (Park and Poo 2013; Mariga et al. 2017; Mitre et al. 2017). In neurons, the expression of the *BDNF* gene is regulated by neuronal activity, in a calcium-dependent manner (Tao et al. 1998). The genomic organisation of the *BDNF* gene is complex and comprises at least 9 different promoters encoding a number of splice variants as well as an antisense mRNA (for review, see West et al. 2014). *BDNF* has the hallmark of a gene that is expressed as a function of demand, a property that is not shared with *NTF3* (NT3) whose genomic organisation is much less complex than that of *BDNF* (for review, see West et al. 2014). NT3 expression is regulated by mechanisms distinct from those regulating BDNF expression such as for example thyroid hormone and not by stimuli typically increasing *BDNF* expression such as kainic acid (Katoh-Semba et al. 1999; Hernandez-Echeagaray 2020). As the differential regulation of *BDNF* and *NTF3* has important implications for the interpretation of the main results presented in the following chapters, this specific feature is further commented in the General Discussion (see Chapter 9).

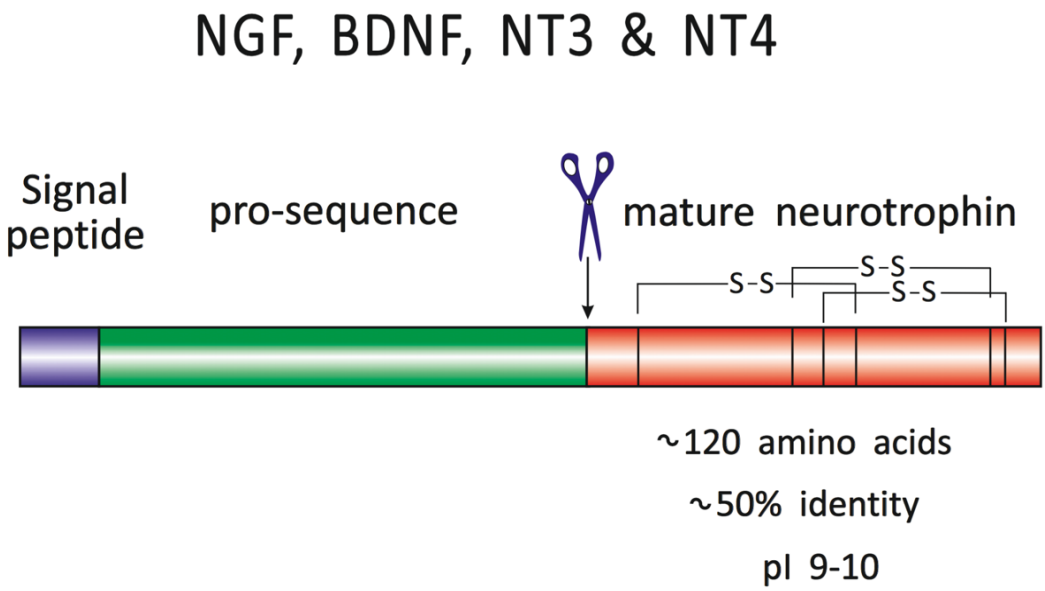

Figure 1.1. Generic representation of the neurotrophins as secretory proteins.

The signal peptide (purple) directs the neurotrophins to the secretory pathway and is followed by a pro-sequence (green) that show moderate conservation between the neurotrophins. The main function of the pro-sequence is thought to permit the folding of the mature sequence (red) including the formation of the cysteine knot (S-S). Various proteases can cleave pro-neurotrophins at furin-like cleavage sites. In the absence of cleavage pro-neurotrophins may be released and interact with the neurotrophin receptor p75 (see below) which can cause apoptosis during development or in the adult after lesion.

1.2.2. The role of neurotrophins in the nervous system

In humans, a number of mutations and polymorphisms have been identified in neurotrophin genes and their Trk receptors and this has further increased the interest for the neurotrophin signalling system and its role in dysfunction of the nervous system. These include in particular memory-related mechanisms, mood disorders and neurodegeneration (Eisenberg et al. 2013; Honea et al. 2013; Mitre et al. 2017; Bochukova et al. 2018; Sonoyama et al. 2020). Improving neurotrophin signalling has thus become a major area of interest, further fuelled by recent observations indicating that synaptic plasticity, thought to be compromised in conditions such as depression in particular, can improved by antidepressants (Castren and Kojima 2017).

1.2.2.1. NGF

With regard to their physiology, neurotrophins are best known for their survival promoting activities in the PNS (for reviews, see Davies 1994; Bibel and Barde 2000; Huang and Reichardt 2001; Bothwell 2014). NGF is essential for the survival of peripheral sympathetic neurons and of most sensory neurons derived from the neural crest. With regard to the role of NGF in the CNS, it is limited to a small, yet physiologically important population of cholinergic neurons in the basal forebrain identified in retrograde transport studies using radiolabelled NGF (Schwab et al. 1979). Unlike PNS neurons, these neurons do not die in the absence of NGF but fail to reach their normal size (Crowley et al. 1994). This is in line with the general notion that whilst the role of neurotrophins as essential survival factors is well established in the PNS, such is not the case in the CNS in the absence of lesion such as axotomy. NGF is best known for its role in all aspects related to pain-related mechanisms that go beyond its ability to promote the survival of small diameter sensory neurons in dorsal root ganglia. This notion is now firmly established and is not only based on a very large number of experiments with rodents but also by human genetics. In humans, mutations in the protein-coding sequence of NGF (Einarsdottir et al. 2004) or its receptor tyrosine kinase TrkA (Indo et al. 1996) render the carriers pain-insensitive. This body of work has led to the development of monoclonal antibodies blocking the biological activity of NGF, now used in large-scale clinical trials in conditions associated with chronic pain including rheumatoid arthritis (for reviews, see Barker et al. 2020; Wise et al. 2021).

1.2.2.2. BDNF

Whilst BDNF also supports the survival of some neural crest-derived sensory neurons, its most important targets in the PNS are neurons derived from epidermal placode (Lindsay et al. 1985). It is the loss of these neurons that are critical for the regulation of respiration, balance

and blood pressure that causes the post-natal death of new-born mice lacking BDNF (Ernfors et al. 1994a; Jones et al. 1994) or its tyrosine kinase receptor TrkB (Klein et al. 1993). In contrast to the PNS, BDNF does not play a major role as a survival factor in the CNS whereby in its absence, cell bodies, especially those of inhibitory neurons fail to reach their normal size. Likewise, the size of dendritic arbors and the number of branches is reduced in mutant animals (Gorski et al. 2003; Rauskolb et al. 2010). Following the demonstration that long-term potentiation fails to reach its full extent in the hippocampus (Korte et al. 1995), much of the attention subsequently focused on the role of BDNF in synaptic plasticity (for review, see Park and Poo 2013). At the molecular level, one of the most studied molecules associated with post-synaptic changes is Arc/Arg3.1 whereby its levels have been shown to be substantially and rapidly altered following activation of TrkB (Bramham et al. 2008). The focus on the role of BDNF in the adult brain further increased following the discovery of a polymorphism in humans linking the substitution of an amino acid in the pro-sequence of BDNF with mild memory deficits (Egan et al. 2003). BDNF is now linked with a large range of conditions including neurodegeneration, the regulation of food intake and mood disorders (for reviews, see Castren and Kojima 2017; Mariga et al. 2017; Jones et al. 2021). Furthermore, recent findings indicate that the BDNF receptor TrkB (see below) is a target of all antidepressants. (Casarotto et al. 2021, reviewed in Ateaque and Barde, 2021).

1.2.2.3. NT3

With regard to NT3, a prominent physiological role in the PNS has been firmly established with regard to the survival of sub-populations of sensory neurons including in particular those involved in proprioception and audition. Indeed, NT3 has been shown to be essential for the survival of large myelinated neurons and axons in dorsal root ganglia and of neurons in the spiral ganglia (Ernfors et al. 1994b; Farinas et al. 1994; Ernfors et al. 1995). Its role in preventing the toxicity of drugs compromising the survival of the corresponding neurons is also well documented and there is a currently a great deal of interest in delivering NT3 as well as BDNF to improve impaired functions of neurons innervating the inner ear and treat deafness in particular (for review, see Leake et al. 2020). As the nerve terminals innervating the inner ear are thought to be more readily accessible to selective reagents such as receptor-activating antibodies there is an interest in developing such reagents (Szobota et al. 2019). Whilst far fewer data are available on the role of NT3 in the CNS compared with BDNF, the available data suggest that their roles may be similar and both are involved in synaptic plasticity including the facilitation of neurotransmission and the development of dendrites (see Joo et al. 2014; Hernandez-Echeagaray 2020). However, unlike is the case with BDNF, very little is known about molecular mechanisms related to synaptic plasticity downstream of TrkC

activation.

1.2.2.4. NT4

NT4 also uses the TrkB receptor to transduce its biological activity whereas less is known about its functional relevance whereby it seems to largely overlap with that of BDNF as can be expected given that share the same tyrosine kinase receptor. However, unlike is the case with the other neurotrophin genes, mice carrying homozygote deletions of the *Ntf4* gene are viable and only show a mild phenotype compared with other neurotrophins (Liu et al. 1995).

1.3. Neurotrophin receptors

1.3.1. The neurotrophin receptor p75

As the neurotrophin field began with the discovery of NGF (see above), the first neurotrophin receptor characterised was designated the NGF receptor. Two groups followed the same strategy of expression cloning and used monoclonal antibodies to isolate cells expressing the receptor at their surface following transfection with human (Johnson et al. 1986) or rat genomic DNA (Radeke et al. 1987). Following the realisation that BDNF also binds to this receptor (Rodriguez-Tébar et al. 1990), it was renamed the neurotrophin receptor p75 (structure of p75 shown in Figure 1.2). By contrast with the Trk receptors, the cytoplasmic domain of p75 is devoid of enzymatic activity. P75 was the first member to have been characterised of what later turned out to be a large family of receptors designated the Tumour Necrosis Factor Receptor Superfamily (TNFRSF). The distinct feature of this family is the recruitment of cytoplasmic interactors allowing these receptors to transduce their activity following ligand binding (Locksley et al. 2001). Many TNFRSF members are primarily expressed in cells of the immune system and often bind trimeric ligands whilst p75 is primarily, but not exclusively, expressed in the developing nervous system. Unlike the Trk receptors that bind neurotrophins (see below), p75 has been reported to also bind a number of different ligands including unprocessed neurotrophins (designated pro-neurotrophins), Aβ and proteins of viral envelopes (for review, see Malik et al. 2021). Like all TNFRSF members, p75 transduces its effects by recruiting cytoplasmic interactors of which about 30 have been characterised (Malik et al. 2021). This diversity explains in part why by comparison with the Trk receptors it has been difficult to understand the biological relevance of p75, especially *in vivo*. In addition, p75 levels of expression vary considerably during development and in the adult whereby in the adult brain, p75 expression is largely restricted to basal forebrain cholinergic neurons, one of very few neuronal populations also expressing the NGF receptor TrkA in the CNS. One the best understood functions of p75 is its ability to cause cell death following binding of pro-

neurotrophins, i.e. un-cleaved neurotrophins where the pro-domain is still attached to the mature protein (Lee et al. 2001). Like other TNFRSF members the role of p75 may be particularly relevant in pathological situations as for example its levels of expression in neurons have long been known to be significantly upregulated after axotomy (Ernfors et al. 1989).

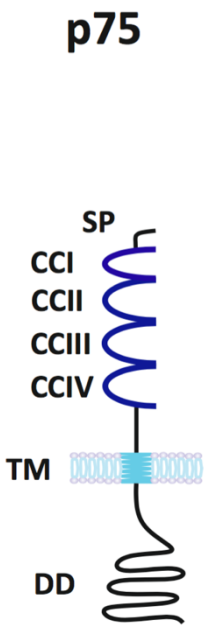

Figure 1.2. The neurotrophin receptor p75 is a member of the tumour necrosis factor receptor superfamily (TNFRSF).

Scheme showing the structure of p75. The 4 neurotrophins bind to p75 with nanomolar affinities. P75 was the first TNFRSF member to have been identified and later members were added to the family based on the extracellular cysteine-rich motifs in their extracellular domains (4 in the case of p75 as indicated). It is also referred to as TNFRSF16 or CD271. Like all members of the family and unlike the neurotrophin tyrosine kinase receptors (see below) no enzymatic activity is intrinsically linked with the protein coding sequence of the receptor and signalling is mediated by interactions with cytoplasmic interactors, of which large numbers have been identified (for review, see Yuan et al. 2019). Note also that the cytoplasmic domain, despite the lack of catalytic activity has a structure that is similar to the death domain of members of the tumour necrosis receptor family whereby p75 is known to induce cell death (Liepinsh et al. 1997). The designations are: SP: signal peptide, CCI: cysteine-rich cluster I, CCII: cysteine-rich cluster II, CCIII: cysteine-rich cluster III, CCIV: cysteine-rich cluster IV, TM: transmembrane domain and DD: death domain. Scheme is approximately to scale. Scheme adapted from previous images in use in the Barde Lab.

1.3.2. The neurotrophin tyrosine kinase receptors

The discovery of the first neurotrophin receptor tyrosine kinase originates from studies aiming to define the cause of solid tumours. Specifically, what later turned out to be a receptor for NGF was first described as “a human oncogene formed by the fusion of truncated tropomyosin and protein tyrosine kinase sequences” (Martin-Zanca et al. 1986). The subsequent cloning of the corresponding proto-oncogene resulted in clues as to the possible function of this then receptor as it allowed *in situ* hybridisation studies to be performed in the developing mouse embryo. These experiments revealed a restricted expression pattern essentially limited to the developing peripheral nervous system (Martin-Zanca et al. 1990). The notion that NGF may activate a then unknown tyrosine kinase receptor emerged from experiments indicating that cell extracts of the pheochromocytoma cell line (PC12), responded to NGF by proliferation arrest and neurite outgrowth (Greene and Tischler 1976) and increased tyrosine phosphorylation (Maher 1988). It was then revealed that PC12 cells expressed the proto-oncogene Trk, later renamed TrkA, and that NGF binds to, and can be cross-linked to, the tyrosine phosphorylated receptor (Hempstead et al. 1991; Kaplan et al. 1991; Klein et al. 1991a). The availability of cDNA clones encoding TrkA also led to the accidental discovery of TrkB during the course of a cDNA library screening (Klein et al. 1989). Sequence analyses revealed striking homologies with TrkA, especially in the intracellular domain encoding the kinase domain. Northern blot as well as *in situ* hybridisation experiments revealed a strong expression in the nervous system, both during development and in the adult.

Following the demonstration that TrkA was an NGF receptor (see above), it rapidly became clear that TrkB was the BDNF tyrosine kinase receptor (Glass et al. 1991; Klein et al. 1991b; Soppet et al. 1991), later shown to also bind and be activated by Neurotrophin-4 (Klein et al. 1992). Similarly, the availability of TrkA clones also allowed the isolation by homology cloning of the third member of the family, TrkC that turned out to be a receptor for NT3 (Lamballe et al. 1991). TrkC turned out to be the most neurotrophin-specific receptor, it has no measurable affinity for neurotrophins other than NT3 (neurotrophin-Trk receptor interactions shown in Figure 1.3B). By contrast, it also binds a neurotrophin unrelated ligand, an axonal tyrosine phosphatase receptor PTPσ. The interaction of this receptor with TrkC modulates the formation of glutamatergic synapses (Takahashi et al. 2011). The TrkC/PTPσ interaction was mapped and shown not to involve the NT3 binding site on TrkC whereby the addition of NT3 to excitatory synapses involving presynaptic PTPσ and postsynaptic TrkC enhances synapse formation (Ammendrup-Johnsen et al. 2015). These intriguing data positions TrkC uniquely in the context of Trk receptor function in the CNS, even if still very little is known about TrkC signalling following its kinase domain activation by NT3. This question is at the core of the

results presented in the following Chapters that also deal with the intricacies of studying TrkC activation by NT3 in neurons.

1.3.3. The structure of the Trk receptors

As their method of discovery suggests, the 3 mammalian Trk receptors are closely related in structure (Figure 1.3A). This not only relates to their cytoplasmic tyrosine kinase domains (over 80% amino acid identities in the corresponding domain) but also to their extracellular domains (about 40%). All three receptors are single-pass transmembrane receptors that are heavily N-glycosylated comprising a signal sequence followed by leucine-rich repeats flanked by cysteine-rich sequences followed by immunoglobulin-like domains. X-ray diffraction studies have mapped the binding site of NGF to the second immunoglobulin-like repeat of TrkA (Wiesmann et al. 1999). Dimerisation of the receptors is thought to lead to the activation of the kinase domain and transphosphorylation of tyrosine residues, therefore it is conceivable that the sequences upstream of the juxta-membrane immunoglobulin-like repeat may help prevent the dimerisation and activation of Trk receptors in the absence of ligands as can be observed upon overexpression of Trk receptors in heterologous systems. In addition, attention increasingly focuses on the transmembrane domains of the Trk receptors. Recent work revealed that the transmembrane domains of TrkA plays a role in its dimerisation (Franco et al. 2020). In addition, in a major recent development (see also Chapter 7), antidepressants have been shown to selectively bind to the transmembrane of TrkB in a cholesterol-dependent manner (Casarotto et al. 2021). A tyrosine residue has been identified in the transmembrane domain of TrkB that is thought to play a key role in the interactions of TrkB with the lipids found in neuronal membranes (Casarotto et al. 2021).

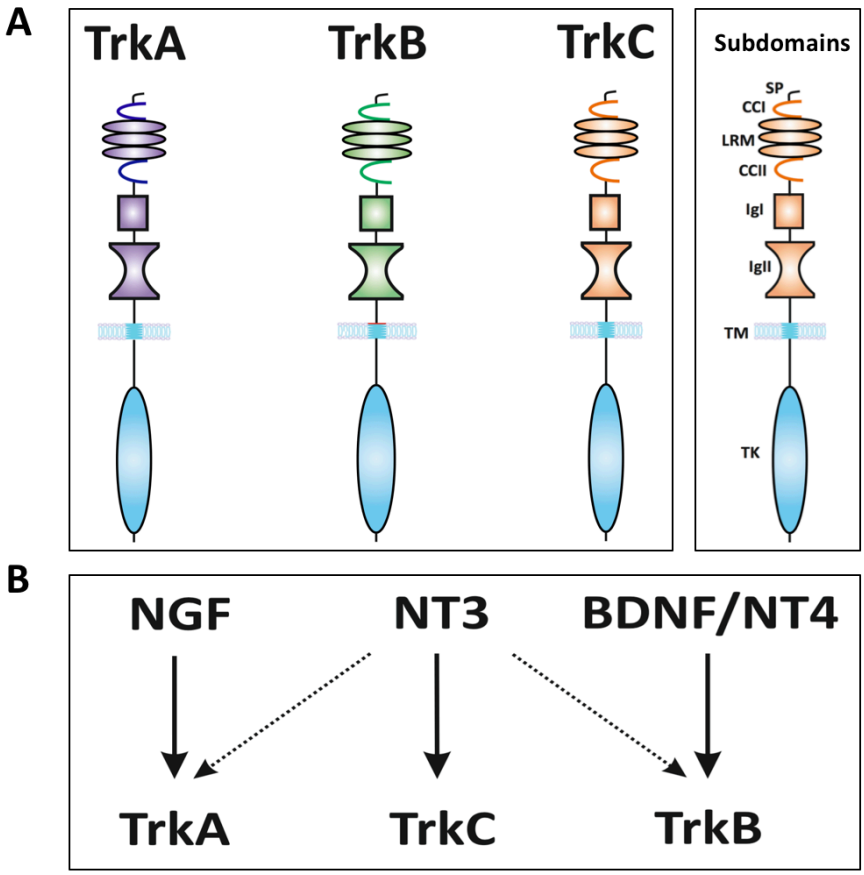

Figure 1.3. The Trk receptors.

Scheme depicting the three Trk receptors, TrkA, TrkB and TrkC (A left panel) whereby the different domains are also indicated (A right panel). The designations are: SP: signal peptide, CCI: cysteine-rich cluster I, LRM: Leucine rich motif, CCII: cysteine-rich cluster II, IgI: immunoglobulin-like domain I, IgII: immunoglobulin-like domain II, TM: transmembrane domain and TK: tyrosine kinase domain. (C). indicates ligand preference whereby NT3 also binds to TrkA and TrkB as well as TrkC. Schemes (A). and (B). are approximately to scale. Schemes adapted from previous images in use in the Barde Lab.

1.3.4. Biological relevance of the Trk receptors *in vivo*

By the time the 3 Trk receptors had been discovered, extensive work with cultured neurons as well as some work *in vivo* had established the functional relevance of their neurotrophin ligands (Bibel and Barde 2000; Huang and Reichardt 2001; Bothwell 2014). In particular, the experiments performed by Levi-Montalcini and Cohen had demonstrated the relevance of NGF as the post-natal injections of antibodies to new-born rodents massively impacted the development of the peripheral sympathetic system (Cohen 1960; Levi-Montalcini and Booker 1960). *In vitro* work had demonstrated that BDNF prevents the death of sensory neurons not responding to NGF, including those derived from epidermal placodes (Lindsay et al. 1985) and that the addition of BDNF to developing quail embryos prevented naturally occurring neuronal death (Hofer and Barde 1988). The selective elimination of the genes encoding the Trk receptors *NTRK1* (TrkA) (Klein et al. 1993) and *NTRK3* (TrkC) (Klein et al. 1994) greatly helped delineating the *in vivo* relevance of neurotrophin-Trk interactions *in vivo* as around the same time, results became available related to the elimination of the corresponding neurotrophin genes (Crowley et al. 1994; Ernfors et al. 1994a; Ernfors et al. 1994b; Farinas et al. 1994; Jones et al. 1994). The majority of these studies focused on the peripheral nervous system as a substantial body of work preceding the gene targeting experiments had established that neurotrophins prevent the death of distinct sub-populations of neurons of the peripheral nervous system. By contrast, the deletion of Trk receptors in the CNS, like is the case with the neurotrophins only causes mild defects in the CNS, unless an imbalance is created by the sparse deletion of a Trk receptor or of the ligand as has been demonstrated with TrkC in cerebellar Purkinje cells (Joo et al. 2014 and see Discussion) and with BDNF in the cerebral cortex (English et al. 2012).

Functionally, there is overwhelming evidence to indicate that the neurotrophin signalling system is involved in synaptic plasticity, as exemplified by the role of BDNF/TrkB signalling in long-term potentiation (Korte et al. 1995; Minichiello et al. 2002). Beyond modulation of synaptic transmission by neurotrophins, there is also strong evidence that they modulate dendritic branching as well as spine formation (Rauskolb et al. 2010; Park and Poo 2013; Zagrebelsky and Korte 2014). The most studied biochemical downstream target of Trk activation is the actin-associated protein Arc/Arg3.1 and its levels rapidly increase following TrkB activation by BDNF. This short-lived protein is rapidly transferred to dendrites following the activation of afferent pathways and is thought to link neurotransmitter receptors with the actin cytoskeleton (for review, see Zhang and Bramham 2021). Given these crucial properties of Arc/Arg3.1 it is a much-studied target in the context of BDNF-mediated synaptic plasticity. By contrast, very little is known about the role of NT3/TrkC signalling even though most

neurons in the human prefrontal cortex co-express *NTRK2* (TrkB) and *NTRK3* (TrkC) mRNA and the levels of both have been reported to be decreased in the brain of schizophrenic patients (Weickert et al. 2005).

1.4. Research aims

The research project had the following aims:

1. Validate antibodies ensuring the unambiguous identification of TrkB and TrkC
2. Establish a robust cell culture system allowing the generation of neurons expressing the neurotrophin receptors TrkB and TrkC
3. Eliminate the expression of ligand activatable forms of TrkB using CRISPR/Cas9
4. Examine Trk activation as a function of BDNF and NT3 concentrations
5. Study gene expression downstream of TrkC activation and compare the results with TrkB activation, with a focus on genes involved in synaptic plasticity

Chapter 2 - Methods and Materials

2.1. CHO cell culture

2.1.1. CHO cell thawing

CHO cells overexpressing human cDNAs encoding TrkA, TrkB or TrkC (a kind gift from Dr. Jia Xie, Scripps Institute) were partially thawed by incubation in a 37°C water bath until only a small wedge of ice remained in the vial. 2 ml of CHO media consisting of DMEM:F12 containing 10% FBS (Biosera), 5% Glutamax and 1% Penicillin/Streptomycin (all from Thermo Fisher Scientific unless otherwise indicated) was added directly to the vial, the cells were then collected and centrifuged at 2000 rpm for 3 min. The supernatant was removed, the pellet resuspended in 2 ml CHO media and the suspension added to a single well of a Nunc cell-culture treated 6-well plate (Thermo Fisher Scientific). Cells were maintained in a 37°C and 7% CO_2 incubator. A complete media change was performed the following day.

2.1.2. CHO cell freezing

Cells were treated with 0.05% trypsin (Thermo Fisher Scientific), placed in the incubator for 3 min and manually dissociated repeatedly during incubation by swirling the plate. The trypsin-cell suspension was then added to an equal volume of CHO media (described above) and centrifuged at 2000 rpm for 3 min. The supernatant was removed and the pellet resuspended in 0.5 ml CryoStor (StemCell Technologies) before transfer to a Cryovial (Elkay). Cryovials were placed in a freezing container (“Mr Frosty”, Thermo Fisher Scientific) and transferred to liquid nitrogen storage the following day.

2.1.3. CHO cell passaging

Cells were treated with 0.05% trypsin and dissociated as described above whereby the pellet was resuspended in the appropriate volume of CHO media. The volume of cell suspension added to the plate was adjusted depending on whether cells were being plated onto a Nunc treated 10 cm dish, 5 cm dish, 6-well plate, 12-well plate or a 24-well plate (all Thermo Fisher Scientific). After passaging, a full media change was performed the following day followed by media changes every other day or as required.

2.2. hES cell culture and neuronal differentiation

2.2.1. hESC thawing

Cryovials containing hESCs were partially thawed by incubation in a 37°C water bath until only a small wedge of ice remained in the vial. 2 ml of mTeSR medium (STEMCELL Technologies) was added directly to the vial, the cells collected and centrifuged at 2000 rpm for 3 min. The supernatant was removed and the pellet resuspended in 2 ml of mTeSR containing Rho-kinase inhibitor (STEMCELL Technologies, 1:1000 dilution) and plated onto Matrigel (Corning) plates pre-coated with Matrigel for 1 hour at 37°C. When thawed hESCs were plated into a single well of a Nunc cell culture treated 6-well plate.

2.2.2. hESC freezing

HESCs were treated with ReLeSR (STEMCELL Technologies) for 1 min and placed in the incubator. ReLeSR was aspirated from the well and cells collected from the well using 2 ml of mTeSR medium (STEMCELL Technologies). The cell suspension was centrifuged at 2000 rpm for 3 min, the supernatant removed and the pellet resuspended in 0.5 ml CryoStor (STEMCELL Technologies) before transfer to a Cryovial (Elkay). Cryovials were placed in a freezing container ("Mr Frosty", Thermo Fisher Scientific), transferred to -80 °C and placed in liquid nitrogen storage the following day.

2.2.3. hESC growth and passaging

The human embryonic stem cell line hESC H9, WAe009-A (Thomson et al. 1998) and isogenic *NTRK2* (TrkB) targeted or non-targeted clones C9, D2, B1 and A10 (see Chapter 5) were grown on Matrigel-coated plates and maintained in mTeSR medium. Medium was changed daily and hESCs were passaged using ReLeSR (STEMCELL Technologies). HESCs were treated with ReLeSR (STEMCELL Technologies) for 1 min and placed in the incubator. ReLeSR was aspirated from the well and cells were collected from the well using 2 ml of mTeSR medium (STEMCELL Technologies). The cell suspension was centrifuged at 2000 rpm for 3 min and the supernatant aspirated. Cells were resuspended in mTeSR with Rho kinase inhibitor and split at either a 1:3, 1:4 or 1:6 ratio onto Nunc treated 6-well plates.

2.2.4. Neuronal differentiation

Neuronal differentiation was performed as previously described (Merkouris et al. 2018). HESCs were sub-cloned until the desired cellular morphology was observed (see Chapter 3), grown to confluency and passaged using Accutase (Life Technologies) at a 1:3 ratio onto Matrigel-coated Nunc treated 6-well plates. Cells were incubated for 1 hour with Rho-kinase

inhibitor, the culture medium removed and Accutase added to the cells followed by incubation for 5-8 min followed by gentle cell resuspension achieved by swirling the plate. The resuspended cells were then added to an equal volume of medium, and plated with Rho-kinase inhibitor. When cells had reached 70% confluency (DIV 0), they were washed 3 times with PBS (Invitrogen Life Technologies) and fed daily with a “neural induction medium” containing Advanced DMEM:F12 (with Glutamax); 1 % Penicillin/Streptomycin (all from Thermo Fisher Scientific); 10 µM SB431542 (Abcam) 1 µM LDN 193189 (Stemgent); 1.5 µM IWR1 (Tocris) and 2 % NeuroBrew-21 without retinoic acid (Miltenyi Biotec). At day 8 neural progenitors were dissociated with Accutase as described above (Life Technologies) and re-seeded with Rho-kinase inhibitor at a 1:4 ratio onto Matrigel-coated plates in expansion medium containing Advanced DMEM-F12 supplemented with 2% NeuroBrew-21 without retinoic acid (Miltenyi), 0.2 µM LDN193189, 1.5 µM IWR1 and 25 ng/ml Activin A (Peprotech).

Subsequent neuronal differentiation and maturation were performed as previously described (Telezhkin et al. 2016b). Neural progenitors were seeded on poly-D-lysine (Thermo Fisher Scientific) and Matrigel-coated surfaces (Poly-D-lysine was added to wells for 1 hour followed by 3 DPBS washes before wells were coated with Matrigel) at a density of 1 million cells per well of 12-well plates or 150,000 cells per 13 mm coverslip and cultured for 7 days in SJA (Synaptojuice A) medium containing Advanced DMEM F12 (with Glutamax), 1% penicillin/streptomycin, 2 % NeuroBrew21 with retinoic acid (Miltenyi Biotec), 2 µM PD0332991 (Tocris Bioscience), 10 µM DAPT (Sigma-Aldrich), 0.6 mM $CaCl_2$ to give 1.8 mM $CaCl_2$ in final complete medium (Sigma-Aldrich), 3 µM CHIR 99021 (Tocris Bioscience), 10 µM Forskolin (Tocris Bioscience), 300 µM GABA (Tocris Bioscience) and 200 mM ascorbic acid (Sigma- Aldrich). The medium was replaced at day 7 post-plating by SJB (Synaptojuice B) medium which contained equal parts Advanced DMEM/F12 with Glutamax and Neurobasal A (Thermo Fisher Scientific), 1% penicillin/streptomycin (Life Technologies), 2% NeuroBrew-21 with retinoic acid (Miltenyi Biotec), 2 µM PD0332991 (Tocris Bioscience), 3 µM CHIR 99021 (Tocris Bioscience), 0.3 mM $CaCl_2$ (1.8 mM $CaCl_2$ final), and 200 µM ascorbic acid (Sigma-Aldrich). Plated progenitors and the resulting neurons were maintained for up to day 33 before experimentation.

All cultures were regularly checked for mycoplasma contamination using the LookOut Mycoplasma PCR Detection kit (Sigma-Aldrich) according to the manufacturer’s instructions. Cultures were also monitored daily (see Chapter 3) and observed for signs of bacterial and yeast contamination by phase contrast microscopy.

2.3. CRISPR targeting

NTRK2 mutant H9 hESC clones were generated by CRISPR gene editing. Guide RNAs targeting exon1 of *NTRK2* were selected using Deskgen CRISPR design tools (www.deskgen.com) with the help of Nick Allen. CRISPR was performed using ribonucleoprotein technology (RNP) following an established protocol (Bruntraeger et al. 2019). Briefly, 2 nM of each guide RNA (TCGTCCTGGATAAGGTGGCATGG, GTCGCTGCACCAGATCCGAGAGG, ACACTGTTAGGCTCCAATCTCGG) and 20 nmol ATTOTM 550 labelled Alt-R® CRISPR-Cas9 tracrRNA were complexed in IDT buffer. The RNP complexes were formed immediately prior to use by mixing the crRNA:tracrRNA complexes with Alt-R® S.p. HiFi Cas9 Nuclease V3. All CRISPR reagents were purchased from Integrated DNA Technologies. RNP complexes were delivered to H9 hESCs by Amaxa nucleofection. Briefly, H9 hESCs pre-treated for 1 hour with Rho-kinase inhibitor and were dissociated into single-cell suspension using Accutase. 1×10^6 cells were resuspended in Amaxa P3 nucleofection buffer (Lonza), mixed with Cas9 RNP complex and nucleofected using program CA137 on the Amaxa-4D nucleofector. After overnight culture in mTesR medium containing Rho-kinase inhibitor nucleofected cells were sorted by flow cytometry (BD FACS Aria Fusion) with the help of Mark Bishop and the brightest ATTO550 labelled cells (~5000 cells) re-plated at clonal density onto Matrigel-coated 10 cm plates. Cells were fed with mTesR medium containing Rho-kinase inhibitor and penicillin/streptomycin for the first 3 days followed by mTesR only thereafter. Colonies derived from single cells were manually picked on day 7 into Matrigel coated Nunc treated 96 well plates (Thermo Fisher Scientific) under the guidance of Nick Allen and Bridget Allen. 96 well plates were replica-plated by passaging with ReLeSR, allowing one plate to be used for DNA analysis.

2.4. DNA analysis

2.4.1. DNA extraction

Clone genotyping was carried out using DNA extracted from each well of the 96 well plate using QuickExtract DNA Extraction Solution (Lucigen) according to the manufacturer's instructions. The cells were washed once with PBS and 50 µl QuickExtract DNA solution added per well. The wells were scraped to dislodge cells and the cell suspension transferred to PCR tubes/96 well PCR plate (depending on how many clones to be screened). The samples were placed in a thermal cycler and heated for 5 min at 68°C before vortexing and further heating at 95°C for 15 min. DNA was then stored at -80°C until PCR.

2.4.2. Genotyping

Samples were genotyped using PCR primers (forward: 5′-CCCTGTAAAGCGGTTCGCTA-3′ and reverse: 5′-CCCACTCTTGGGACAGCATT-3′) designed to flank the CRISPR targeted region. 1 µl of DNA was used per PCR reaction. Each well/tube contained 10 µl PCR Biosystems red master mix (PCR Biosystems), 0.1 µl of each forward and reverse primer and made up to 20 µl with ddH_2O. The samples were placed in a thermal cycler and the PCR was run using the following program: 95°C 3 min; (95°C 30 s, 58°C 30 s, 86 °C 1 min) x 35; 4°C ∞. PCR products for wild type and mutant alleles were analysed by 2% agarose gel electrophoresis.

2.4.3. DNA sequencing

PCR amplicons from candidate edited clones were gel extracted (Qiagen) for Sanger sequencing (Eurofins) and sequences analysed using CRISPR-ID software (http://crispid.gbiomed.kuleuven.be/).

2.5. RNA analysis

2.5.1. RNA extraction

Total RNA was extracted from human neurons using the RNeasy Mini kit (Qiagen). Cultures were washed with DPBS and lysed with 350 µl of RLT RNA lysis buffer (Qiagen) containing 1% β-2-mercaptoethanol (Sigma-Aldrich). Lysates were either frozen at -80°C or processed with the RNeasy Mini Kit according to the manufacturer's instructions, including a DNase treatment for 15 min at room temperature (Sigma-Aldrich).

2.5.2. RNA quality and quantity checks

2.5.2.1. Qubit Analysis

To measure the concentration of RNA in each sample, a Qubit Fluorometer (Invitrogen by Life Technologies) was used. Two assay tubes for the standard samples were set up as well as one per sample to be tested. A working solution consisting of the Qubit reagent (from Qubit kit) being diluted 1:200 in Qubit buffer (from Qubit kit). 200 µl of working solution was prepared for each standard and sample. The standards were prepared by adding 190 µl of working solution and 10 µl of standards 1 and 2 (from Qubit kit) respectively. For the sample, 198 µl working solution was added followed by 2 µl of the RNA sample. The tubes were briefly vortexed and then incubated for 2 min at room temperature prior to Qubit analysis.

2.5.2.2. Tapestation analysis

The 2200 Tapestation (Aglient Technologies) performed an RNA ScreenTape Assay and gave an indication of the quality of RNA in our samples. The RNA ScreenTape Sample Buffer and RNA ScreenTape Ladder (both Agilent Technologies) were allowed to equilibrate to room temperature. 5 µl of Sample Buffer was added to 1µl RNA Ladder for the standard, or 1 µl RNA sample. The tubes were then vortexed (IKA vortexer and adaptor) at 2000 rpm for 1 min. The samples were then spun down briefly. The samples were heated to 72°C for 3 min, then placed on ice for 2 min. The samples were briefly centrifuged before loading onto the Tapestation.

2.5.3. RT-qPCR

The levels of full-length, kinase domain-positive *NTRK2* and *NTRK3* mRNAs were quantified by RT- qPCR relative to a geometric mean of mRNAs for *GAD1* and *GAD2* by Sean Wyatt. 5 µl total RNA was reverse transcribed, for 1 hour at 45°C, using AffinityScript (Agilent) in a 25 µl reaction according to the manufacturer's instructions. 2 µl of cDNA was amplified in a 20 µl reaction volume using Brilliant III ultrafast qPCR master mix reagents (Agilent Technologies).

PCR products were detected using dual- labelled (FAM/BHQ1) hybridisation probes specific to each of the cDNAs (Eurofins). The PCR primers were: *NTRK2* (TrkB) forward: 5′-TTCCCATCACCAGAAATG-3′ and reverse: 5′-GCTTGAGAAACAAACCAG-3′; *NTRK3* (TrkC) forward: 5′-TCTGCTAGTGAAGATTGG-3 ′ and reverse: 5′-TCCCACCCTGTAATAATC-3′; *GAD2* forward: 5′-CCAGAAGTCAAGGAGAAA-3′ and reverse: 5′-GTCTGTTCCAATCCC AA-3′; *GAD1* forward: 5′-CAGAGAAGAATTTGAGATGG-3′ and reverse: 5′-GGCTTTGTGGAATATACC-3′. Dual-labelled probes were: *NTRK2*: 5′-FAM-CTATCATCACAACCTACGAAGACAAA-BHQ1-3′; *NTRK3*: 5′-FAM-ATGTCCAGAGATGTCTACAGC-BHQ1-3′; *GAD2*:5′-FAM-TGCTCTTCCCAGGCTCATTGC-BHQ1-3; *GAD1*: 5′-FAM-CAATGGCGAGCCTGAGCACA-BHQ1-3. Forward and reverse primers were used at a concentration of 250 nM and dual-labelled probes were used at a concentration of 500 nM. PCR was performed using the Mx3000P platform (Agilent) using the following conditions: 95°C for 3 min followed by 45 cycles of 95°C for 10 s and 60°C for 35 s. Reverse transcribed *NTRK2*, *NTRK3*, *GAD1* and *GAD2* cDNAs were quantified by reference to a standard curve comprising serial 5-fold dilutions of a 250 bp synthetic DNA template corresponding to the transcript being amplified. Each synthetic DNA template comprised the PCR amplicon flanked by 50-100 bp of transcript sequence. Primer and probe sequences were designed using Beacon Designer software (Premier Biosoft).

2.5.4. RNAseq analysis

H9 and A10 neurons were treated for 2 hours and 24 hours with BDNF and NT3 respectively (2 nM) and RNAseq was performed by Angela Marchbank in the Genomics Hub of Cardiff University. RNA was extracted and integrity assessed on an Agilent RNA 6000 Pico chip using the Agilent 2100 Bioanalyzer (Agilent Technologies). RNA (500 ng) was used to produce the cDNA library with the Tru-Seq protocol (Illumina) and sequenced with an Illumina HiSeq 4000 system. Initial data processing was carried out by Sumukh Deshpande and Robert Andrews. RNA-seq single-end fastq files were mapped to human assembly genome GRCh38 using the STAR package and transcript counts were generated using FeatureCounts and the results normalized using the Bioconductor R package. Gene expression values and differentially expressed genes were obtained using DeSeq2 package in fragments per kilobase of transcript per million mapped reads (FPKM). Principal component analysis (PCA) was used to analyse how different samples relate to each other based on overall expression profiles.

The analysis also included the Glimma package that generated interactive graphics, allowing a detailed exploration of the data at both sample and gene-level – this was not possible with the use of static R plots. This analysis was carried out by Spyros Merkouris. The RNA-sequencing data in the form of gene-level counts were imported into R, organized, filtered and

normalised using edgeR package, followed by the limma package whereby linear modelling and empirical Bayes moderation was used to assess differential expression. Note that the full RNAseq datasets will be deposited into an online database upon publication of this data.

2.6. Protein analysis

2.6.1. Protein extraction

Neurons were incubated with the appropriate ligand for various lengths of times as indicated in the Results section Prior to lysis, the cultures were washed with PBS, and subsequently lysed with 70 µl of RIPA lysis buffer: 50 mM Tris- HCl, pH 7.4, 150 mM NaCl, 1 mM EDTA, 1% Triton-X-100, 0.2% sodium deoxycholate, 0.1% SDS and supplemented with a cocktail of protease and phosphatase inhibitors (Sigma-Aldrich) at 1:100 dilution containing 100 mM 1,10-Phenanthroline, 100 mM 6-aminohexanoic acid, 10 mg/ml aprotinin and 2 mM sodium orthovanadate. Cell lysates were kept on ice for 10 min, then centrifuged for 15 min at 15,000 rpm and the supernatant transferred to a new tube prior to western blot analysis, or storage at -80°C.

2.6.2. BCA

The protein concentration of lysates was determined using the Thermo fisher Scientific Pierce BCA Protein Assay Kit (Thermo Fisher Scientific) according to the manufacturer's instructions. Protein samples were diluted 1:50 in ddH_2O and prepared in triplicates. Both samples and BSA standards (25-2000 µg/ml) were incubated in working reagent (prepared according to the manufacturer's instructions) for 1 hour at 60°C. Absorbances were recorded on a FLUOstar® Omega microplate reader (BMG Labtech, Aylesbury, UK) and the protein concentration of each sample determined using the calibrated BSA standard curve. Following the realisation that the differences in protein concentrations across 5 independent differentiations were negligible, Ponceau Red stains was then routinely used instead after every transfer to ensure that similar volumes of lysates were loaded and transferred.

2.6.3. Western blotting

4 X NuPAGE loading buffer (containing 0.666 g Tris HCl, 0.682 g Tris Base, 0.8 g LDS (lithium dodecyl sulfate), 0.006 g EDTA (ethylenediaminetetraacetic acid), 4 g glycerol, 0.75 ml SERVA Blue G250 (1% solution) and 0.25 ml phenol red (1% solution) and 10 X DTT (dithiothreitol) (Sigma-Aldrich) was added to each sample before heating at 70°C for 10 min (in cases where DTT was omitted, samples were heated for 5 min). Samples were then loaded onto a 4-12% Bis-Tris NuPAGE gel (Invitrogen) and the gel run at 120 V for 1.5 hours. Protein

was transferred to nitrocellulose membranes using the wet transfer Mini-Trans Blot Cell (Bio-Rad). The membrane was then washed with PBS and stained with Ponceau Red to allow visualisation of transferred protein. The membrane was then blocked for 1h with blocking solution (5% western blotting grade blocker (BIO-RAD) and 1% BSA (Sigma-Aldrich) in 1 X TBS-T) (described below). Following this the blots were probed with rabbit monoclonal anti-P-Trk (Cell Signaling, mAb #4621) diluted 1:4000, goat polyclonal anti-TrkB (R&D Systems) diluted 1:2000, goat polyclonal anti-TrkC (R&D Systems) diluted 1:2000, mouse monoclonal anti-synaptophysin (Sigma-Aldrich S5768) diluted 1:2000 or anti-arc mouse monoclonal (Santa Cruz sc – 17839). The primary antibody was diluted in blocking solution and incubation was overnight at 4 °C.

The membranes were then washed 3 times with 20 ml TBS-T (10 X TBS (10 X TBS – 25 mM Tris Base, 1.37 mM NaCl, 2.6 mM KCl dissolved in ddH_2O. TBS-T: 1 X TBS & 1% Tween-20 (Sigma-Aldrich) for 10 min per wash on a rocker and incubated with the secondary antibody (1:2000) in blocking solution for 1 hour. The primary antibodies were detected with donkey anti-Rabbit HRP-conjugated, anti-goat HRP-conjugated and anti-Mouse HRP-conjugated secondary antibodies (Promega). The membrane was developed using the WesternBright ECL Kit (Advansta). Blots were visualized with the Image Lab software and the Universal Hood III camera system (BIO-RAD). Densitometry analysis of the bands with ImageJ was used to calculate the intensity of the signal for each band. The quality of protein transfer was checked in every case by staining the membranes with Ponceau Red. Normalisation in all cases was deemed acceptable based Ponceau staining as the volume as well as the protein concentrations were found to be consistent between samples (see above). Synaptophysin was therefore not routinely used as a normalisation control.

2.7. Immunocytochemistry

Coverslips were prepared by incubating them in 100% nitric acid overnight, then washed 3 times with water, once with ethanol and autoclaved. Cells grown on coverslips were washed once with PBS and fixed with 4% paraformaldehyde for 30 min except when stained for TrkC, in which case the cells were fixed for 10 min. The coverslips were then washed 3 times for 5 min with 0.1% Tween-20 in PBS at room temperature, and blocked for 1 hour with 3% donkey serum and 0.1 % BSA in 0.1% Tween-20/PBS and incubated for 1 hour at room temperature with any of the following antibodies: anti-β-III-tubulin (Tuj1) mouse polyclonal (Abcam) diluted 1:1000, goat polyclonal anti-TrkB (R&D Systems) diluted 1:2000, or rabbit monoclonal anti-TrkC (Cell Signalling) diluted 1:2000. Subsequently the cultures were incubated for 1 hour at room temperature with the corresponding secondary antibodies (Alexa fluor 488 donkey anti-rabbit, Alexa fluor 488 donkey anti- goat or Alexa fluor 488 donkey anti-mouse; Invitrogen). Cells were then washed 3 times for 5 min with 0.1% Tween-20 in PBS at room temperature before incubation with DAPI in PBS (1:10,000). Cells were washed once with PBS and mounted using DAKO mounting medium (Agilent). Coverslips were left to dry overnight before imaging with a Nikon Eclipse Ni-U epifluorescence microscope using iLabCam iPhone 11 adapter (iDu Optics). Images were taken via an iPhone as the Trk signal was found to be very weak using the standard camera attached to the microscope and the exposure was optimised for the TrkB and TrkC staining to enable clear visualisation of the Trk staining pattern.

2.7.1. Cell counting

H9 TrkB-, H9 TrkC-, H9 Tuj1-, A10 TrkB-, A10 TrkC- and A10 Tuj1-positive cells were counted in 20 randomly selected field, 2 coverslips each using a Nikon Eclipse Ni-U epifluorescence microscope at 40 X magnification. The number of TrkB- or TrkC-positive cells was found not to be significantly different from the number of Tuj1-positive cells, neither for H9 nor A10 neurons.

Chapter 3 - Neurons derived from wild-type human embryonic stem cells express the Neurotrophin-3 receptor TrkC

3.1. Short Introduction

Culture work with embryonic stem cells has opened the possibility to direct their differentiation into cells with relevant features, in this case human neurons expressing growth factor receptors of interest. Successful differentiation of hESCs has been previously achieved in a related study centred around the characterisation of a new antibody activating the BDNF receptor TrkB (Merkouris et al. 2018). The differentiation procedure used in this previous project was shown to generate cultures containing over 80% of BDNF-responsive neurons (Merkouris et al. 2018). Beyond the large population of BDNF-responsive neurons indicative of significant homogeneity of the neurons generated by the culture procedure, this procedure was also highly reproducible between experiments and consistently generated a small proportion of non-neuronal cells. These features justified a mass analysis of cells treated with various reagents, including various ligands activating TrkB (Merkouris et al. 2018). Accordingly, it was essential to ensure that TrkC-expressing neurons in cultures of similar quality could also be reproducibly generated. The same hESC clone used in this related project, designated H9, was also used here and it is one of the most extensively used hESC lines in the field. It possesses 2 XX chromosomes and was described in the first publication documenting the successful isolation of human stem cells (Thomson et al. 1998). A key characteristic of the differentiation protocol, now widely used in the field, is that it involves dual inhibition of TGF- β signalling that efficiently promotes neuronal differentiation (Chambers et al. 2009). Activin A addition is also a key part of this differentiation protocol and promotes the differentiation of GABAergic, long projection neurons with characteristics resembling those of medium spiny neurons in the striatum (Arber et al. 2015). In the mouse system, these neurons are amongst the most BDNF-responsive neurons, both *in vivo* and *in vitro* (Rauskolb et al. 2010).

The main aim of this chapter was to successfully differentiate H9 hESCs into neurons, to demonstrate TrkC expression in these neurons and to explore the characteristics of TrkC activation by NT3.

3.2. Results

3.2.1. Generating neurons from H9 human embryonic stem cells

The process of successful neuronal differentiation from hESCs (summarised in Figure 3.1) heavily relies on detailed examination of cultures by phase contrast microscopy. Accordingly, hESC cultures were assessed daily and experience accumulated to allow reliable conclusions to be made about the ideal cell morphology of undifferentiated hESCs as the quality of hESCs determines the quality of the neurons produced. The morphology of hESCs deemed promising in terms of suitability for neuronal differentiation is illustrated in Figure 3.2A. This is a key aspect in this type of project as it takes about a month for neurons to be generated from undifferentiated hESCs and to be ready for experimentation. In addition to morphology, a key additional criterion was the rate of cell division. Upon thawing, hESCs were sub-cultured for various lengths of time depending on the quality of cells prior to freezing, the freezing procedure, the length of storage and the thawing procedure - all factors potentially impacting the quality of hESCs. Subsequently, hESCs were repeatedly passaged to ensure the selection of the most rapidly dividing cells. If a differentiation was initiated before the cells were of sufficient quality and homogeneity, the neurons produced were of poor quality (illustrated in Figure 3.3) or most commonly the cells died and/or detached during the earlier stages of the differentiation procedure. Promising hESCs not only looked homogenous by phase contrast microscopic examination, but also typically formed large, tightly packed colonies with round edges and a high nucleus-to-cytoplasm ratio (Figure 3.2A). After a split at day 8 of the differentiation procedure, rosettes began to form - a reliable indication that neural progenitors had been generated (Figure 3.2B). At day 16, progenitors were counted and 1 million cells were added to each well of a 12-well plate. From this time onwards, neurons began to elongate processes (Figure 3.2C) and the last differentiation medium was added to cells at day 23. Subsequently, the cellular morphology did not dramatically change and neurons remained evenly distributed (Figure 3.2D). Possible contaminations by bacteria and mycoplasma were regularly checked whereby antibiotics were used from day 0 of the differentiation procedure and throughout (see Chapter 2, Materials and Methods).

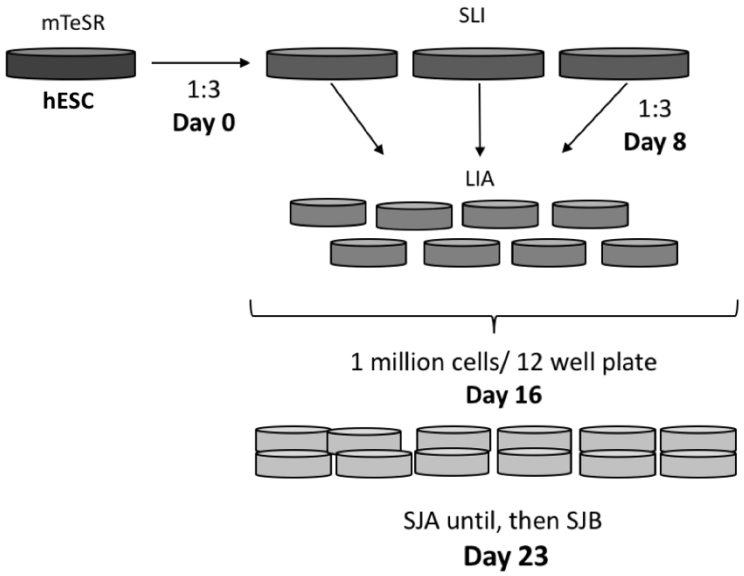

Figure 3.1. Scheme of the differentiation procedure.

Summary of the differentiation protocol described in Materials and Methods with the gradual expansion of cells and most typical split ratios indicated at each stage.

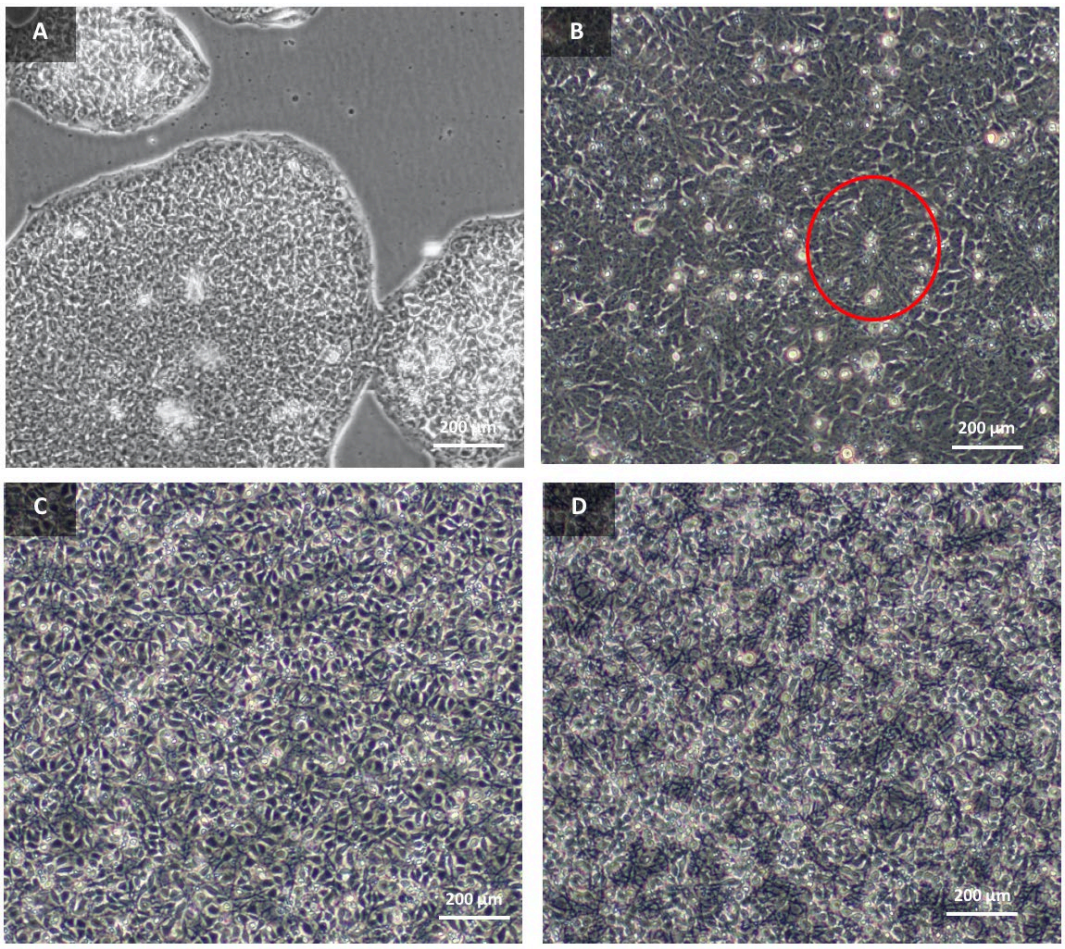

Figure 3.2. Phase contrast images of H9 cells illustrating the different phases of the differentiation procedure.

Phase contrast images (20 X magnification) showing optimal cultures of: H9 hESCs ready for differentiating (A), day 10 progenitors showing neural progenitor rosettes (B, red circle indicates a neural rosette), day 19 neurons (C) and day 27 neurons (D) that had been in terminal differentiation medium for 4 days and were ready for experimentation.

To ensure the generation of reproducible results, it was important to identify cultures unlikely to be suitable for further experimentation whereby slight inconsistencies in cell density and clustering between differentiations were difficult to eliminate entirely. The most common identified factor accounting for experimental variability was the Matrigel solution used for coating the wells. This coating matrix is relatively ill-defined and significant batch-to-batch variability was noted, leading in some cases to the clustering of neurons and the formation of thick cable-like structures (Figure 3.3A). These lead to the gradual detachment of neurons and sparse cultures with increasing number of dead cells over time (Figure 3.3B).

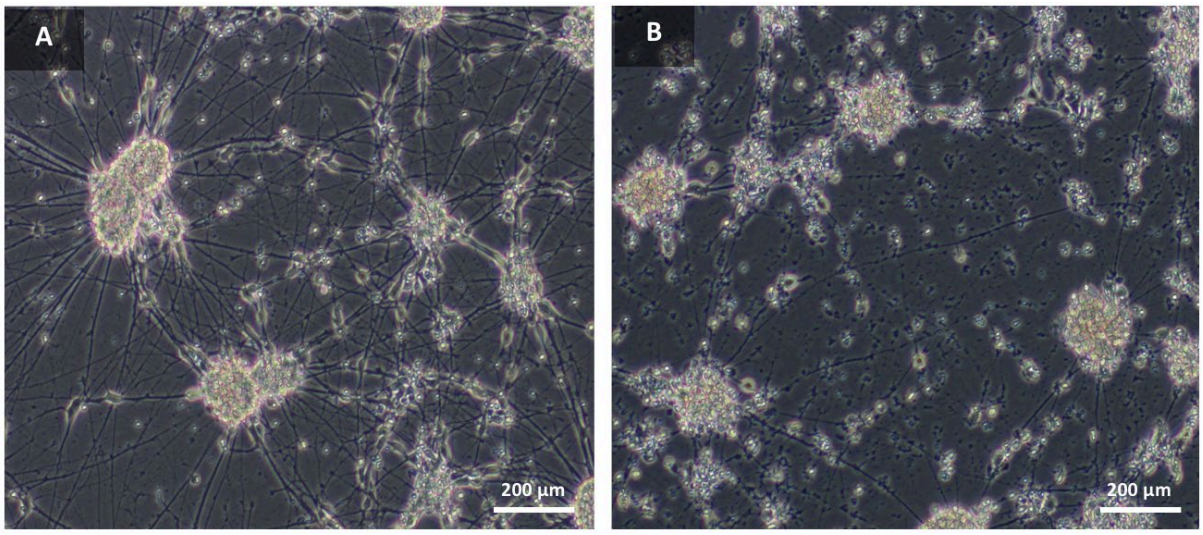

Figure 3.3. Examples of neuronal morphology unsuitable for experimentation.

Phase contrast images (20 X magnification) of sub-optimal neuronal cultures of H9 neurons. Cellular clumps and thick cables have formed (A). Cells have also gradually detached from the well resulting in the accumulation of debris from dead cells and processes resulting in low cell density (B).

3.2.2. Detection of TrkC by Western blot in lysates of cells transfected with Trk receptors

A previous set of results using the same differentiation protocol and the same H9 hESCs indicated significant expression of TrkC (AKA *NTRK3*) as a result of the RNAseq experiments performed with these cells (Merkouris et al. 2018). The same analysis also indicated barely detectable expression of other NT3-binding receptors, namely TrkA (AKA *NTRK1*) and p75 (AKA *NGFR*, see General Introduction). These results were replicated here (see Chapter 8). Such low levels of RNA expression are unlikely to generate detectable levels of the corresponding proteins.

Using lysates of transfected CHO cells constitutively expressing human TrkA, B or C, affinity purified goat polyclonal anti-TrkC antibodies were then tested using lysates of these cells (Figure 3.4A) as well as TrkA, TrkB, TrkC or non-transfected (designated HEK293 control) HEK293 lysates (Figure 3.4B). Only very small amounts of the corresponding HEK293 cell lysates were available (kind gift from Dr. Jia Xie), whilst the TrkB- and TrkC-expressing CHO cells could be grown as needed (these cells were originally generated by Dr. Jia Xie also and kindly gifted for use in this project). The TrkC polyclonal antibodies used here have been raised against the secreted extracellular domain of mouse myeloma cell line NS0 using the human TrkC sequence comprising Cys31 to Asp428. It is thus likely that these antibodies recognise conformation-dependent epitopes imposed by the formation of disulfiide bridges, known to be present in Trk receptors including TrkC. As illustrated in Figure 3.4, these antibodies turned out to be specific for TrkC, with no sign of cross-reactivity with either TrkA or TrkB. Given the way these antibodies were raised (see above) it was of interest to test CHO and HEK293 lysates with and without reduction with DTT prior to separation by SDS gel electrophoresis. As could be expected, the absence of reduction led to a more intense TrkC signal, both with CHO and HEK293 lysates (Figure 3.4A and B).

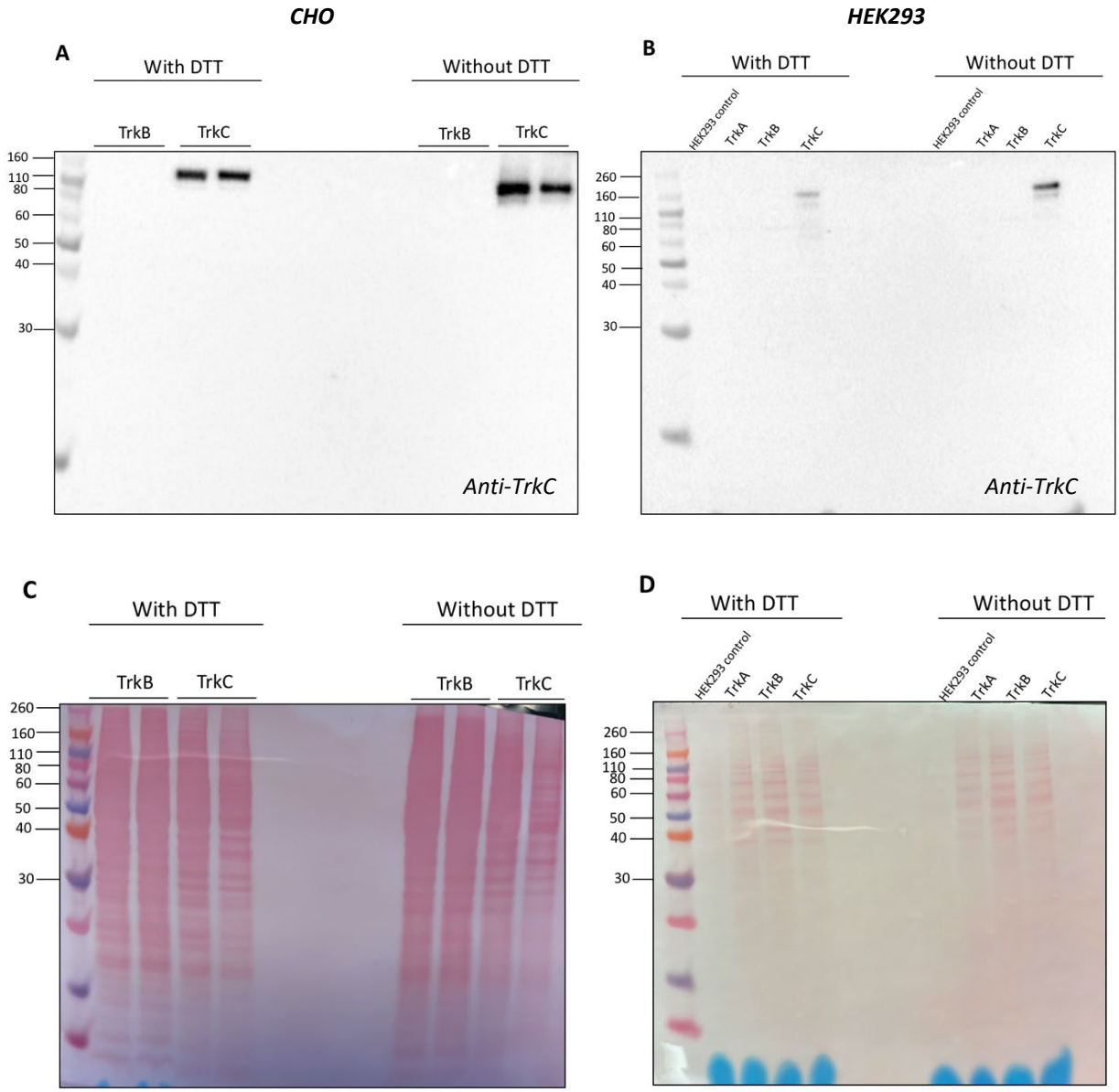

Figure 3.4. Validation of an anti-TrkC antibody using transfected CHO and HEK293 cells.

Lysates of CHO cells transfected with either TrkB or TrkC cDNAs were subjected to SDS gel electrophoresis and probed with an anti-TrkC antibody (A). Note the absence of signal in lysates of cells transfected with TrkB. (B). Lysates of HEK293 cells transfected with either TrkA, TrkB or TrkC or non-transfected (HEK293 control). Note the absence of signal with TrkA and TrkB. With both CHO and HEK293 cells the signal intensity for TrkC was increased in the absence of DTT treatment of the cell lysates. (C). and (D). show Ponceau stains corresponding to both blots.

3.2.3. Detection of TrkC by Western blot in lysates of H9 neurons

Following validation of the TrkC antibody with transfected cells, H9 neuronal lysates were then probed also with and without DTT treatment (Figure 3.5). A clear signal could be detected yet several bands could also be detected with and without DTT treatment of the lysates, presumably reflecting different degrees of N-glycosylation. Indeed, all Trk receptors are known to be heavily N-glycosylated whereby it is interesting to note that these multiple TrkC-reactive bands were observed with H9 neurons, but not with HEK293 or CHO cell lysates.

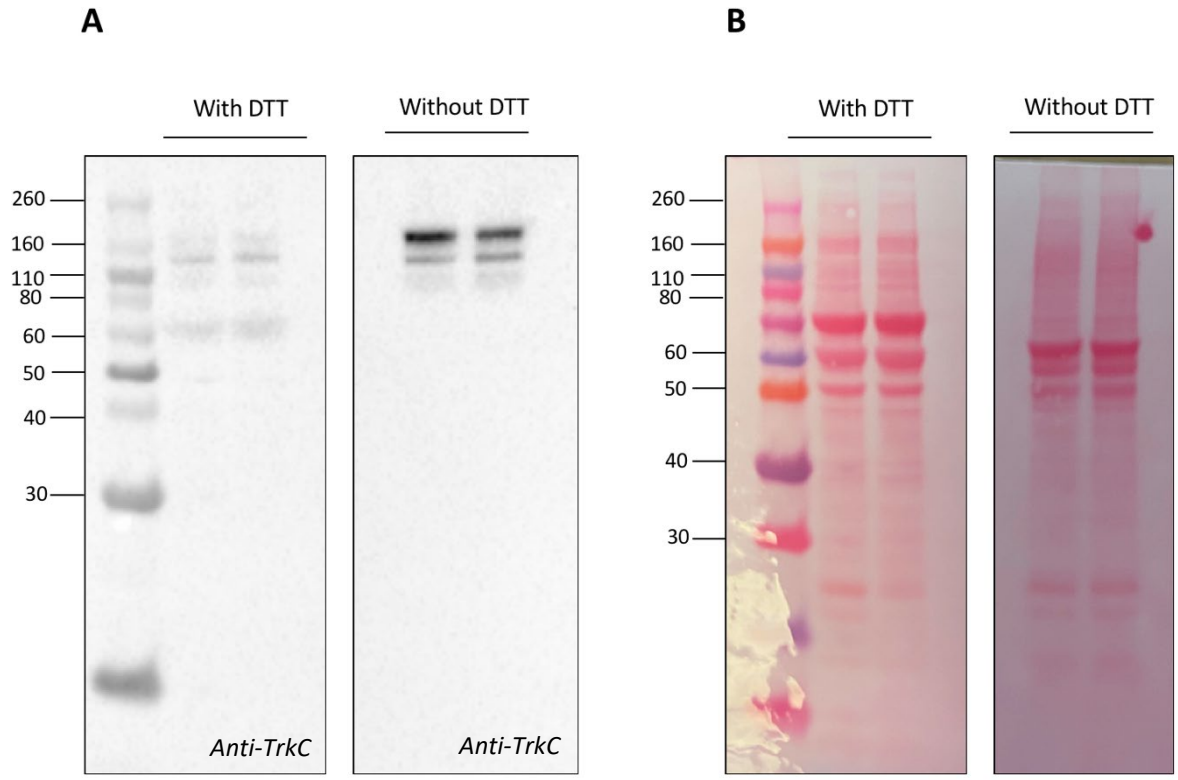

Figure 3.5. Expression of TrkC by H9 neurons

Western blots of H9 neuronal lysates that were subjected to SDS gel electrophoresis and probed with the anti-TrkC antibody showing that TrkC is expressed in terminally differentiated H9 neurons and is detected more readily when lysates are not denatured in the presence of DTT (A). (B). shows Ponceau stains corresponding to both blots.

3.2.4. Time course of TrkC expression in lysates of H9 neurons

Having established the specificity of the TrkC polyclonal antibodies and that H9 neurons expressed the receptor, the timing of TrkC expression during the course of neuronal differentiation was then explored. Lysates were prepared at several DIV (days *in vitro*), namely DIV 17, 21 and 30, separated by gel electrophoresis and probed for TrkC expression with the TrkC polyclonal antibody described in the above. TrkC was shown to be expressed at DIV 21 and at clearly higher levels than at DIV 17 (Figure 3.6) showing that neuronal maturation impacted the expression of TrkC. In view of these results, cells were not used for experiments before day 27, with most experiments performed between DIV 27-33. .

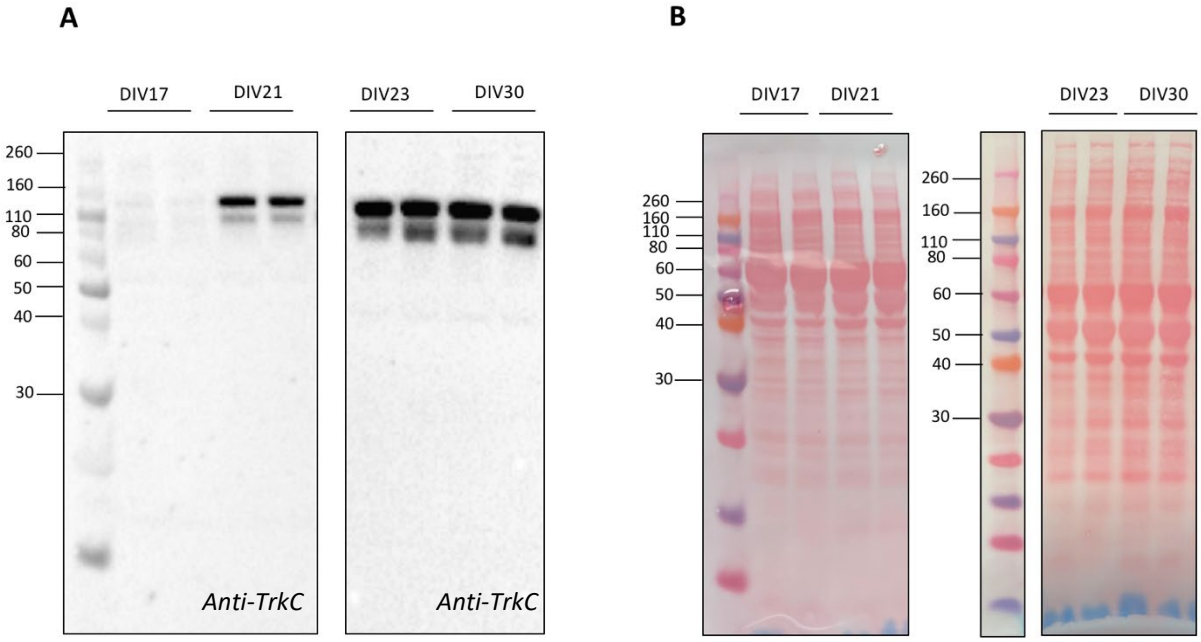

Figure 3.6. Expression of TrkC during neuronal maturation.

H9 neuronal lysates were separated by SDS gel electrophoresis and probed with anti-TrkC. The Western blots suggest that TrkC begins to be expressed robustly between DIV 17 and DIV 21 (A, left panel), to reach maximum expression at DIV 23 (A right panel). Expression is then maintained throughout terminal differentiation (A right panel). (B). shows Ponceau stains corresponding to both blots. This result was reproduced 3 times with 3 different differentiations.

3.2.5. Quantification of TrkC expression by cultured neurons

To determine the proportion of TrkC-expressing neurons, progenitors were plated at low density on poly-D-lysine-coated coverslips and stained with a β-III-tubulin (Tuj1) monoclonal antibody, or a previously characterised rabbit monoclonal anti-TrkC antibody suitable for this purpose (Takahashi et al. 2011). The use of this monoclonal antibody followed a large number of experiments performed with the TrkC goat polyclonal antibody described in the above leading to the conclusion that it cannot be used for immunocytochemistry experiments, possibly because the epitopes are sensitive to the fixation procedure. This interpretation is in line with the results presented in the above indicating that the epitopes recognised by the goat polyclonal anti-TrkC antibody are conformation-sensitive, with the signal intensity markedly decreasing following reduction with DTT (see above). The mean percentages ± SEM of Tuj1-positive neurons were 72.9 ± 3.1 (Figure 3.7 left panel) and 68.9 ± 1.9 (Figure 3.7 middle panel) for neurons stained with TrkC. The remaining 21.7% of neurons that were not stained with Tuj1 were considered to correspond to the nuclei of dead cells, known to readily take up DAPI rather than to non-neuronal cells in the culture. This was confirmed using phase contrast observation (Figure 3.7 bottom left panel) where no non-neuronal cell morphology was observed whereby dead cells were observed in the culture (red arrows) possibly due to the low density of cell plating. As dead cells do not synthesise protein, it was concluded that these cells could not contribute to the TrkC-positive cell count and therefore that the Tuj1-expressing and TrkC-expressing cells overlapped. This means that essentially all Tuj1-expressing cells express TrkC.

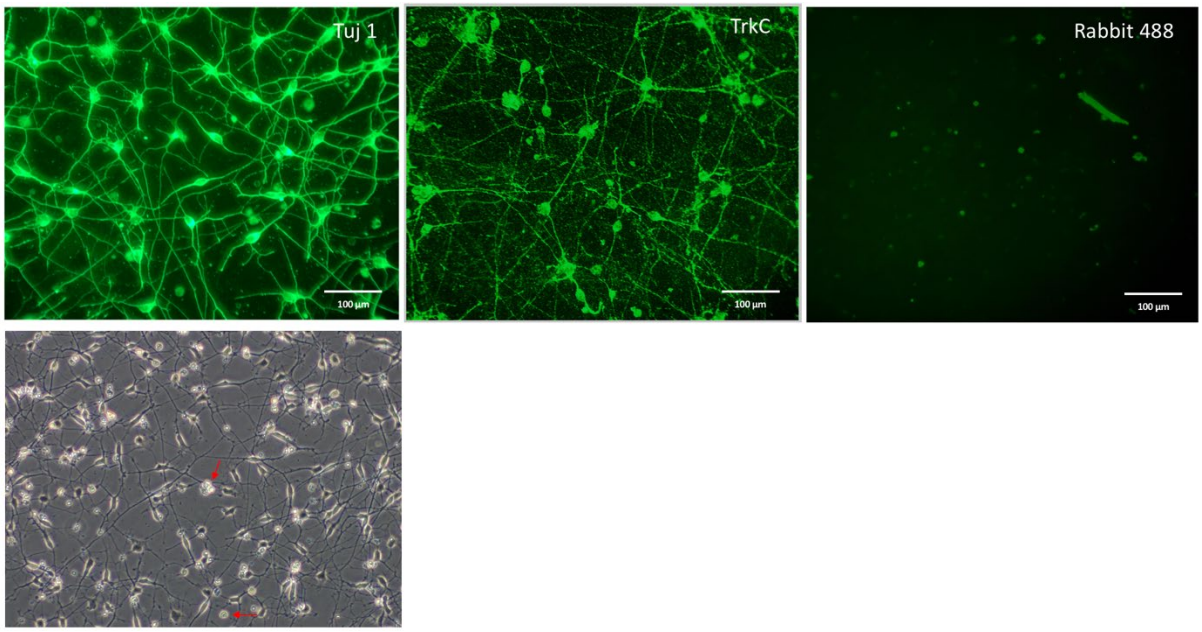

Figure 3.7. Expression of TrkC by H9 neurons: Immunofluorescence.

H9 neuronal progenitors were plated at low density on coverslips and stained with a rabbit TrkC monoclonal antibody (middle panel) or an anti-β-III-tubulin (Tuj1) mouse polyclonal antibody (left panel). Note the punctate appearance of TrkC staining, both on processes and cell bodies. The image in the right panel was obtained by omitting incubation with the primary antibody. The anti-rabbit secondary antibody only gives a barely detectable signal (right panel).The mean numbers ± SEM of Tuj1-positive neurons were 72.9 ± 3.1 and 68.9 ± 1.9 for neurons stained with TrkC. The bottom left panel shows a phase contrast image of H9 neurons on coverslips and examples of dead cells within the culture are indicated by the red arrows.

3.2.6. Activation of TrkC by NT3 and comparison with TrkB activation in transfected cells

To determine TrkC activation in response to NT3, an anti-phospho-Trk antibody was used that targets phosphorylated tyrosine residues 701 and 702 in the activation loop of TrkC, thus reflecting the activity of the kinase domain of TrkC. This is important as Trk receptors can also be tyrosine phosphorylated by other kinases thereby acting as substrates rather than active enzymes (see Discussion). Also, it is critical to note that owing to the near identical kinase domains of the Trk receptors, antibodies directly reflecting receptor activation do not distinguish between P-TrkB and P-TrkC.

The results with the TrkC- and TrkB-expressing CHO cells indicate that comparatively high concentrations of NT3 are needed to activate TrkC (Figure 3.8A). Whether such concentrations are ever reached *in vivo* is questionable and subsequent experiments with neurons revealed that TrkC activation actually occurs at much lower concentrations (see Chapter 7). Compared with TrkC, a stronger NT3-induced P-Trk signal was observed with TrkB-expressing CHO cells (Figure 3.8B), possibly due to a larger number of TrkB receptors being present in these cells. This interpretation is supported by the observation that a P-Trk signal was observed in the absence of NT3, suggesting receptor autophosphorylation known to occur with overexpressed Trk receptors. These results confirmed previous results by others that TrkB can be readily activated by NT3 in heterologous system (for review, see Barbacid 1994).

These results indicate that NT3 signalling through TrkC cannot be studied unequivocally in neurons co-expressing TrkB such as those derived from H9 hESCs or indeed most neurons in the mammalian brain. As detailed in Chapter 5, TrkB was then eliminated in hESCs in order to study TrkC signalling without also activating TrkB.

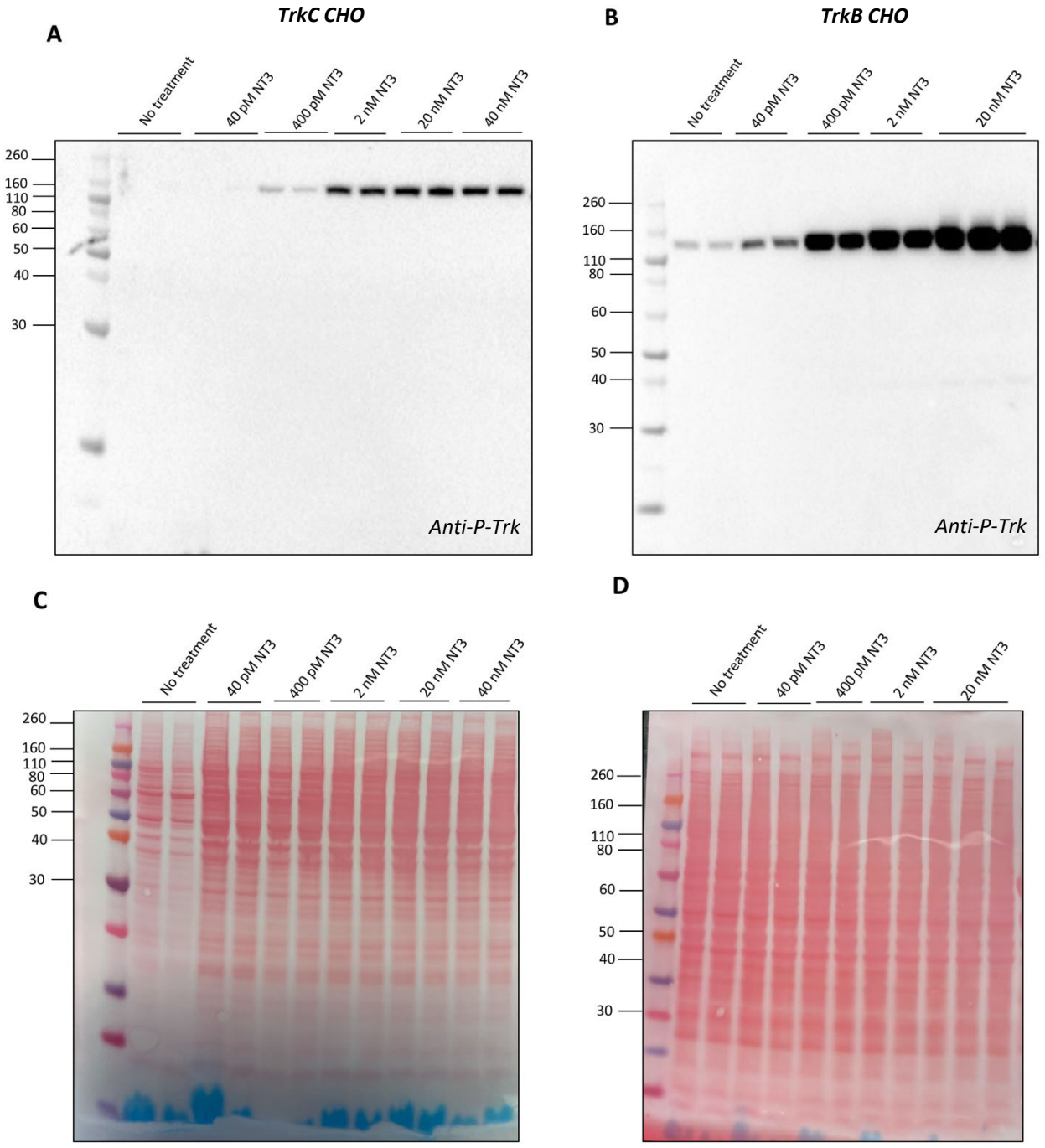

Figure 3.8. TrkB and TrkC activation by NT3 in transfected CHO cells: Dose response.

CHO transfected cells were treated for 20 min with various concentrations of NT3, the lysates separated by SDS gel electrophoresis and probed with anti-phospho-Trk. Note that whilst the P-Trk signal saturates at about 2 nM NT3 with the TrkC cells (A) it keeps increasing with the TrkB cells (B). (C). and (D) show Ponceau stains corresponding to both blots.

3.3. Short Discussion

The main result detailed in this Chapter indicates that neurons generated from the hESC clone H9 express the NT3 receptor TrkC, not only at the RNA, but also at the protein level. This conclusion was reached using 2 different antibodies: a monoclonal antibody validated for immunocytochemistry (Takahashi et al. 2011) and polyclonal antibodies suitable for Western blot shown not to cross-react with TrkA and TrkB (Figure 3.4). The TrkC signal observed with these polyclonal antibodies was considerably more intense when the cell lysates applied to the gel were not incubated with reducing agent DTT, in line with the fact that these TrkC antibodies were raised against the secreted, presumably glycosylated extracellular domain of TrkC that contains several cysteine residues involved in the formation of disulfide bridges.

The presence of multiple bands suggests that TrkC is likely N-glycosylated in neurons in a more heterogenous fashion than is the case in CHO or HEK293 cells for reasons that are unclear. Whether or not neuron-specific glycosylation may be related to the ability of TrkC to be activated by much lower concentrations of NT3 in neurons than is the case in other systems (see Chapter 7) is unclear at this point. Whatever the explanation may be, these results further emphasise the need to study receptor activation, TrkC in this case, in a relevant neuronal context as opposed to heterologous systems involving over-expression. This may be particularly important in the case of TrkB and TrkC as both receptors are closely related and share the same biosynthetic pathways, including N-glycosylation and the formation of disulfide bridges.

Determining the proportion of TrkC-expressing neurons was essential, given the assumption underlying these types of studies that all cells react similarly when exposed at the same time to the same reagent. The immunocytochemistry experiments needed to quantify receptor expression were complicated by the observation that the antibody used for Western blot did not allow a reproducible staining of fixed neurons, presumably because the epitopes recognised by this antibody may be conformation dependent and did not survive the fixation procedure. Quantification of the percentage of TrkC-expressing neurons could be achieved using a previously validated monoclonal antibody suitable for immunostaining (Takahashi et al. 2011). Crucially, this antibody revealed that essentially all Tuj1-postive, process-bearing cells derived from H9 hESCs expressed TrkC, thus justifying the further use of these neurons in mass analyses following the lysis all neurons exposed to NT3 (see Chapters 6, 7 and 8).

In addition, this culture system is particularly suitable for the study of downstream events triggered by NT3 and solely downstream of TrkC activation as the two other NT3 receptors to

consider, namely p75 and TrkA are not expressed at detectable levels in H9 neurons. The same characteristics apply to A10 neurons (see Chapter 8). P75 expression would have significantly complicated the analyses as it has been reported to bind NT3 with high affinity (Dechant et al. 1993). Furthermore, the co-expression of p75 together with TrkB dramatically reduces the ability of NT3 to activate TrkB, at least in heterologous overexpression systems (Bibel et al. 1999a). With regard to the NGF receptor TrkA, activation by NT3 has been proposed to explain some of the differences observed when comparing the sympathetic systems of animals lacking either NT3 or TrkC (Kuruvilla et al. 2004).

This leaves TrkB as the only plausible receptor to be activated by NT3 in H9-derived neurons and clearly, NT3 is a potent activator of TrkB in transfected CHO cells (Figure 3.8B), confirming previous well known observations in the field (for review, see Barbacid 1994). As most neurons in the mammalian CNS co-express TrkB and TrkC (see General Discussion), TrkB expression was then investigated in these cells (see Chapter 4).

Chapter 4 - Neurons derived from wild-type human embryonic stem cells express the BDNF/NT4 receptor TrkB at higher levels than TrkC

4.1. Short Introduction

Previous work with neurons derived from human H9 hESCs has established that the kinase domain of TrkB can be activated by BDNF, NT4 and a novel TrkB-activating antibody (Merkouris et al. 2018). As TrkB can also be activated by NT3 (see Introduction), the question arose as to whether TrkB can also be activated by NT3 in H9 human neurons and if so, how TrkC signalling could then be meaningfully studied in this system. Previous work revealed that the ability of NT3 to activate TrkB is context-dependent and that for example in rodent neurons, higher NT3 concentrations are needed to activate TrkB than in transfected cells (see for example Boltaev et al. 2017). This is possibly due to the co-expression of other NT3-binding receptors such as the neurotrophin receptor p75 (Dechant et al. 1993). Whilst RNAseq data indicates that H9 neurons do not express the NGF receptor TrkA (*NTRK1*) or the pan neurotrophin receptor p75 (*NGFR*) at significant levels, the question arose as to whether TrkB activation by NT3 may mask TrkC activation, especially if TrkB levels of expression would be significantly higher than those of TrkC as suggested by RNAseq data (Merkouris et al. 2018). Also, no tools are available allowing a distinction of the kinase-active form of the different Trk receptors.

Therefore, the main aim of this chapter was to explore TrkB expression and activation in H9 neurons and to try and quantify the relative degree of expression of TrkB and TrkC. A further aim was to investigate whether all cultured neurons also express TrkB, as was shown to be the case for TrkC (see Chapter 3). Last, given recent results that all drugs used to treat depression bind to TrkB (Casarotto et al. 2021), it was of interest to explore whether some of the most commonly used antidepressants may modulate TrkB signalling in human neurons.

4.2. Results

4.2.1. Validating commercially available antibodies for TrkB detection

Polyclonal anti-TrkB antibodies were first validated using lysates of CHO cells overexpressing either TrkB or TrkC (Figure 4.1A) or of transfected HEK293 cells overexpressing either TrkA, TrkB or TrkC (Figure 4.1B) (both CHO and HEK293 cells were also used in Chapter 3). A weak cross-reactivity with TrkC was observed with CHO cell lysates expressing TrkC in the absence of reduction and at a high protein concentration of the lysates treated with DTT (Figure 4.1C). Both with and without DTT, the same polyclonal antibodies failed to reveal significant cross-reactivity with TrkA or TrkC (Figure 4.1B) whereby for reasons explained in Chapter 3, the protein load was less in the case of HEK293 cell lysates (compare Figure 4.1C with Figure 4.1D). The overall conclusion of these experiments is that the TrkB antibody used recognises TrkB much more readily than TrkC.

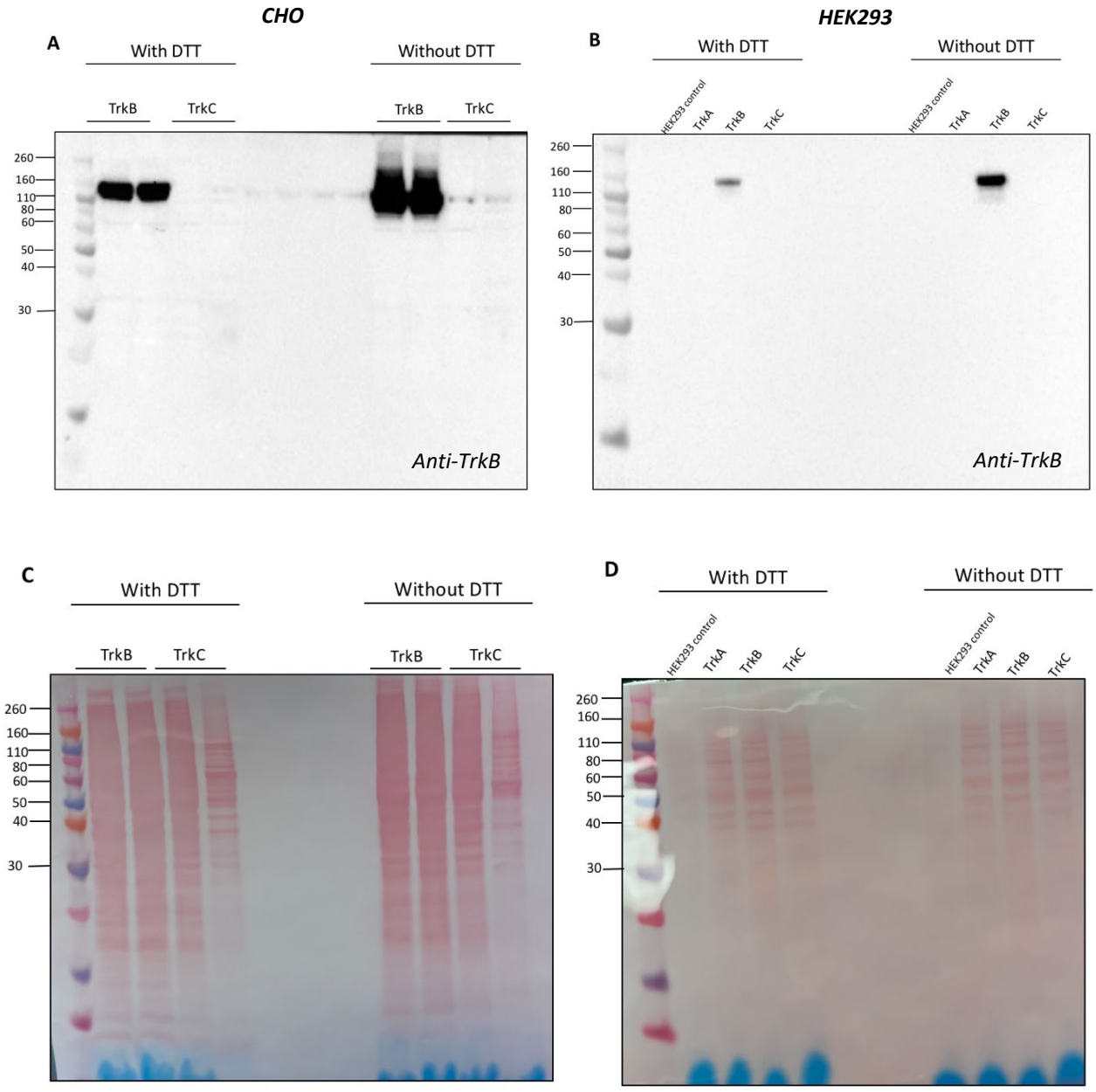

Figure 4.1. Validation of polyclonal anti-TrkB antibodies using transfected CHO and HEK293 cells.

(A). Lysates of CHO cells transfected with either TrkB or TrkC cDNAs were separated by SDS gel electrophoresis and probed with anti-TrkB polyclonal antibodies. (B). Lysates of HEK293 cells transfected with either TrkA, TrkB or TrkC or non-transfected (HEK293 control). Note the absence of signal with TrkA and TrkC. With both CHO and HEK293 cells the signal intensity for TrkB was increased in the absence of DTT treatment of the cell lysates. Also note the very slight cross reactivity in lysates of cells overexpressing TrkC when protein concentration was high (C) and lysates were not denatured with DTT (A). (C). and (D). show Ponceau stains corresponding to both blots.

4.2.2. TrkB expression in H9 neurons

H9 neuronal lysates were then analysed by Western blot and probed with anti-TrkB (Figure 4.2). As with the detection of TrkC (see Chapter 3) and as shown in the above, the absence of reduction with DTT also increased the signal strength (Figure 4.2A). The rationale for omitting DTT was the same as for the anti-TrkC, given that the antigen used for immunisation has been generated under the same conditions, presumably involving the formation of disulfide bridges in the secreted material used as the antigen. Using neuronal lysates at different time points, TrkB levels of expression seemed to increase during the course of the differentiation process (Figure 4.2B), roughly paralleling what had been observed with TrkC (see Chapter 3, Figure 3.6).

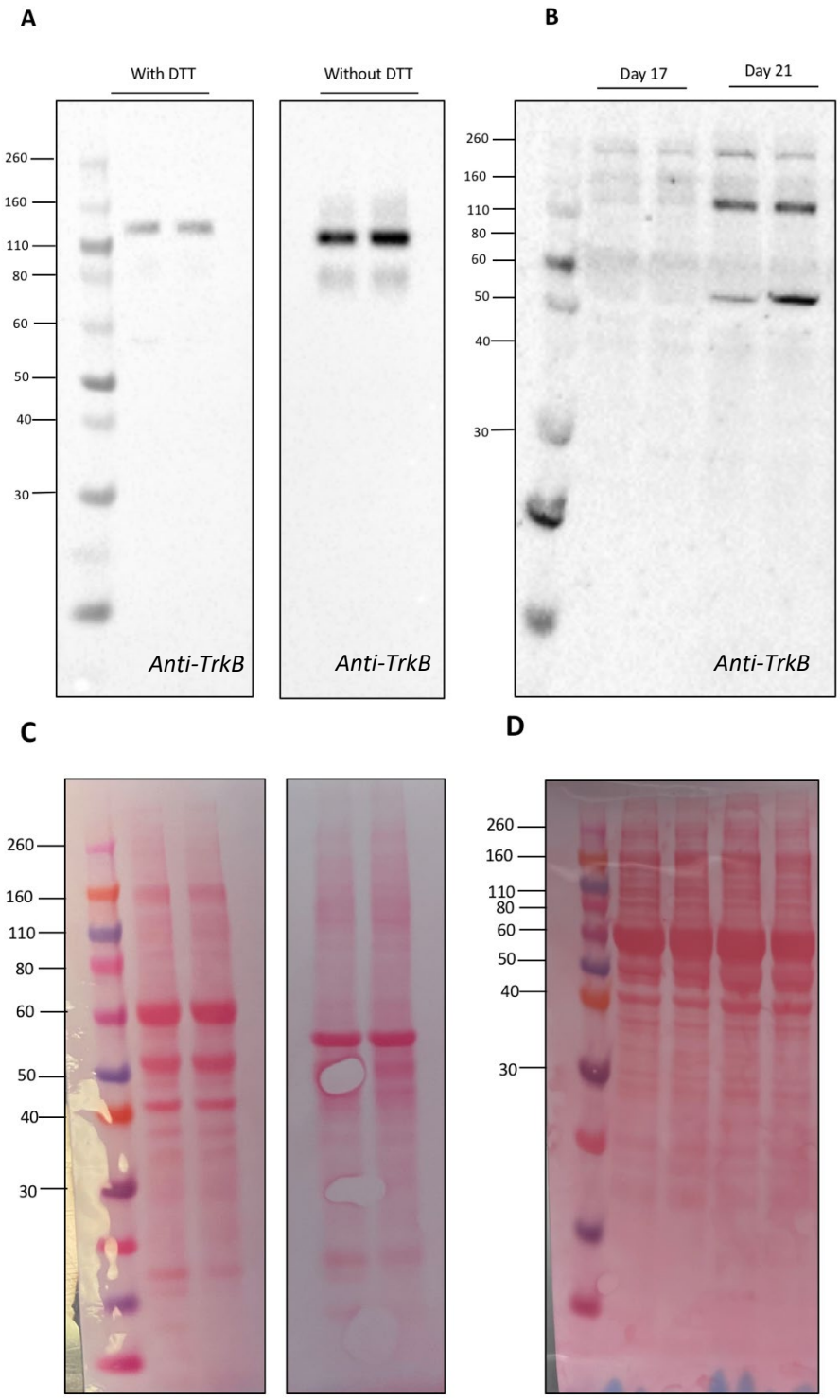

Figure 4.2. TrkB expression by H9 neurons.

H9 neurons were lysed, the lysates separated by SDS gel electrophoresis and probed with anti-TrkB. (A) Note the higher intensity signal in the absence of incubation with DTT (B). The signal intensity increases with time in culture (lysates treated with DTT). Note the presence of multiple bands, the highest molecular weight in (B) possibly corresponding to a TrkB dimer (Shen and Maruyama 2012). (C) and (D) show the Ponceau stains corresponding to both blots.

To investigate whether all neurons expressed TrkB as was found to be the case with TrkC (see Chapter 3), H9 progenitors were plated at low density on coverslips and stained with either the anti-TrkB or the mouse β-III-Tubulin (Tuj1) antibodies to determine the proportion of neurons expressing TrkB (Figure 4.3). The mean percentages ± SEM of Tuj1-positive neurons were 72.9 ± 3.1 (Figure 4.3 left panel) and 72.7± 2.6 neurons were stained with TrkB (Figure 4.3 middle panel) indicating that the all cultured neurons expressed TrkB. As explained in Chapter 3, the identity of the DAPI positive yet not Tuj1 positive cells was concluded to be due to dead cells/debris (Figure 3.7 bottom left panel). The staining was further concluded not to be a result of the secondary antibody given the lack of any signal at all in the processes when the Goat 488 secondary antibody was used without the primary antibody (Figure 4.3 right panel).

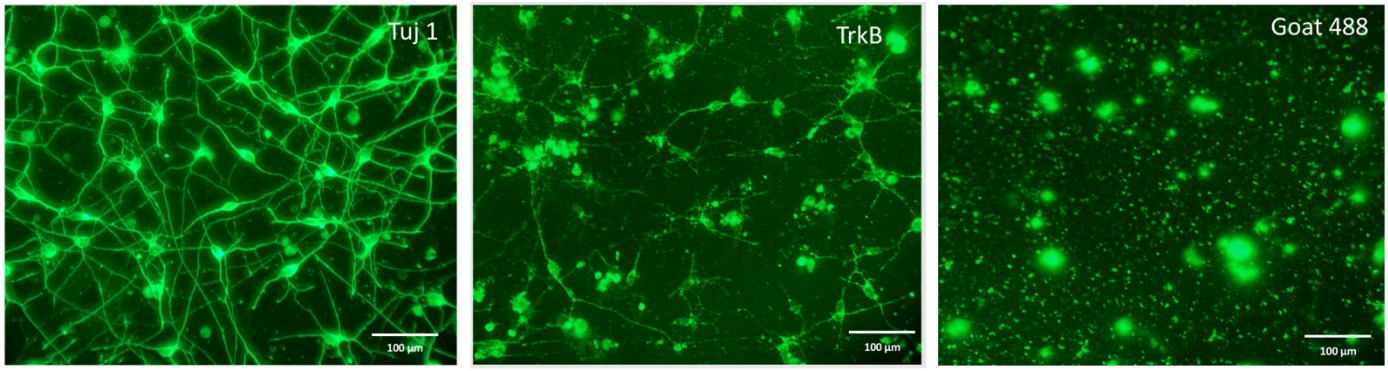

Figure 4.3. Expression of TrkB by H9 neurons: Immunofluorescence.

Neuronal progenitors were plated at low density on coverslips and stained with the anti-TrkB antibodies (middle panel) or an anti- β-III-tubulin (Tuj1) mouse polyclonal antibody (left panel). The image on the right panel was obtained by omitting incubation with the primary antibodies. The mean numbers ± SEM of Tuj1-positive neurons were 72.9 ± 3.1 (left panel) and 72.7 neurons were stained with TrkB (middle panel).

4.2.3. TrkB phosphorylation by multiple ligands

TrkB has been previously shown to be activated by 3 different ligands, namely BDNF, Neurotrophin-4 (NT4) and the TrkB-activating antibody designated ZEB85 (Merkouris et al. 2018). These results were reproduced here and extended with the unexpected observation that the TrkB antibodies used for Western blot experiments also induced TrkB phosphorylation (Figure 4.4A). This result was surprising as these antibodies are described by the manufacturer (see Material and Methods) as blocking BDNF binding to immobilized recombinant mouse TrkB.

The fact that structurally distinct ligands could all induce phosphorylation of TrkB raised the question of whether they all interacted similarly with TrkB. In the context of a collaborative project with Neil McDonald and David Briggs at the Francis Crick Institute, 2 TrkB extracellular domains were generated comprising the TrkB extracellular domain up to either Glycine_383 or Histidine_432. Using these constructs in a Western blot experiment, ZEB85 binding to TrkB could be narrowed to the sequence between Glycine_383 and Histidine_432 (Figure 4.4B). This was an unexpected result in view of the facts that functionally, BDNF and ZEB85 are indistinguishable (Merkouris et al. 2018) and that the binding sites of all neurotrophins have been mapped to the second immunoglobulin-like repeat of the Trk receptors (Banfield et al. 2001). The TrkB sequence between Glycine_383 and Histidine_432 is not part of this immunoglobulin-like domain. A representation of the binding sites of TrkB ligands BDNF, NT4 and ZEB85 is shown in Figure 4.4C.

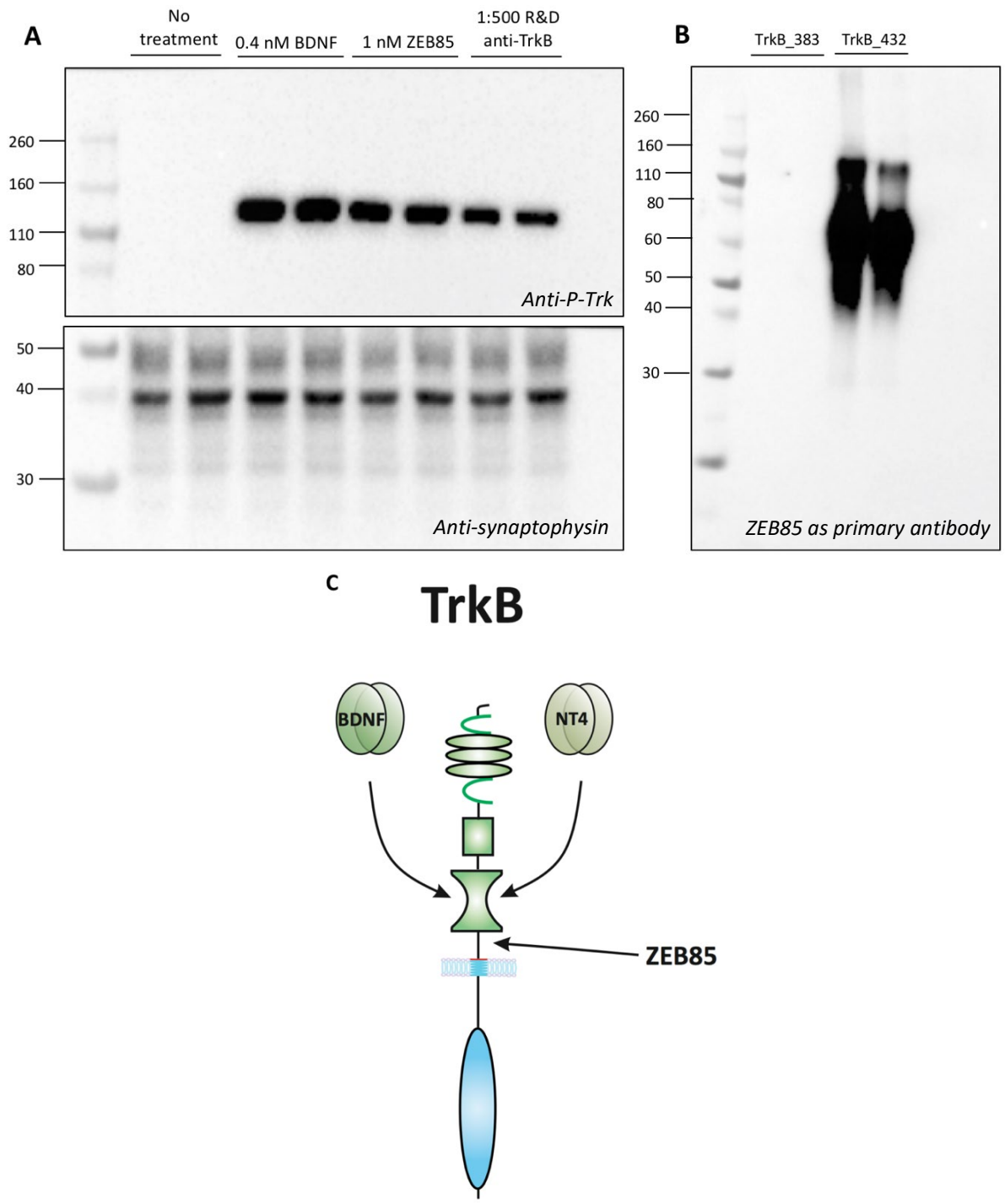

Figure 4.4. Activation of TrkB by multiple ligands.

H9 neuronal lysates were separated by SDS gel electrophoresis and probed with anti-P-Trk showing ligand-induced phosphorylation by BDNF, ZEB85 and anti-TrkB. All treatments were for 1 hour (A). (B). Western blot analysis of 2 TrkB sequences extending from the TrkB amino terminal to either Glycine 383 or Histidine 432 and probed with ZEB85 as the primary antibody. Histidine 432 is the last amino acid in TrkB ECD before the transmembrane domain (C). Illustration approximately to scale depicting the TrkB receptor and the binding sites of ligands used in this project, namely BDNF, NT4 and ZEB85. BDNF and NT4 both bind to the second immunoglobulin-like domain whereas ZEB85 does not. Scheme (C) adapted from previous images in use in the Barde Lab.

4.2.4. TrkB expression relative to TrkC expression

As comparing the endogenous levels of TrkB and TrkC proteins with antibodies would include the unsubstantiated assumption that the corresponding antibodies would bind their respective targets similarly, comparisons were made instead at the levels of gene expression. First, a detailed examination of the available RNAseq data (Merkouris et al. 2018) revealed higher levels of *NTRK2* (TrkB) expression compared with *NTRK3* (TrkC) (Figure 4.5). Second, RNA was extracted from H9 neurons and RT-qPCR performed with *NTRK2* and *NTRK3* primers optimised for similar GC contents. These results (Figure 4.6) confirmed that *NTRK2* levels are about 3-fold higher than those of *NTRK3*. As these results suggest distinctly higher levels of receptor expression of TrkB compared with TrkC, they should caution any interpretation of Trk activation by NT3 in TrkB-expressing H9 neurons. Indeed, TrkB activation is likely to mask TrkC activation, even at relatively low NT3 concentrations because of the higher levels of *NTRK2* expression compared with *NTRK3*.

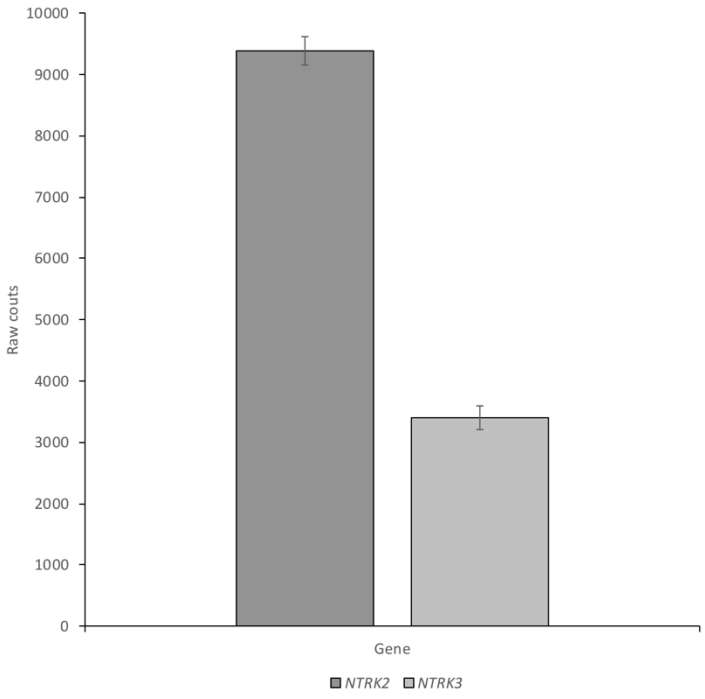

Figure 4.5. *NTRK2* and *NTRK3* raw counts from RNA extracted from H9 neurons.

Expression levels of *NTRK2* (TrkB) mRNA and *NTRK3* (TrkC) mRNA in untreated DIV 30 H9 neurons. Error bars refer to SEM and n = 12 for both genes.

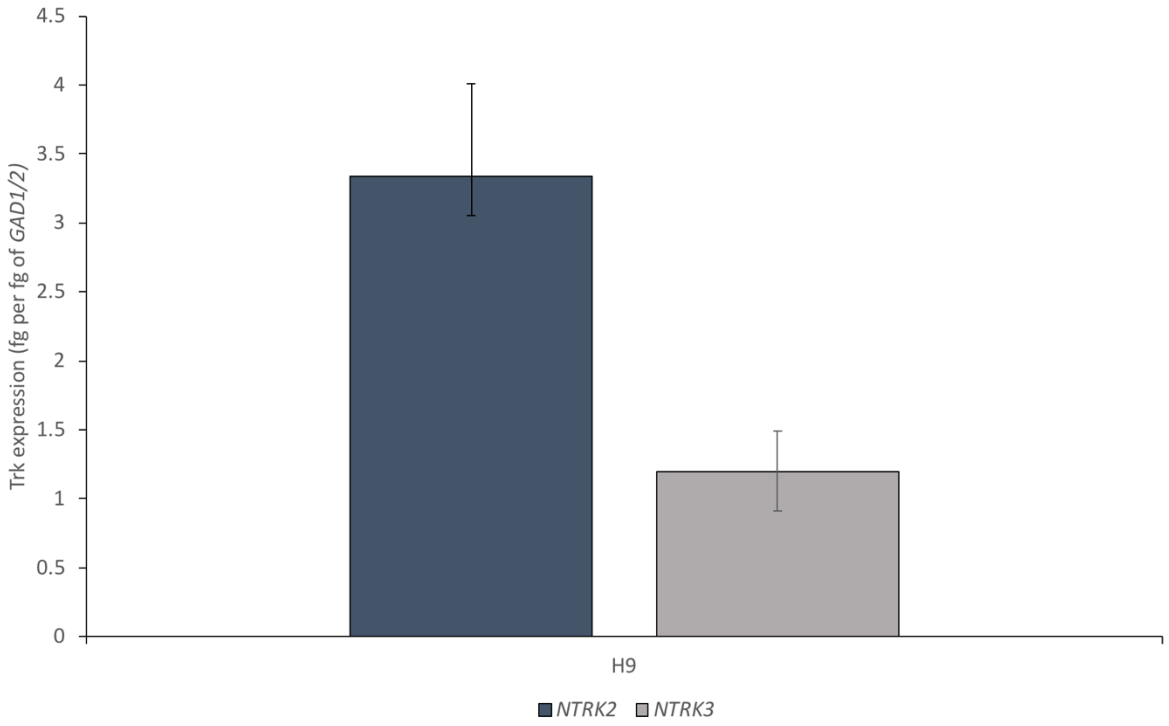

Figure 4.6. Quantification of *NTRK2* and *NTRK3* mRNAs in H9 neurons by RT-qPCR.

RT-qPCR following RNA extraction from H9 neurons shows higher expression of *NTRK2* mRNA relative to *NTRK3*. Error bars refer to SEM and n = 8 for each gene. All values were normalised to an average of *GAD1* and *GAD2* mRNA expression.

4.2.5. Modulation of TrkB signalling in human neurons by small molecules

Given the poor bioavailability of BDNF, there has been a great interest in the pursuit of small molecules reportedly activating TrkB whereby the results obtained with some of the most frequently reported compounds could not be readily replicated (see in particular Boltaev et al. 2017) More recently, a report was published (that our group was asked to comment upon, see Ateaque and Barde 2021) indicating that all drugs commonly used to treat depression, including those that are structurally unrelated, bind TrkB and potentiate its activation by BDNF in a cholesterol-dependent manner (Casarotto et al. 2021). In Figure 4.4C, a red line at the top of the TM points to a CHOL-recognition and alignment (CRAC) motif thought to bind cholesterol (Casarotto et al. 2021) and is not found in TrkA or TrkC (see short discussion). It was thus of interest to test whether some of the most commonly used antidepressants may modulate TrkB activity in cultured H9 human neurons. Accordingly, potentiation of BDNF-induced phosphorylation of TrkB by imipramine and fluoxetine was examined as well as the role of cholesterol. An initial pilot experiment did suggest that the addition of cholesterol to the culture may cause a slight potentiation of BDNF-induced TrkB phosphorylation (Figure 4.8A and B, red circles) whereby cholesterol was unable to independently induce phosphorylation of TrkB (Figure 4.8C). No changes were observed with regard to the phosphorylation status of TrkB following fluoxetine or imipramine addition, with or without BDNF (Figure 4.8B and C). To test whether these treatments may modify the levels of TrkB expression, lysates of treated cells were examined by Western blot analysis but no differences in protein levels were apparent (Figure 4.7). No activation of TrkB could be observed with any of the small molecules used and the initial observation of the potentiation of BDNF-induced TrkB phosphorylation by cholesterol could be reproduced in some, but not in other experiments. In sum, these preliminary results obtained with antidepressants and cholesterol addition remained inconclusive (see short discussion).

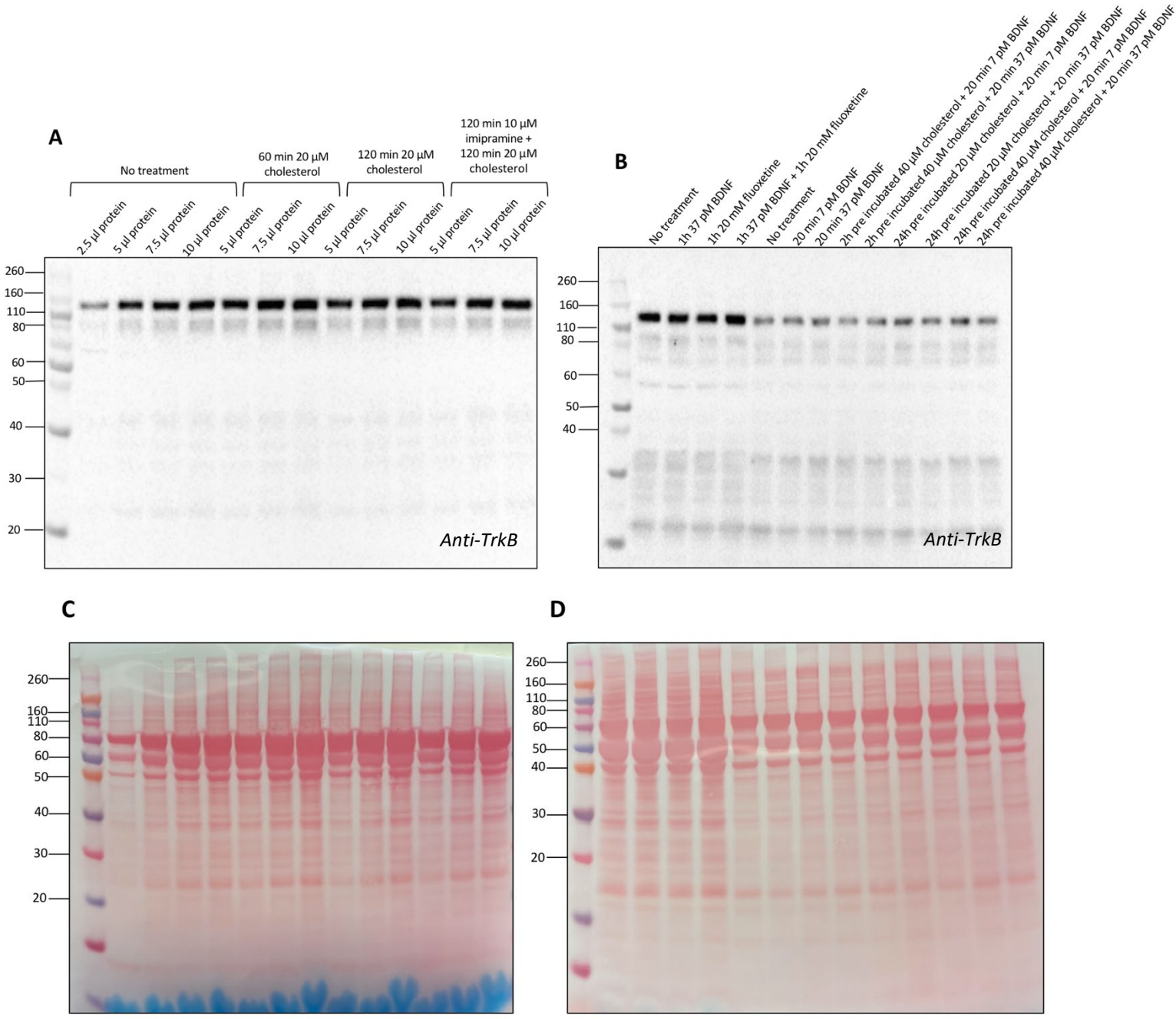

Figure 4.7. Expression of TrkB in H9 neurons treated with cholesterol and/or imipramine/fluoxetine.

Lysates of protein extracted from H9 neurons (denatured in the presence of DTT) were separated by SDS gel electrophoresis and probed with anti-TrkB. (A). TrkB expression is not affected by the addition of cholesterol nor imipramine and levels of receptor expression correlate with amounts of lysates loaded. (B). further shows that TrkB levels are not affected by cholesterol, nor by fluoxetine. (C). and (D). show Ponceau stains corresponding to both blots.

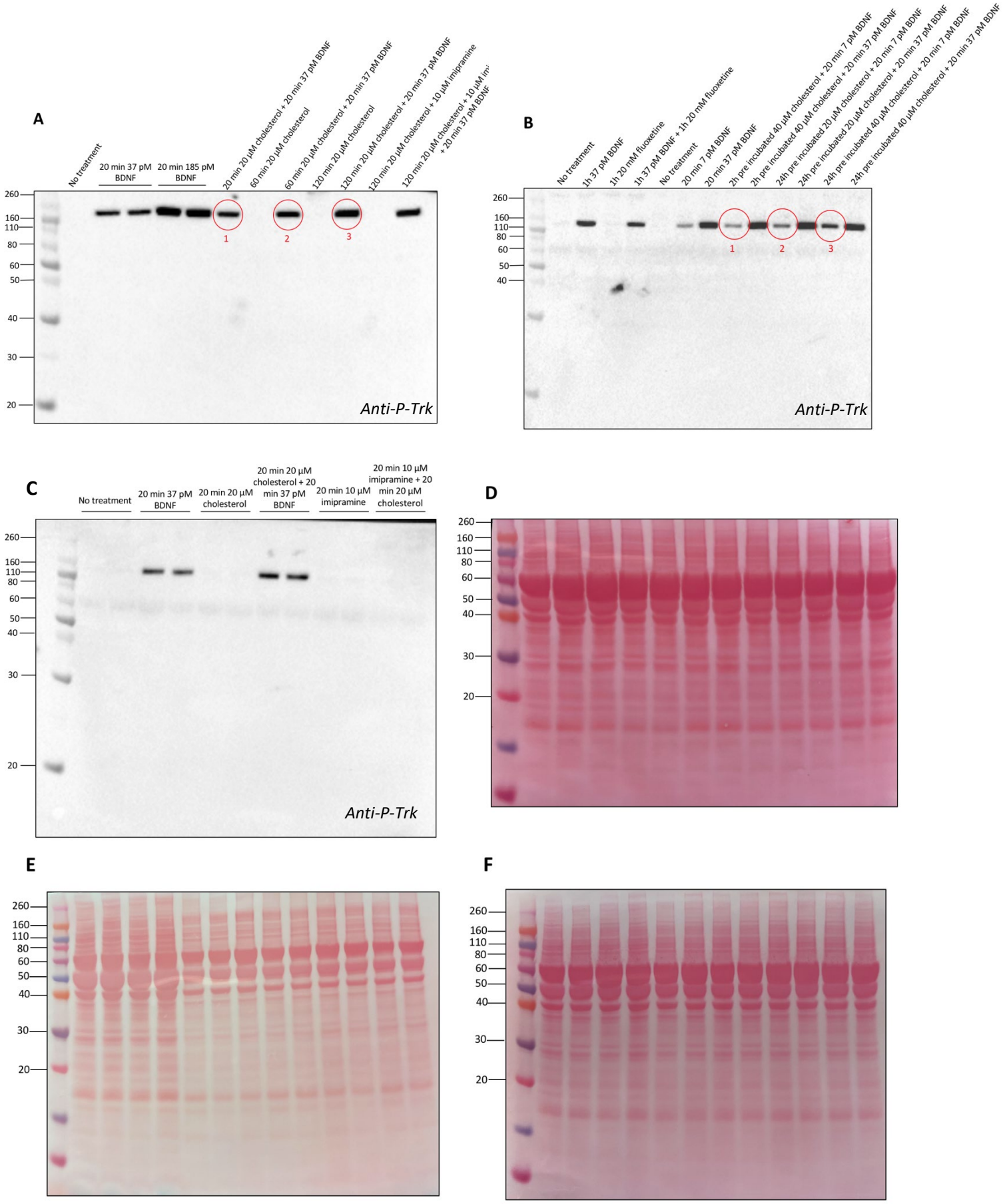
A
No treatment
20 min 37 pM BDNF
20 min 185 pM BDNF
20 min 20 µM cholesterol + 20 min 37 pM BDNF
60 min 20 µM cholesterol
60 min 20 µM cholesterol + 20 min 37 pM BDNF
120 min 20 µM cholesterol
120 min 20 µM cholesterol + 20 min 37 pM BDNF
120 min 20 µM cholesterol + 10 µM imipramine
120 min 20 µM cholesterol + 10 µM imi
+ 20 min 37 pM BDNF
260
160
110
80
60
50
40
30
20
1
2
3
Anti-P-Trk
B
No treatment
1h 37 pM BDNF
1h 20 mM fluoxetine
1h 37 pM BDNF + 1h 20 mM fluoxetine
No treatment
20 min 7 pM BDNF
20 min 37 pM BDNF
2h pre incubated 40 µM cholesterol + 20 min 7 pM BDNF
2h pre incubated 40 µM cholesterol + 20 min 37 pM BDNF
24h pre incubated 20 µM cholesterol + 20 min 7 pM BDNF
24h pre incubated 20 µM cholesterol + 20 min 37 pM BDNF
24h pre incubated 40 µM cholesterol + 20 min 7 pM BDNF
24h pre incubated 40 µM cholesterol + 20 min 37 pM BDNF
260
160
110
80
60
50
40
1
2
3
Anti-P-Trk
C
No treatment
20 min 37 pM BDNF
20 min 20 µM cholesterol
20 min 20 µM cholesterol + 20 min 37 pM BDNF
20 min 10 µM imipramine
20 min 10 µM imipramine + 20 min 20 µM cholesterol
260
160
110
80
60
50
40
30
20
Anti-P-Trk
D
260
160
110
80
60
50
40
30
20
E
260
160
110
80
60
50
40
30
20
F
260
160
110
80
60
50
40
30
20

Figure 4.8. Activation/potentiation of TrkB by BDNF with and without cholesterol and/or imipramine/fluoxetine.

Lysates of protein extracted from H9 neurons were separated by SDS gel electrophoresis and probed with anti-P-Trk. Red circles (A and B 1-3) indicate what appears to be a gradual, albeit modest potentiation of the P-TrkB signal with increasing concentrations of cholesterol, possibly in a time-dependent fashion whereby no potentiation of the BDNF-induced phosphorylation signal is observed by imipramine (A) or fluoxetine (B). Note that neither cholesterol, imipramine or fluoxetine independently induce phosphorylation in H9 neurons (B and C). (D), (E), and (F). show Ponceau stains corresponding to (A), (B) and (C). respectively.

4.3. Short Discussion

The co-expression of TrkB and TrkC in cultured neurons derived from hESCs is a relevant and important feature of the culture system used, given that many neurons in the human CNS co-express TrkB and TrkC (see General Discussion). Also, the observation that essentially all cultured neurons express TrkB (Figure 4.3) and TrkC (Figure 3.7) is important as it justifies mass analyses of cultured neurons, as opposed to single cell RNAseq for example. Previous results with this culture system had also established that functionally, most H9 neurons respond to BDNF addition using c-Fos staining as a quantifiable reporter (Merkouris et al. 2018).

With regard to TrkB activation, it is surprising that this receptor can be activated by a range of different ligands (Figure 4.4). Whilst BDNF and NT4 have some important features in common, and by and large seem to target the same neuronal populations *in vivo* (Liu et al. 1995), NT3 has its own receptor TrkC and unlike is the case with NT4, it is still unclear whether NT3 can activate TrkB *in vivo* (Stenqvist et al. 2005). This is important as most *in vitro* studies indicating TrkB activation by NT3 use saturating concentrations of NT3, unlikely to be reached *in vivo* (see General Discussion).

In addition to neurotrophin ligands, antibodies can also activate TrkB as demonstrated not only by Merkouris and colleagues but also in other studies (Traub et al. 2017; Merkouris et al. 2018; Han et al. 2019). Whilst these antibodies were selected for their ability to activate TrkB, such was not the case for the anti-TrkB antibody used here for Western blot experiments. A further unexpected observation was that this antibody binds to an epitope distinct from the neurotrophin binding site, namely the entire ECD of TrkB. It has been previously suggested that TrkB may exist as pre-formed dimer (Shen and Maruyama 2012) which may also be part of the reasons for a high molecular weight component seen on Western blot (Figure 4.2B). Antibodies such as ZEB85 or the anti-TrkB may thus favour a pre-existing dimer conformation by virtue of these reagents being divalent and not simply because they occupy the BDNF binding pocket. The existence of pre-existing TrkB dimers has been discussed before (Shen and Maruyama 2012) and it has been suggested that the extracellular juxtamembrane motif of TrkB itself has an inhibitory role on receptor dimer formation, and mutating it can promote TrkB dimer formation (Shen et al. 2019). These structural considerations may have important implications. In particular, they may play a role in the potentiating effects of cholesterol and antidepressants on TrkB activation by BDNF. A tyrosine residue uniquely found in the transmembrane domain of TrkB, and not in TrkA or TrkC, was shown to be involved in cholesterol binding (Casarotto et al. 2021). The failure to replicate these findings here with

cultured human neurons, with a read-out targeting the activated domain of the TrkB kinase do not challenge the conclusions reached by (Casarotto et al. 2021). The delivery of cholesterol to cultured cells and its incorporation into cell membranes is a complex issue and would need to be investigated in detail with regard to the mode of delivery as well as the timing of such experiments. Here, cholesterol was simply added to the cell culture medium and given time constraints there was no simple way to ascertain whether cholesterol reached the cell membrane. Astrocytes are thought to be the major source of cholesterol for neurons as the latter have only a limited ability to synthesise cholesterol (for review, see Pfrieger and Ungerer 2011). A limitation of the culture system used here is that it is relatively devoid of non-neuronal cells including astrocytes as such cells tend to interfere with the growth of neurons as monolayers. There was no simple way to assess whether the added cholesterol was inserted at all into the plasma membrane of the cultured neurons, which may require additional steps including internalisation and reexport from lysosomes (Meng et al. 2020). If this is to be re-investigated, methods of controlling cholesterol delivery to the plasma membrane would have to be considered (Zidovetzki and Levitan 2007).

The main conclusion of this Chapter is that H9 neurons express both TrkB and TrkC at the protein level. The mRNA data indicate that the levels of *NTRK2* are significantly higher than those of *NTRK3*, suggesting that the levels of TrkB receptors may be markedly higher than those of TrkC. These results indicate that meaningful TrkC-mediated signalling by NT3 cannot be studied using such cells given the ability of NT3 to also activate TrkB (see Chapter 3) and that further investigations into the activation of TrkC by NT3 in this culture system would require the elimination of ligand-activatable TrkB. Experiments summarising these attempts are described in the next Chapter (Chapter 5).

Chapter 5 - Generation of cells lacking ligand-activatable forms of TrkB

5.1. Short introduction

The results presented in the previous Chapters not only confirm the notion that TrkB can be readily activated by NT3 (see Chapter 3) but also that H9 neurons express the *NTRK2* (TrkB) gene at higher levels than is the case for *NTRK3* (TrkC) (see Chapter 4). It would then seem unlikely that in H9 neurons, TrkC-mediated signalling by NT3 could be studied in isolation, without a contribution of TrkB activation that would be difficult to quantify. In addition, the tools available to study the activation of the kinase domain of Trk receptors cannot distinguish between TrkB and TrkC as the residues flanking the pair of critical phosphorylated tyrosine residues are identical: YSTD**YY**RVGG. The next step was then to eliminate ligand-activatable TrkB by gene targeting. To this end, the CRISPR-Cas9-based system (for review, see Doudna and Charpentier 2014) was used and guide RNAs designed to target the signal sequence of TrkB with the goal of preventing the activation of TrkB by extracellular ligands.

5.2. Results

5.2.1. *NTRK2* targeting of H9 hESCs using CRISPR-Cas9

The tracrRNA (trans-activating CRISPR RNA) making up the crRNA complex along with the guide RNA (gRNA, see Figure 5.1 for definitions and explanations) was labelled with a fluorescent marker thus enabling Fluorescence-Activated Cell Sorting (FACS) of CRISPR-targeted clones that had incorporated the tracrRNA. A simple summary of the process used to target the TrkB gene *NTRK2* is illustrated in Figure 5.1.

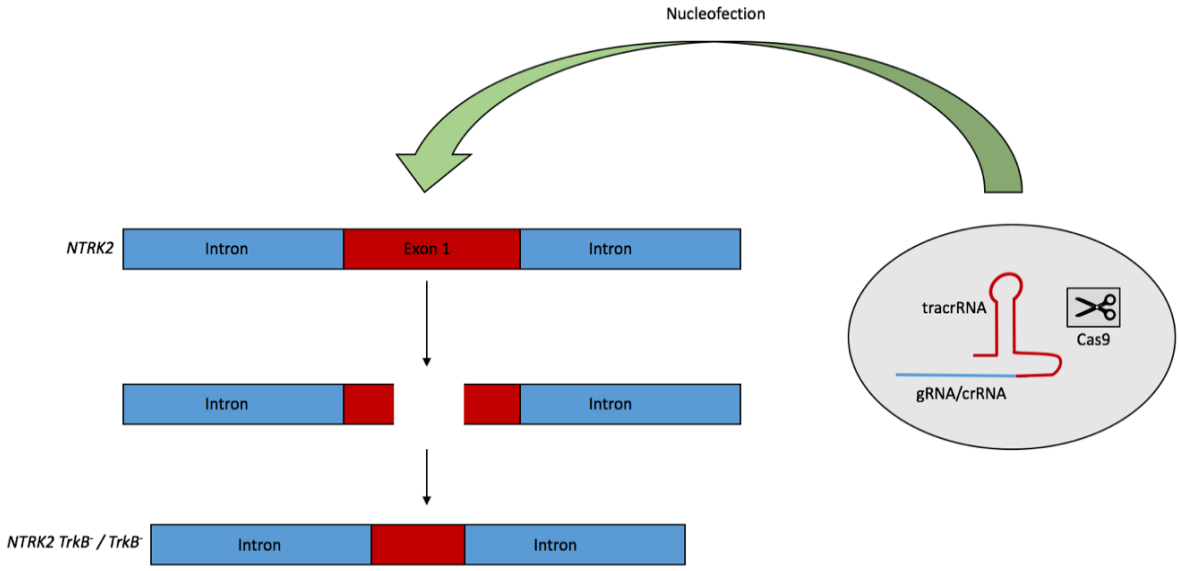

Figure 5.1. Overview of the CRISPR-Cas9 procedure.

Scheme depicting the mature crRNA complex consisting of the gRNA (recognises the target genomic region of interest) and tracrRNA (base pairs with the gRNA to form mature crRNA which is then able to bind to specific genomic sequences of *NTRK2* and guides Cas9 to the cleavage site). This complex (within the grey oval) was introduced into the nuclei of cells along with the Cas9 protein via nucleofection. This process involves a brief voltage pulse altering the membrane properties of the cells, thus allowing the mature crRNA and Cas9 protein to enter the cell. The Cas9 protein contains a nuclear localisation signal (NLS) to ensure efficient targeting of the nuclei of cells.

The gRNAs were designed complementary to a portion of exon 5 of the *NTRK2* gene. As exon 5 of *NTRK2* is known to encode the signal sequence and part of the extracellular domain of TrkB, the deletion was predicted to prevent translation of the ligand-binding domain of the receptor. Importantly, each gRNA contained a protospacer adjacent motif (PAM) allowing exogenous DNA to be distinguished from endogenous DNA and sequence-specific Cas9 cleavage to occur. As shown in Figure 5.2A, the initiation codon of *NTRK2* was targeted and three guide RNAs designed to maximise the chances of a deletion – one was designed to the sense strand and two on the antisense strand (Figure 5.2B). A successful targeting event was predicted to generate amplification products smaller by 47 bp, 104 bp or 151 bp compared with untargeted *NTRK2* (Figure 5.2B). Particularly for the larger deletions, the size differences were readily detectable by gel electrophoresis (Figure 5.4) as the primers (outlined in purple in Figure 5.2A) were designed to flank the CRISPR-targeted region of *NTRK2*.

A

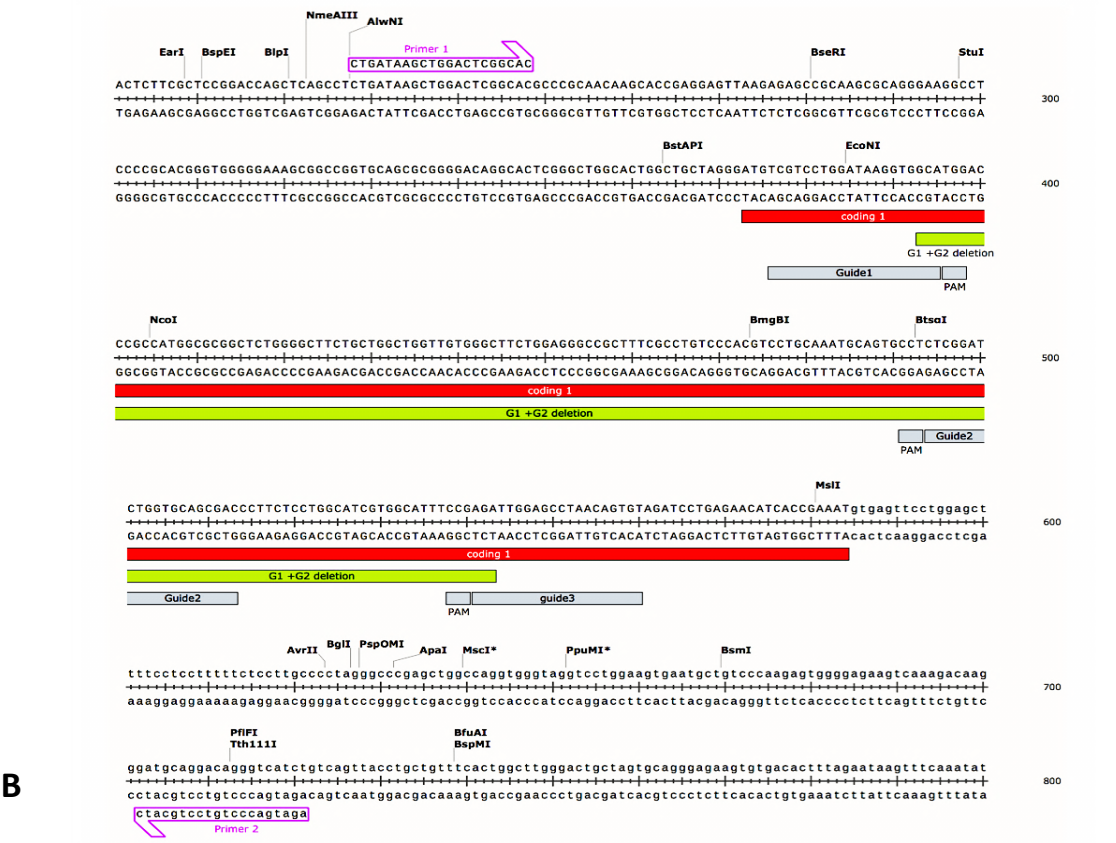

B

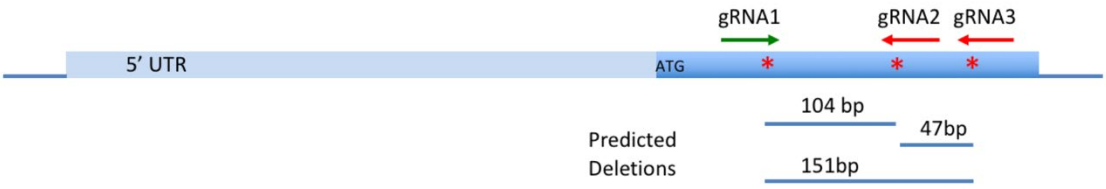

ATG**TCGTCCTGGATAAGGTG*GCATGG**ACCCGCCATGGCGCGGCTCTGGGGCTTCTGCTGGCTGGTTGTGGGCTT

CTGGAGGGCCGCTTTCGCCTGTCCCACGTCCTGCAAATGCAGTG**CCTCTC*GGATCTGGTGCAGCGAC**CCTTCTC

CTGGCATCGTGGCATTT**CCGAGA*TTGGAGCCTAACAGTGT**AGATCCTGAGAACATCACCGAAAT

Figure 5.2. Design of guide RNAs and predicted deletions.

(A). The portion of exon 5 of *NTRK2* targeted (file assembled in SnapGene) as well as primer sequences used in the genotyping to differentiate targeted cells from non-targeted cells. The 3 gRNAs are indicated as well as the portion of *NTRK2* to be deleted. A summary of the CRISPR process is also shown and the possible base pair deletions in (B). The sense strand gRNA sequence is highlighted in green and guide RNA sequences on the antisense strand are highlighted in red. PAM sites are underlined and predicted Cas9 cleavage sites are indicated *. On the coding sequence of *NTRK2* exon 1, the sense strand guide RNA sequence is highlighted in green and guide RNA sequences on the antisense strand are highlighted in red. PAM sites are underlined and predicted Cas9 cleavage sites are indicated *.

Following nucleofection, the cells were plated and cultured overnight before FACS analysis the following day. The success of the FACS procedure was ensured by the detection of highly fluorescent cells in the nucleofected clones (Figure 5.3A), compared to a lack of fluorescence in the non-nucleofected controls (Figure 5.3B). This meant that cells in the nucleofected sample had likely incorporated the fluorescent tracrRNA i.e the crRNA. The top 3% of fluorescing cells were collected (9,500 cells), plated onto a 10 cm dish and cultured until colonies (derived from a single cell) could be manually picked for genotyping. It was important that colonies were plated at low density to prevent them growing into each other and forming heterogeneous clones representing a mixture of targeted and non-targeted cells. Nonetheless, this turned out to be the case for clone E10 (see Figure 5.4).

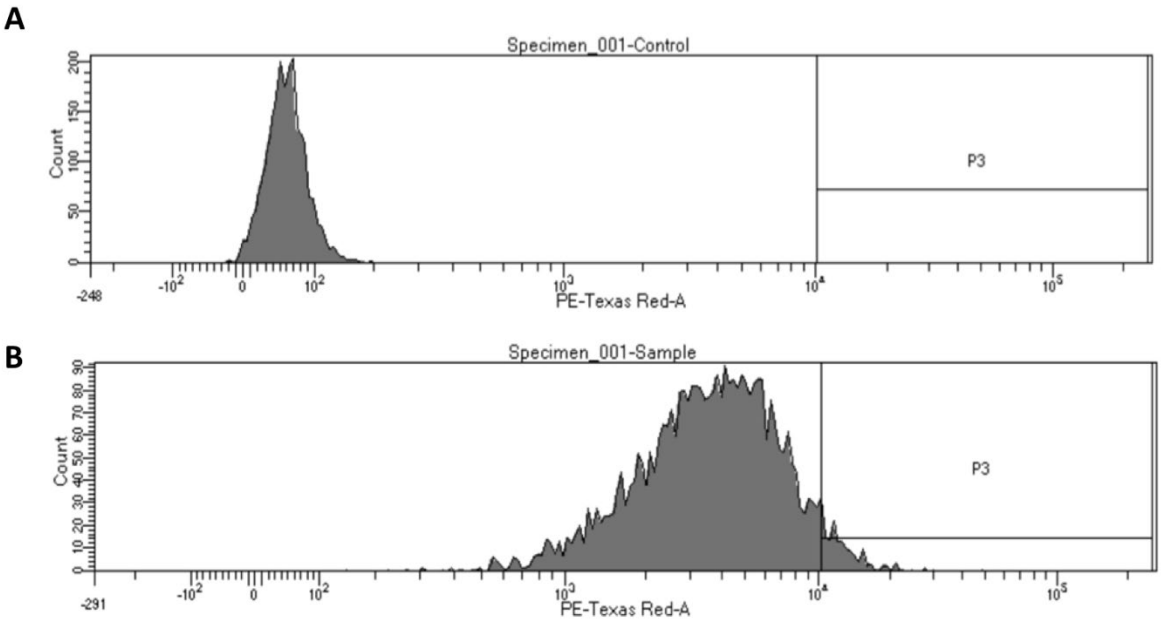

Figure 5.3. Separation of control and transfected cells by fluorescence intensity.

Nucleofected cells were FACS sorted and fluorescence levels of nucleofected cells relative to cell count are shown. (A) indicates non-transfected controls i.e. cells not fluorescing. (B). indicates nucleofected cells showing fluorescence. The P3 section indicates the cells selected for plating. Note that in the nucleofected sample, most cells were fluorescing (B) indicating they had likely incorporated the fluorescent tracrRNA.

5.2.2. Identification of CRISPR/Cas9-targeted clones

Primers were first tested and the PCR protocol optimised using DNA extracted from wild-type H9 hESCs to ensure that a clear single banded product corresponding to *NTRK2* could be observed. Once the colonies had reached a sufficient size, they were manually picked and plated into a 96-well plate for genotyping. Targeted cells were predicted to generate a smaller *NTRK2* fragment caused by the Cas9 endonuclease deletion. After the first round of genotyping, it became apparent that some colonies may have had only one of two alleles targeted, i.e. they were heterozygotes. It was also apparent that due to the differing intensities of the amplified DNA fragments, some clones were likely to consist of a mixture of targeted and untargeted cells (Figure 5.4, E10 clone, left panel circled in red), presumably due to the fact that colonies grew into each other. Subsequently, clone E10 was re-plated as single cells at a very low density and allowed to grow into colonies now with each colony derived from a single cell. Clones were re-genotyped (Figure 5.4 right panel) resulting in multiple clones producing a lighter fragment than the heavier wild-type *NTRK2* fragment. This suggested that E10 did contain a mixture of targeted and non-targeted cells, with the difference in base pairs being around 150 bp, as predicted by the gRNA design. As a result, the clones thought to be *NTRK2* targeted that were selected for validation were A10, B1 and D2. Suspected non-targeted clone C9 was also selected as a control that was subjected to the CRISPR-Cas9 process yet did not appear to contain the deletion (clones selected shown in Figure 5.4 circled in red).

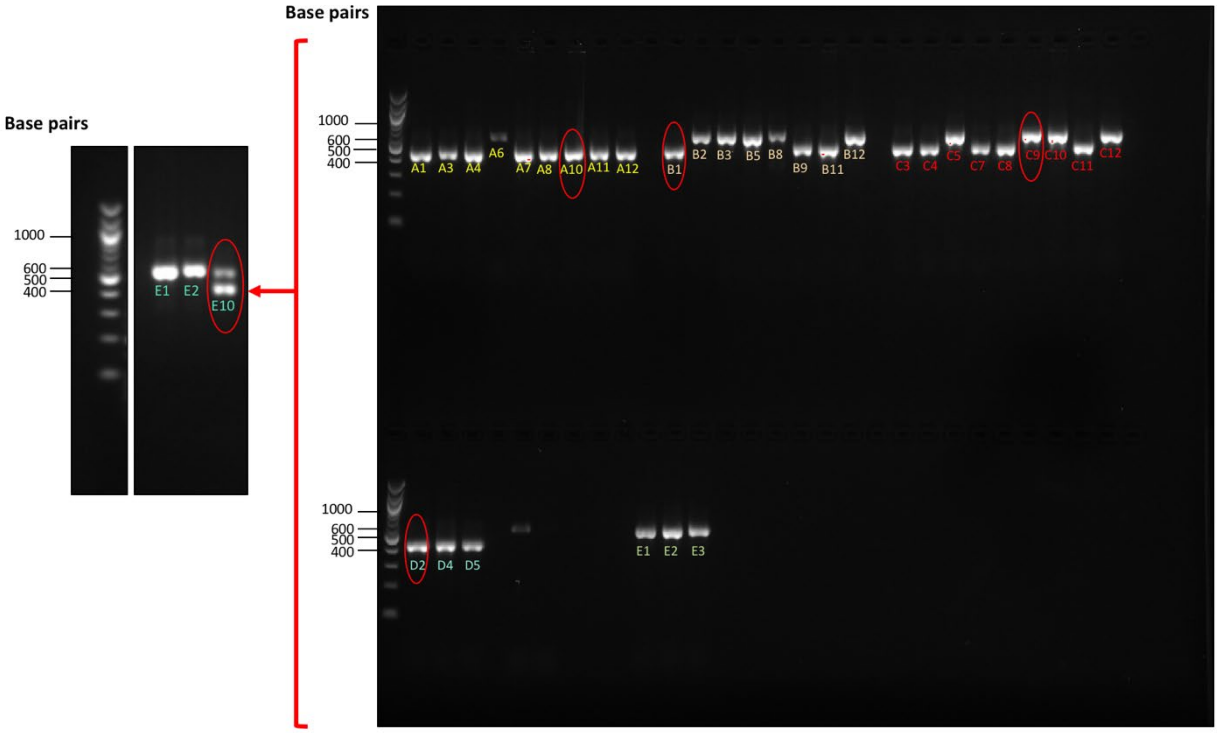

Figure 5.4. Genomic DNA size analysis of selected cells.

DNA was extracted from clones derived from a single cell and subjected to PCR amplification and gel electrophoresis. E10 (left panel, red circle) was hypothesised to be a clone consisting of both targeted and non-targeted cells and this was confirmed by re-plating and re-genotyping of E10 (right panel). Heavier fragments were likely cells that were not targeted by the CRISPR-Cas9 procedure and had therefore retained the full exon 1 sequence. Smaller fragments were hypothesised to contain the exon 1 deletion. Clones circled in red were selected for DNA sequencing.

To confirm that exon 5 sequences encoding the initiation codon of *NTRK2* had been deleted, DNA was extracted from A10, B1, D2, C9 and wild-type H9 and DNA sequencing was performed. C9 was found to be identical to wild-type H9 (sequencing results shown in Figure 5.5) confirming no off-target CRISPR effects on the primer flanking portion of exon 1 of the C9 *NTRK2* gene. This meant that C9 should technically still contain a ligand-activatable form of TrkB, despite going through the targeting process. This clone was then exploited as a relevant control to explore whether the process of nucleofection and FACs had permanently damaged the cells or caused them stress that may have prevented them differentiating as efficiently and homogenously as wild-type cells.

```
6781 gttgggggtc ctacgctcag tcttacgcgt gtctgtttgt cctcagcctc gaggtgcata
6841 ccggaccccc attcgcatct aacaaggaat ctgcgcccca gagagtcccg ggagcgccgc
6901 cggtcggtgc ccggcgcgcc gggccatgca gcgacggccg ccgcggagct ccgagcagcg
6961 gtagcgcccc cctgtaaagc ggttcgctat gccggggcca ctgtgaaccc tgccgcctgc
7021 cggaacactc ttcgctccgg accagctcag cctctgataa gctggactcg gcacgcccgc
7081 aacaagcacc gaggagttaa gagagccgca agcgcaggga aggcctcccc gcacgggtgg
7141 gggaaagcgg ccggtgcagc gcggggacag gcactcgggc tggcactggc tgctagggat
7201 gtcgtcctgg ataaggtggc atggacccgc catggcgcgg ctctggggct tctgctggct
7261 ggttgtgggc ttctggaggg ccgctttcgc ctgtcccacg tcctgcaaat gcagtgcctc
7321 tcggatctgg tgcagcgacc cttctcctgg catcgtggca tttccgagat tggagcctaa
7381 cagtgtagat cctgagaaca tcaccgaaat gtgagttcct ggagcttttc ctccttttc
7441 tccttgcccc tagggcccga gctggccagg tgggtaggtc ctggaagtga atgctgtccc
7501 aagagtgggg agaagtcaaa gacaagggat gcaggacagg gtcatctgtc agttacctgc
7561 tgtttcactg gcttgggact gctagtgcag ggagaagtgt gacactttag aataagtttc
7621 aaatatagat atacatatgc cgattatata tttattcctc gtgggaagga actcactatg
7681 ctttttatat ttcaaagctc tgctgggtgt gctttaggct ttcagtatgc actaacttag
7741 ttttgggcat ttttgtttca taaagtgctg tgtgtatgtt gtgttagaag ttccattaat
7801 attcactaga aaagaggtta aaataattaa ctttcccaaa tctgttgagg gaagtgacag
7861 tctctccctt aacatctttt ttgagattta agttaaccaa tttccctttt cattttatat
```

Figure 5.5. DNA sequence of the wild-type H9 clone at the *NTRK2* exon 1 locus.

DNA sequencing results from hESC H9 wild-type clone. Black bold indicates the last bases of the actual sequence results, red italics indicate the primers used for genotyping of clones, green bold indicates the protein coding exon 1 and green underlined indicates the deleted sequence in A10 and D2 knock out cells as predicted by the gRNAs (Figure 5.2B). This would bring into frame a downstream stop codon which would result in a truncated protein.

Using the DNA sequencing results from clones H9, C9, B1, A10 and D2, the predicted amino acid sequences were translated (Figure 5.6A) following an alignment using CRISPR-ID. The TrkB amino acid sequences of C9 and H9 were found to be identical. Indeed, B1 showed a different translated sequence for allele 2 when analysed by CRISPR-ID and A10 and D2 were also concluded to be differentially targeted due to the amino acid differences after the stop codon (Figure 5.6A). An alignment of the DNA sequences of B1 and A10 also revealed several single nucleotide differences (Figure 5.6B), leading to the conclusion that B1 possessed a different deletion of the TrkB ECD to A10 and D2.

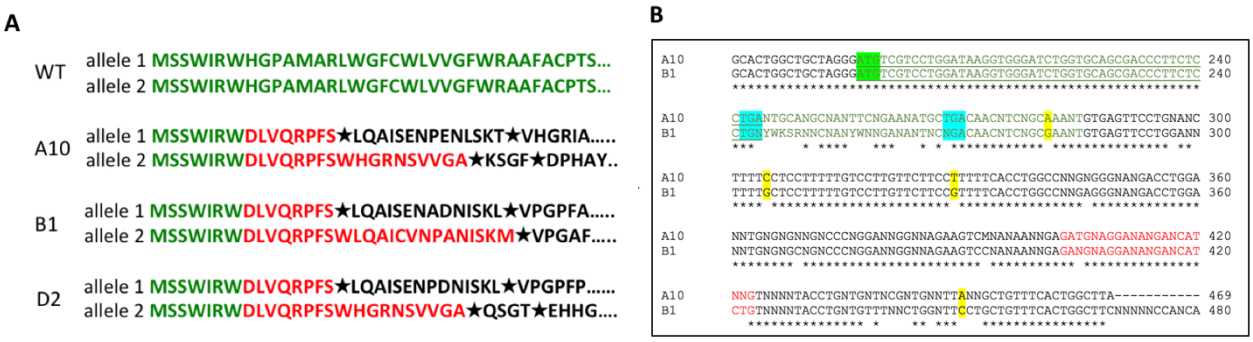

Figure 5.6. Predicted protein sequences of targeted clones.

Predicted N-terminal sequence of TrkB based on the nucleotide sequences determined for clones that remained untargeted (wild-type) and for each allele of the knockout clones A10, B1 and D2 analysed with CRISPR-ID (A). Green sequence shows identity to TrkB. Frameshift-associated translated sequence is shown in red. ★ indicates in-frame stop codons and downstream untranslated sequences are in black. Most subsequent experiments were performed with a clone designated A10 but the deletion of TrkB and the activatability of TrkC by low concentrations of NT3 was also verified with differentially targeted clone B1 (B) and an alignment with A10 shows SNPs indicated in yellow highlight. Green indicates exon 1 and green underlined indicates translated sequence from ATG (green highlight) until one of the TGA stop codons (blue highlight) is brought into frame by the deletion (in the case of A10 the sequencing results are unambiguous, meaning that the first TGA codon would terminate translation). Red indicates reverse primer.

5.3. Short discussion

The main conclusion of this Chapter is that H9 hESCs could be selectively targeted and clones isolated carrying a deletion in exon 5 of the *NTRK2* gene preventing the initiation of the translation of TrkB. The DNA sequences of these clones, A10, D2 and B1 revealed that they were differentially targeted (Figure 5.6). All could be successfully expanded in an undifferentiated state with a similar efficiency to H9 hESCs and their ability to generate neurons was indistinguishable from the H9 and the C9 clones (see Chapter 6), the latter having also been subjected to nucleofection and the sorting procedure. Whilst these results do not rule out off-target effects of the CRISPR procedure, they suggest that the key characteristics of the targeted clones have been preserved. In addition, cells carrying significant chromosomal abnormalities may have been selected against during sub-cloning and would have not differentiated into neurons (see Chapter 6). Indeed, the process of hESC sub-cloning selects for the most rapidly dividing cells, corresponding to the cells that have remained pluripotent (see Yazdani et al. 2012 for discussion). Most importantly, the RNAseq analysis detailed in Chapter 8 indicates that around 95% of the over 14,000 genes analysed are expressed at similar levels in H9 and A10 neurons (see Chapter 8, Figure 8.4).

The demonstration that this strategy led to the elimination of ligand-activatable forms of TrkB is the object of the following Chapter.

Chapter 6 - Characterising neurons lacking ligand-activatable forms of TrkB

6.1. Short introduction

The experiments detailed in the previous chapter led to the generation and isolation of targeted clones A10 and B1. These clones were selected for differentiation and subsequent validation at the protein level. Clone D2 was also differentiated and analysed whereby only the results obtained with A10 are illustrated in this chapter, in addition to the results obtained with differentially targeted clone B1. The first step was to successfully generate neurons from hESCs from all clones, including C9 as a control for the entire procedure (see Chapter 5). The behaviour and differentiation of the targeted clones was monitored in detail and compared at every step with wild-type H9 hESCs, progenitors and neurons. This was especially important given that TrkC, expected to be expressed in the absence of ligand-activatable forms of TrkB, can cause the death of cells and neurons in the absence of TrkC activation by NT3, both *in vitro* and *in vivo* (Tauszig-Delamasure et al. 2007; Nikoletopoulou et al. 2010; Menard et al. 2018). This Chapter also explores in detail whether ligand-activatable forms of TrkB are expressed in targeted clones in which sequencing data indicates that exon 5 of *NTRK2* has been successfully targeted in both alleles.

6.2. Results

6.2.1. Generation of neuronal progenitors and neurons from hESC clones targeted at the *NTRK2* locus

FACS isolated clones were passaged until the morphology and rate of cell division typical of H9 hESCs was achieved (see Chapter 3). Once their phase contrast appearance and rate of cell division was found to be similar to wild-type hESCs (Figure 6.2A-C), they were assessed for their ability to generate progenitors. To this end, progenitors were quantified at day 16 of every differentiation and the number found to be indistinguishable between A10 and H9 clones, regardless of whether progenitors had been stored frozen and thawed or directly taken through the differentiation procedure (Figure 6.1). These results suggest that neither the CRISPR-Cas9 procedure nor the targeting of *NTRK2* (TrkB) significantly affected the processes leading to the generation of neuronal progenitors from hESCs.

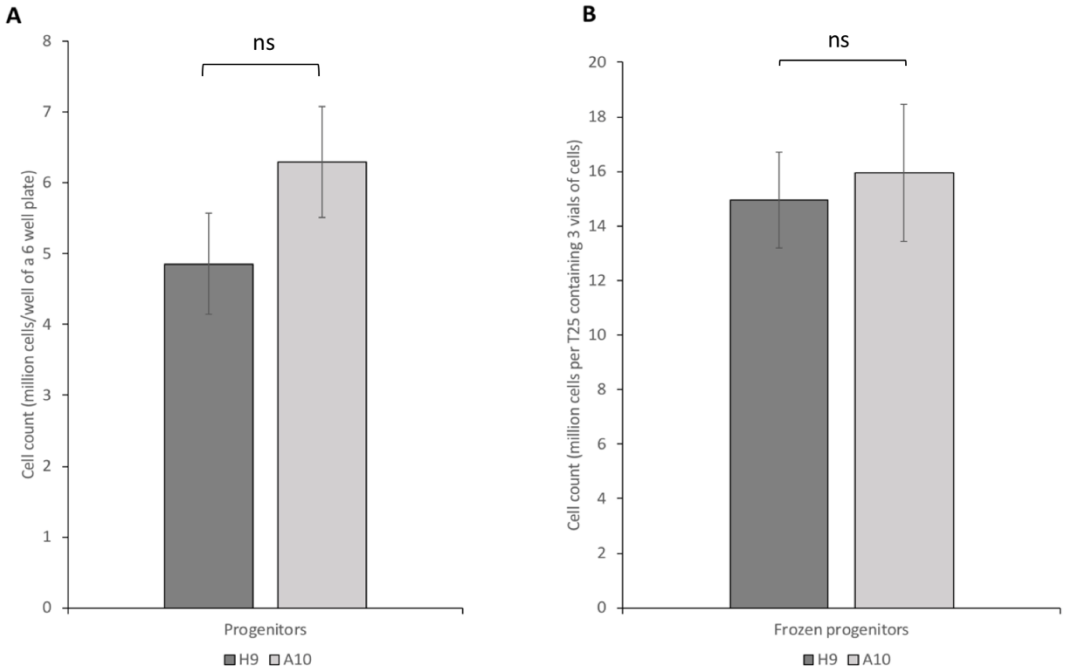

Figure 6.1. Counts of progenitors generated from TrkB-targeted hESC clones.

Quantification of the number of progenitors on day 16 of the differentiation procedure revealed no significant differences between targeted clone A10 and wild-type H9 whether cells were differentiated from hESCs (A) or thawed from 3 pooled vials of frozen progenitors (B). The error bars refer to SEM and significance indicated with asterisks: ***$p < 0.001$, *$p < 0.01$ and ns = $p > 0.05$. For both H9 progenitors and frozen progenitors n = 7, for A10 progenitors n = 6 and frozen progenitors n = 7.

Targeted and untargeted hESC clones (C9, B1 and A10) were then subjected to the exact same differentiation protocol as for wild-type H9 (see Chapter 3). Using this procedure, no apparent abnormal cellular morphology was observed that could be attributed to cells that were targeted, untargeted or wild-type (Figure 6.2). All neurons were also able to be maintained in culture for as long as wild-type neurons, i.e. around 60 days.

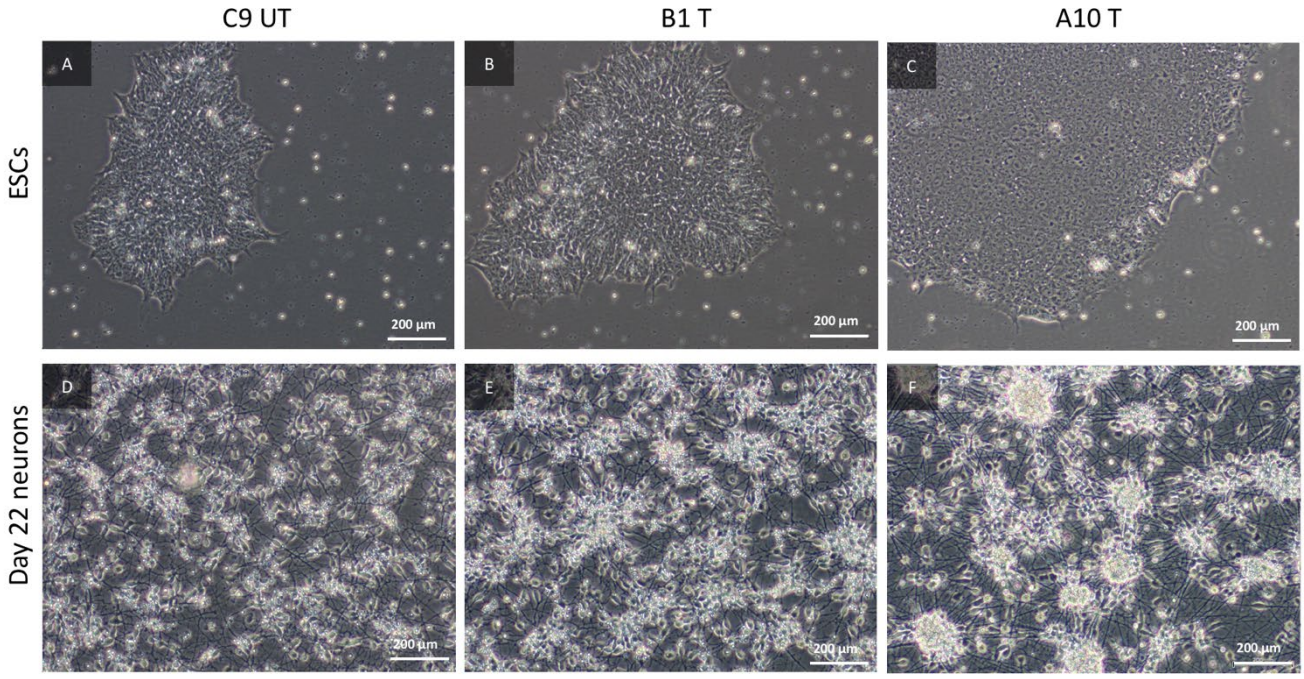

Figure 6.2. Generation of neurons from targeted hESC clones.

Phase contrast images of C9, B1 and A10 undifferentiated hESCs (A-C respectively) and DIV 22 C9, B1 and A10 neurons (D-F respectively). All clones whether targeted (B1, A10) or untargeted (C9) could be maintained in an undifferentiated hESC state and then successfully differentiated into neurons. No morphological differences could be observed between wild-type (H9), untargeted (C9) and targeted (A10, B1) clones at any stage of the differentiation procedure.

To explore whether the addition of NT3 may play a role in the survival of neurons generated from *NTRK2* targeted hESCs, A10 progenitors were plated onto a 12-well plate and all wells supplemented with 2 nM NT3. The following day, NT3 was removed and only half of the wells were re-supplemented with NT3 every other day over the course of 10 days. If TrkC would function as a "dependence receptor" in this experimental setting, then the cultures deprived of NT3 would be expected to exhibit more cell death. However, no clear changes in cell density were observed between A10 cultures supplemented with NT3 and those deprived of it, indicating that TrkC did not function as a dependence receptor in this context or else that the expression levels of TrkC in these neurons are too low to cause cell death.

6.2.2. Validation of *NTRK2* targeted neurons at the mRNA and protein levels

TrkB and TrkC protein levels were then explored in neurons derived from wild-type H9, untargeted C9 and targeted A10 and B1 hESCs. To this end, protein was extracted and analysed by Western bot. The membranes were probed after transfer with the anti-TrkB and anti-TrkC antibodies validated in Chapters 3 and 4. As the results presented in these previous chapters indicated that the TrkC and TrkB antibodies give a stronger signal in the absence of DTT treatment of the cell lysates, DTT was omitted prior to electrophoresis, unless otherwise indicated. Under these conditions and compared with H9 neurons, a faint signal was detected in A10 cell lysates (Figure 6.3A), possibly due to the weak cross reactivity of anti-TrkB with TrkC in the absence of DTT or of a minor TrkB isoform encoded using an alternative initiation codon (see Chapter 8). Crucially, TrkC was detected at comparable levels in A10 neurons relative to H9 at the protein level (Figure 6.3B). Using quantitative RT-PCR, *NTRK3* (TrkC) mRNA levels were also found to be comparable across all clones tested, whether targeted, untargeted or wild-type (Figure 6.3C).

Further analyses with TrkC antibodies revealed that TrkC receptor levels were similar in B1 and C9 neuronal lysates (Figure 6.3E). Additionally, it was confirmed that despite the fact that B1 and A10 had been differentially targeted (see Chapter 5), they both lacked clearly detectable levels of TrkB protein (Figure 6.3D), yet both expressed similar levels of TrkC, comparable to those observed in H9 and C9 neuronal lysates.

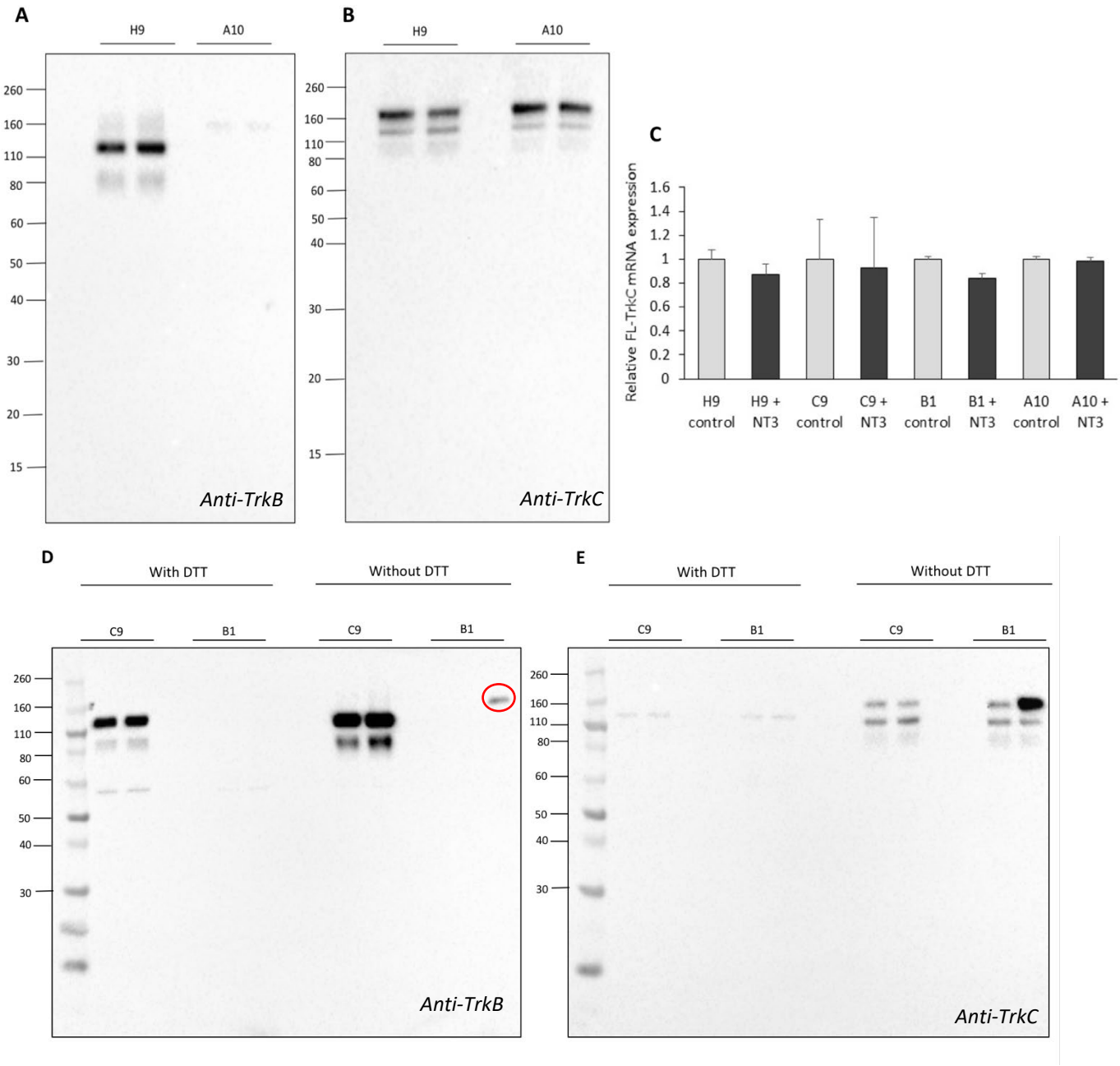
A
H9
A10
260
160
110
80
60
50
40
30
20
15
Anti-TrkB
B
H9
A10
260
160
110
80
60
50
40
30
20
15
Anti-TrkC
C
Relative FL-TrkC mRNA expression
1.6
1.4
1.2
1
0.8
0.6
0.4
0.2
0
H9 control
H9 + NT3
C9 control
C9 + NT3
B1 control
B1 + NT3
A10 control
A10 + NT3
D
With DTT
Without DTT
C9
B1
C9
B1
260
160
110
80
60
50
40
30
Anti-TrkB
E
With DTT
Without DTT
C9
B1
C9
B1
260
160
110
80
60
50
40
30
Anti-TrkC

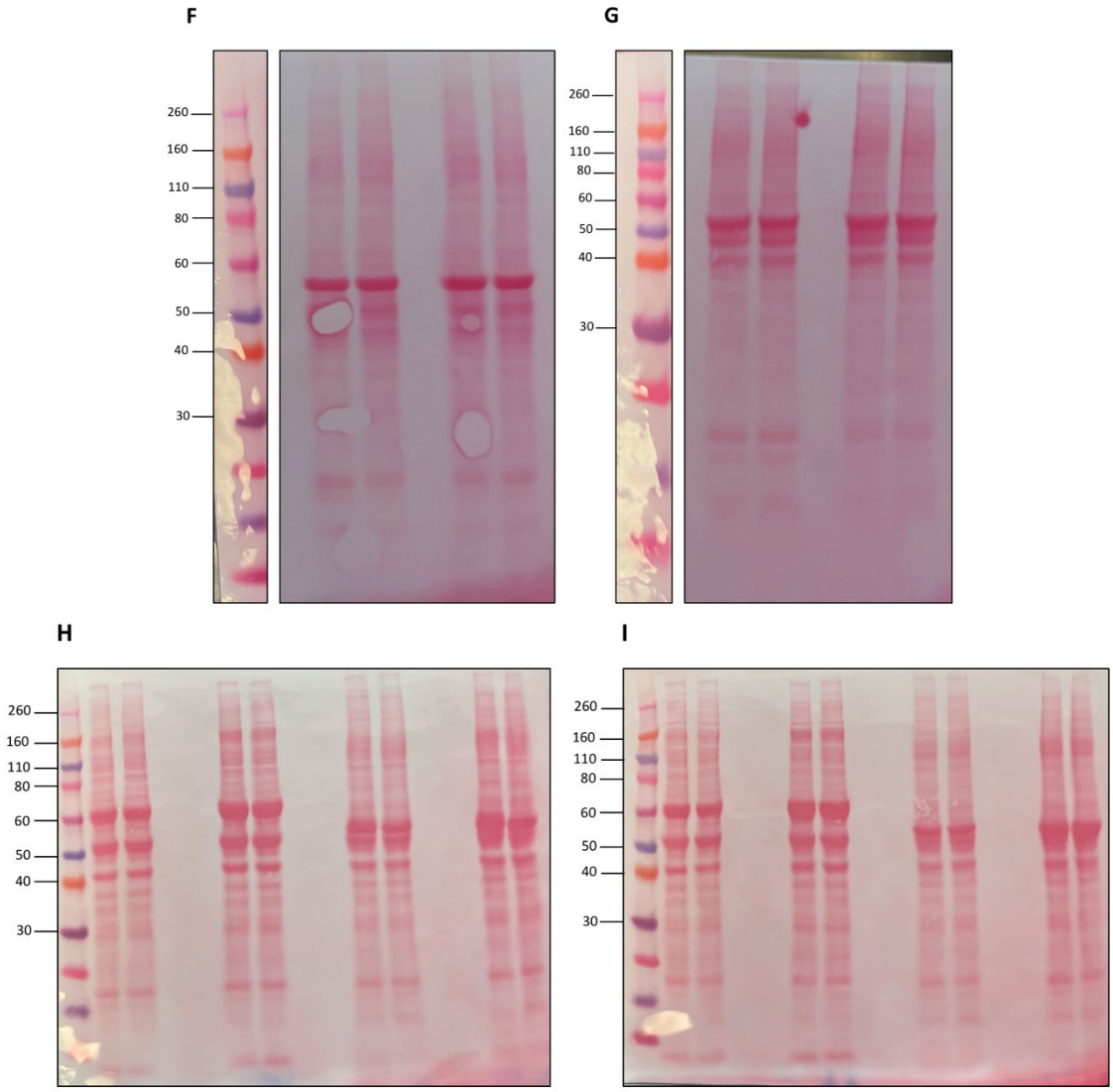

Figure 6.3. Expression of TrkC, but not TrkB in neurons generated from hESC targeted clones.

Western blots of H9 and A10 lysates probed with anti-TrkB and anti-TrkC antibodies. Unless otherwise indicated, samples were not denatured in the presence of DTT (see Chapters 3 and 4 for discussion). TrkB is readily detectable in wild-type H9 but not *NTRK2* targeted A10 (A) whereby TrkC is expressed at similar levels in H9 and A10 (B). Using RT-qPCR, TrkC mRNA levels were found to be expressed at similar levels for both differentially targeted clones A10 and B1, and non-targeted C9 relative to wild-type H9 (n = 3) (C). The faint signal observed with the lysates of A10 neurons (A) probed with anti-TrkB may reflect a weak cross-reactivity of the TrkB antibodies with TrkC (see Chapter 4) or else a TrkB isoform using an alternative initiation codon. (D, E) Western blots with lysates of C9 (untargeted) neurons and B1 (targeted) neurons probed with TrkB and TrkC antibodies respectively. Note that TrkB is readily detectable in untargeted C9 lysates, but not in B1 targeted lysates. The nature of the band in the red circle seen in (D) is unknown but was concluded to be an artefact due to its presence on both blots (D) and (E) and unexplainable high molecular weight. As with H9 and A10, TrkC was readily detectable in both C9 and B1 lysates when DTT was not used (E). (F), (G), (H) and (I). are Ponceau stains corresponding to (A), (B), (D) and (E). respectively.

The possible presence of activatable forms of TrkB was then investigated using neurons derived from the A10, B1 and C9 clone. To this end, neurons were exposed to BDNF, with A10 neurons also being exposed to the TrkB-activating antibody ZEB85 and the anti-TrkB antibody used for the detection of TrkB, following the surprising observations that it also activated TrkB (see Chapter 4, Figure 4.4A). As expected, a Trk phosphorylation signal was not detected following the addition of BDNF to A10 and B1 neurons (Figure 6.4A and B) whereby untargeted C9 had clearly retained ligand-activatable TrkB (Figure 6.4B). In the case of A10, treatment with ZEB85 and anti-TrkB further confirmed that ligand activatable TrkB was no longer present (Figure 6.4A). In addition, a phosphorylation signal was detected following the addition of NT3 to all cell lines (Figure 6.4A and B), indicating that these TrkC-expressing neurons responded to NT3 as expected, in spite of the absence of ligand-activatable forms of TrkB in A10 and B1.

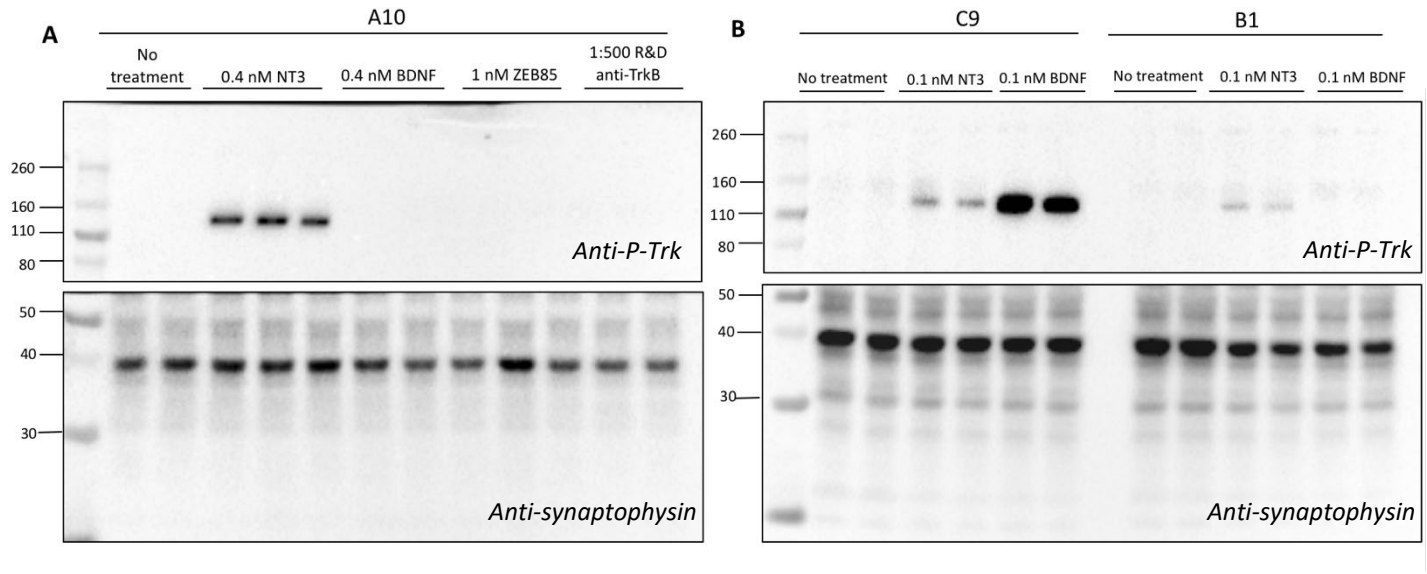

Figure 6.4. Lack of TrkB activation by multiple ligands.

Lysates of A10, C9 and B1 were treated with various ligands and separated by SDS gel electrophoresis. The membranes were probed with anti-phospho-Trk (upper panels) or the neuronal marker anti-synaptophysin (lower panels). The various ligands (indicated) were added to neurons at the indicated concentrations for 1 hour before cell lysis. Note the inability of any of the 3 TrkB activators to trigger Trk phosphorylation in A10 neurons whilst NT3 clearly triggers a P-Trk signal due to TrkC phosphorylation (A). Also note the inability of BDNF to generate a P-Trk signal in B1 neurons (B), a clone that is behaving similarly to A10 but that has been targeted differently according to the results of DNA sequencing. Last, even though the C9 hESCs went through the same procedure as A10 and B1, they somehow escaped the targeted deletion of TrkB and behave similarly to wild-type H9 neurons (B). Note that the B1 and C9 data was reproduced 3 times with 3 independent differentiations and the A10 data was consistently reproduced throughout the project.

Having established that the kinase domain of TrkC can be activated in neurons derived from hESCs successfully targeted at the *NTRK2* locus, it was important to determine the proportion of neurons expressing TrkC within the culture. Whilst the results presented in Chapter 3 and in this Chapter indicate TrkC expression at the protein level (in addition to the gene expression data), whether most or all neurons expressed TrkC in A10 cultures remained to be shown. To this end, A10 neuronal progenitors were plated at low density on coverslips and stained with either β-III-Tubulin, a previously validated anti-TrkC monoclonal antibody (Takahashi et al. 2011), or anti-TrkB as a further validation of the absence of the extracellular domain of TrkB in A10 neurons. No staining in neuronal processes was observed for anti-TrkB in A10 cells (Figure 6.5 upper left panel) with the TrkB staining in A10 cells resembling the goat 488 secondary only control (Figure 6.5, middle panel) meaning that the form of TrkB recognised by the TrkB antibody (i.e. the TrkB ECD) was not present in A10 cells. TrkC staining also revealed a punctate staining (Figure 6.5 lower left panel) (also shown in Chapter 3 with H9 neurons, Figure 3.7) as previously reported (Takahashi et al. 2011). Incubation with the fluorescent-labelled, rabbit secondary antibody (Figure 6.5 lower middle panel) failed to reveal any staining in neuronal processes (see Chapter 3, Figure 3.7). Quantification of Tuj1-positive cells (Figure 6.5, upper right panel) and TrkC-positive cells revealed that the mean number ± SEM of Tuj1-positive and TrkC-positive neurons were virtually identical: 72.8 ± 1.6 and 73.7 ± 2.0 for neurons stained with TrkC indicating that essentially all A10 neurons expressed TrkC. As shown in Chapters 3 and 4, as with H9 neurons, the identity of the DAPI-positive, Tuj1-negative signals was concluded to correspond to the nuclei of dead cells via phase contrast observation (Figure 6.5 bottom right panel, red arrows) confirming the homogeneity of the culture system and that therefore essentially all neurons express TrkC.

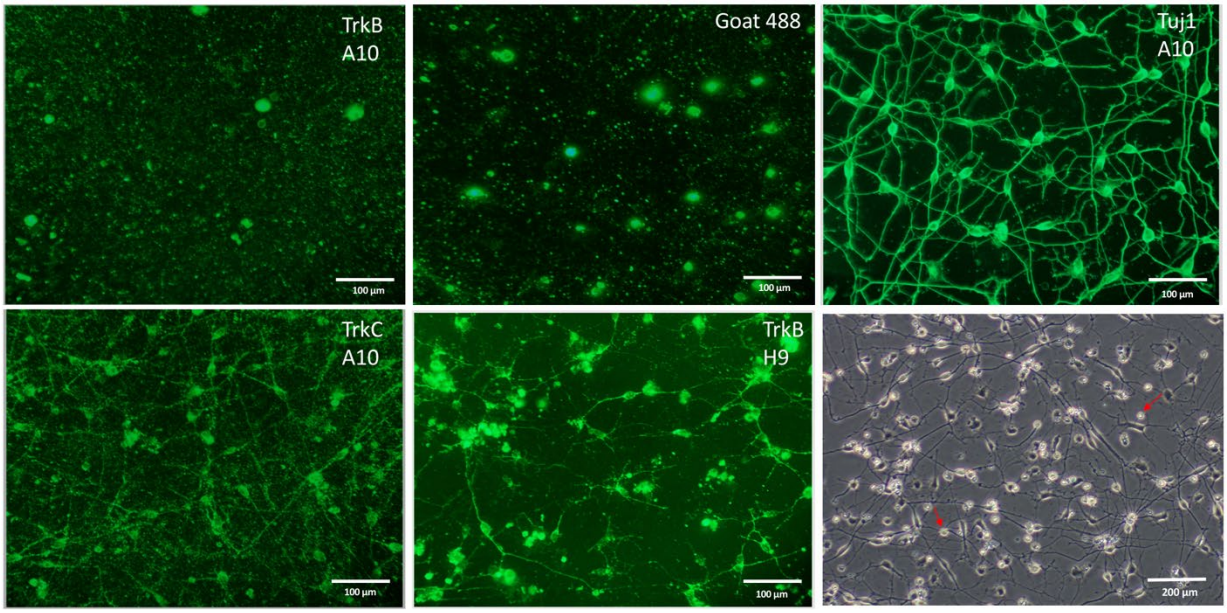

Figure 6.5. Expression of TrkC by A10 neurons: Immunofluorescence.

A10 neuronal progenitors were plated at low density on coverslips and stained with anti-TrkB (upper left panel), the TrkC monoclonal antibody also used in Chapter 3 (lower left panel) or a β-III-Tubulin (Tuj1) antibody (upper right panel). Upper and lower middle images were obtained by omitting incubation with the primary antibodies. Staining of A10 neurons with the TrkB antibodies (upper left panel) does not show any staining of neuronal processes. Apparent cell body staining is also seen with the anti-goat secondary antibody only (upper middle panel). By contrast, the anti-rabbit secondary antibody only gives a barely detectable signal (lower middle panel). The mean number ± SEM of Tuj1-positive neurons for A10 was 72.8 ± 1.6 and 73.7 ± 2.0 for neurons stained with TrkC. The bottom left panel shows a phase contrast image of A10 neurons on coverslips and examples of dead cells within the culture are indicated by the red arrows.

6.3. Short discussion

The main conclusion of this Chapter is that the hESC clones targeted at the *NTRK2* locus allowed the generation of neurons expressing TrkC, at levels comparable to those observed in neurons generated from non-targeted hESCs. Crucially, no activation of TrkB was detected using 3 different TrkB activators (Figure 6.4A).

Two of these clones (A10 and B1) were analysed in some detail and found to behave identically despite their differential targeting with regard to their ability to generate progenitors and subsequently neurons expressing comparable levels of synaptophysin with H9 and C9 neurons. The similarities between the C9 and H9 clones indicated that the properties of these cells had not been measurably affected by the CRISPR procedure including the FACS sorting process, neither with regard to growth rates nor ability to generate neurons.

Given previous work indicating that TrkC is a dependence receptor, i.e. that it can cause the death of cells in the absence of a ligand (Tauszig-Delamasure et al. 2007; Nikoletopoulou et al. 2010), a property not shared with TrkB, it was important to establish that similar numbers of progenitors and neurons could be generated from hESCs expressing only TrkC and not TrkB. No differences in cell numbers were observed, possibly due to the use of Rho-kinase inhibitor included in the differentiation procedure (see Material and Methods) and/or lower levels of expression of TrkC expression compared with previous studies where TrkC expression was found to cause cell death (Tauszig-Delamasure et al. 2007; Nikoletopoulou et al. 2010). It cannot be excluded that TrkC expression in the absence of TrkB may lead to increased cell death, but the additional finding that the levels of synaptophysin does not seem to vary between cell lines whether targeted or untargeted (see above), suggests that TrkC does not act as a death-inducing receptor in this context.

In line with the absence of ligand-activatable forms of TrkB (Figure 6.4), Western blot as well as immunocytochemistry experiments confirmed the absence of detectable TrkB in neurons derived from A10 hESCs. By contrast, TrkC was expressed at similar levels and crucially could still be activated by NT3. A lack of phosphorylation in response to multiple TrkB ligands (Figure 6.4A) was important, as the ligands used bind to different parts of TrkB (see Chapter 4), suggesting that the targeting event had eliminated most, if not all of the TrkB ECD. Indeed, ZEB85 binding was mapped close to the transmembrane domain (see Chapter 4, Figure 4.4B and C). Despite these results, the lack of TrkB activation and of a TrkB signal in Western blot or immunocytochemistry experiments does not imply that all isoforms of TrkB protein have been eliminated by the CRISPR/Cas9 procedure as the gRNAs did not target the TrkB

promoter. Indeed, minor alternative promoters encoding intracellular forms of TrkB have been described in the developing human brain (Luberg et al. 2010a).

In summary, this chapter demonstrates that a cell line possessing ligand activatable TrkC and not TrkB has been generated. In addition, combined with the negligible values of TrkA and p75 mRNA levels (see Chapters 3 and 8) in this cellular system allows NT3-mediated TrkC signalling to be investigated without the complications of autophosphorylation of Trk receptors (see Chapter 3) and NT3-mediated activation of receptors other than TrkC.

Chapter 7 - Trk activation by NT3 in neurons lacking activatable forms of TrkB

7.1. Short Introduction

The generation of a cellular model lacking ligand-activatable TrkB permitted NT3-mediated TrkC signalling to be studied without the problems resulting from concomitant TrkB activation. As no such models have been available thus far, the key question of the concentrations of NT3 needed to activate TrkB in neurons could not be answered. Accordingly, the main objective of this Chapter was to use A10 neurons exposed to increasing concentrations of NT3 and to quantify Trk activation using anti-P-Trk antibodies. The second objective was to compare the A10 results with those obtained with H9 neurons and increasing concentrations of BDNF and of NT3. A third objective was to explore whether the loss of P-Trk signal observed with neurons upon prolonged exposure to BDNF (Merkouris et al. 2018) would also be observed with NT3.

7.2. Results

7.2.1. Trk activation by NT3: Dose-responses and comparison between A10 and H9 neurons

Following the generation of the A10 cells lacking ligand-activatable TrkB, and after ensuring that the cells could be successfully differentiated into neurons and validated in terms of TrkC expression, a dose-response was established using increasing concentrations of NT3 with Trk tyrosine phosphorylation (P-Trk) as a target, using the same anti-P-Trk antibody as in the previous chapters. A10 neurons were treated with NT3 for 1 hour, the cells then lysed and analysed by Western blotting with membranes probed with anti-P-Trk (Figure 7.1) as well as the previously used synaptophysin antibody. Remarkably, a NT3-induced phosphorylation signal could be detected at concentrations as low as 10 pM (Figure 7.1A). Saturation also occurred at a much lower concentration than with CHO cells, i.e. 100 pM for neurons compared with 2 nM for CHO cells (Figure 7.1 and compare with Chapter 3, Figure 3.8A). The EC50 for NT3 using A10 neurons and P-Trk signal intensity as readout was estimated to be around 40 pM, more than an order of magnitude lower than with TrkC expressed in CHO cells (see Chapter 3, Figure 3.8A).

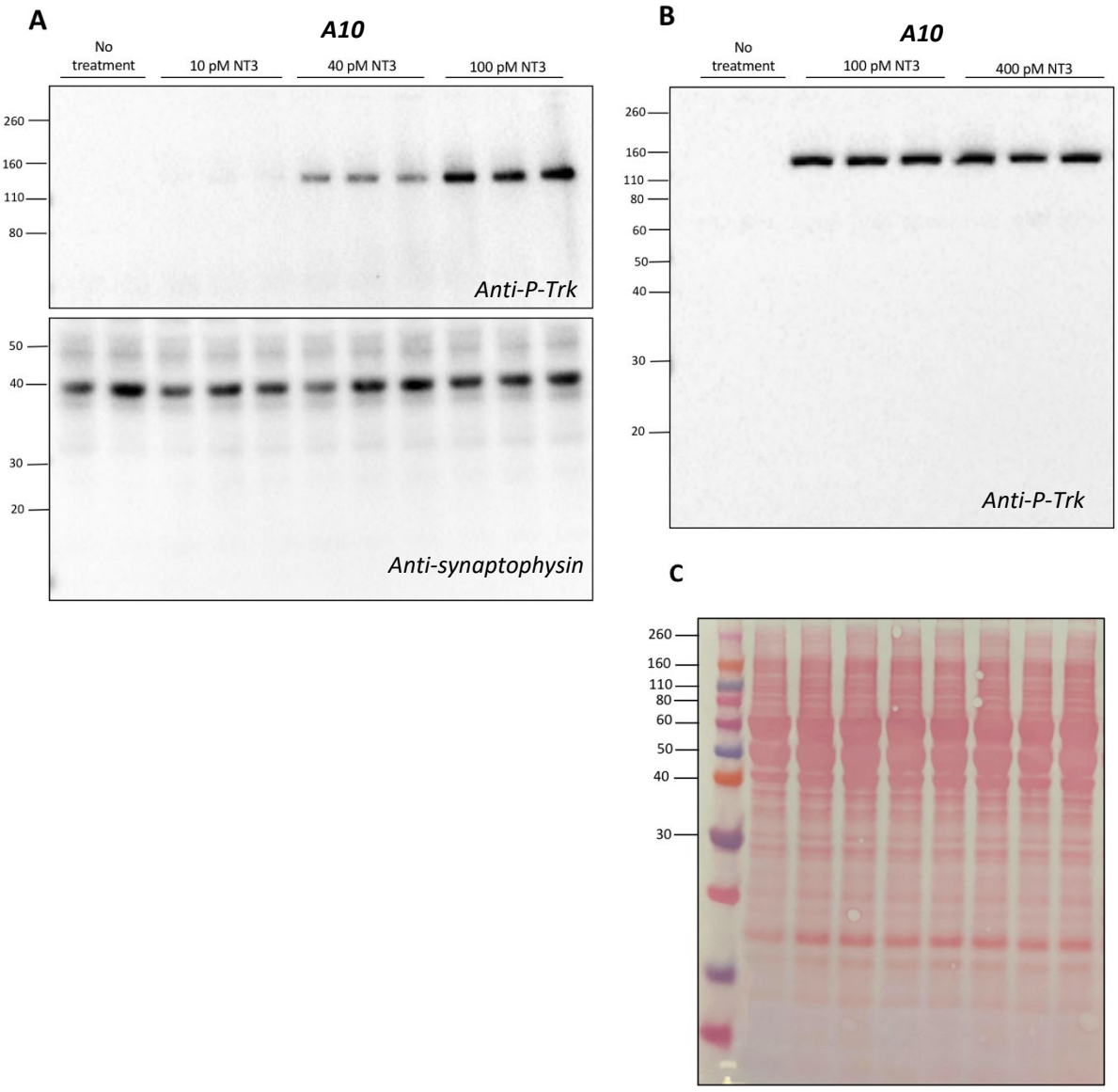

Figure 7.1. TrkC activation by NT3 in A10 neurons: dose response.

A10 neurons were treated with increasing concentrations of NT3 for 1 hour and the lysates separated by SDS gel electrophoresis. Western blots were probed with anti-P-Trk (A upper panel and B) and/or cut horizontally and probed with anti-synaptophysin (A lower panel). Note that the phosphorylation signal appears to saturate at 100 pM NT3. (C). shows a Ponceau stain corresponding to (B).

A comparative NT3 dose-response was also performed with wild-type H9 neurons with BDNF and NT3, also using Trk phosphorylation as read-out (Figure 7.2). As expected, given the higher levels of expression of TrkB compared with TrkC in H9 neurons (see Chapter 4, Figure 4.5 and Figure 4.6), compared to NT3, BDNF induced a significantly higher level of phosphorylation at low ligand concentrations (Figure 7.3A). At higher concentrations of NT3 (400 pM and above), the P-Trk signal elicited by NT3 markedly increased. The densitometry analysis of the band intensity of the phosphorylation signal induced by NT3 in both H9 and A10 neurons confirmed a comparable signal intensity until the NT3 concentration exceeded 100 pM (Figure 7.3B). In A10 neurons, TrkC phosphorylation saturated at 100 pM (see above), but continued to increase in H9 neurons. This was an expected result given that H9 neurons express ligand-activatable TrkB whereas A10 do not. The similarities between H9 and A10 neurons with regard to the intensity of the P-Trk signal up until 100 pM NT3 suggested that at concentrations lower than 100 pM NT3 selectively activated TrkC whereas at higher concentrations, NT3 also activates TrkB.

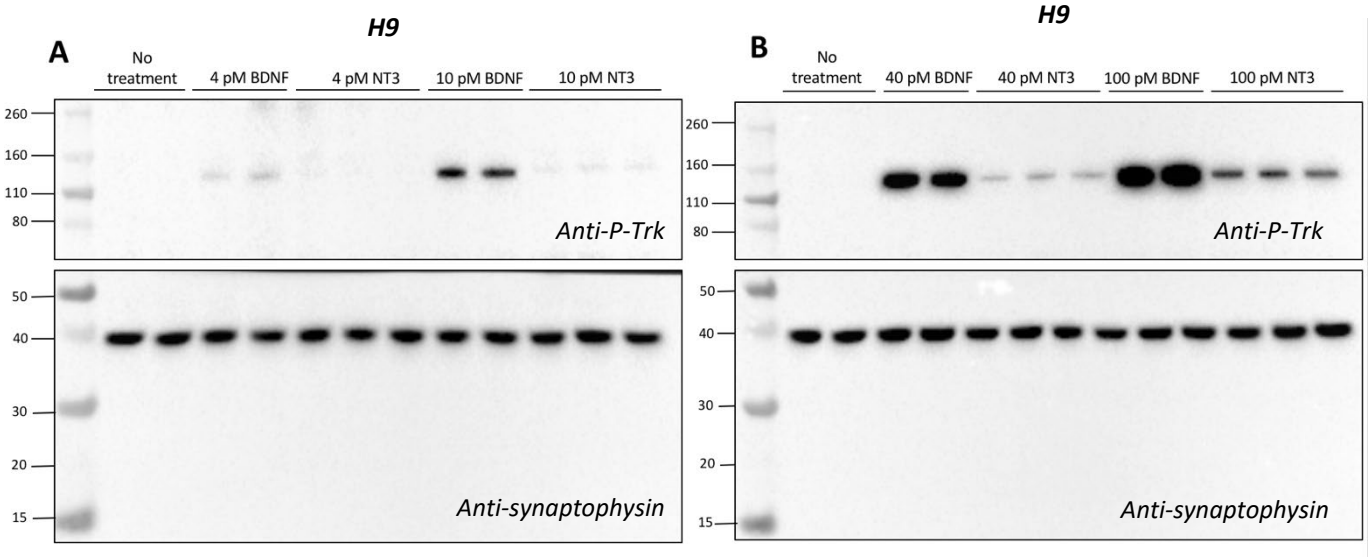

Figure 7.2. Trk activation by BDNF and NT3 in H9 neurons: dose response.

H9 neurons were treated with the indicated low (A) or high (B) concentrations of BDNF or NT3 for 1 hour and the lysates were separated by SDS gel electrophoresis. Membranes were cut horizontally and incubated with either anti-P-Trk (upper panels) or anti-synaptophysin (lower panels). (A). Note that the lowest NT3 concentration generating a quantifiable signal was 10 pM (see Figure 7.3)

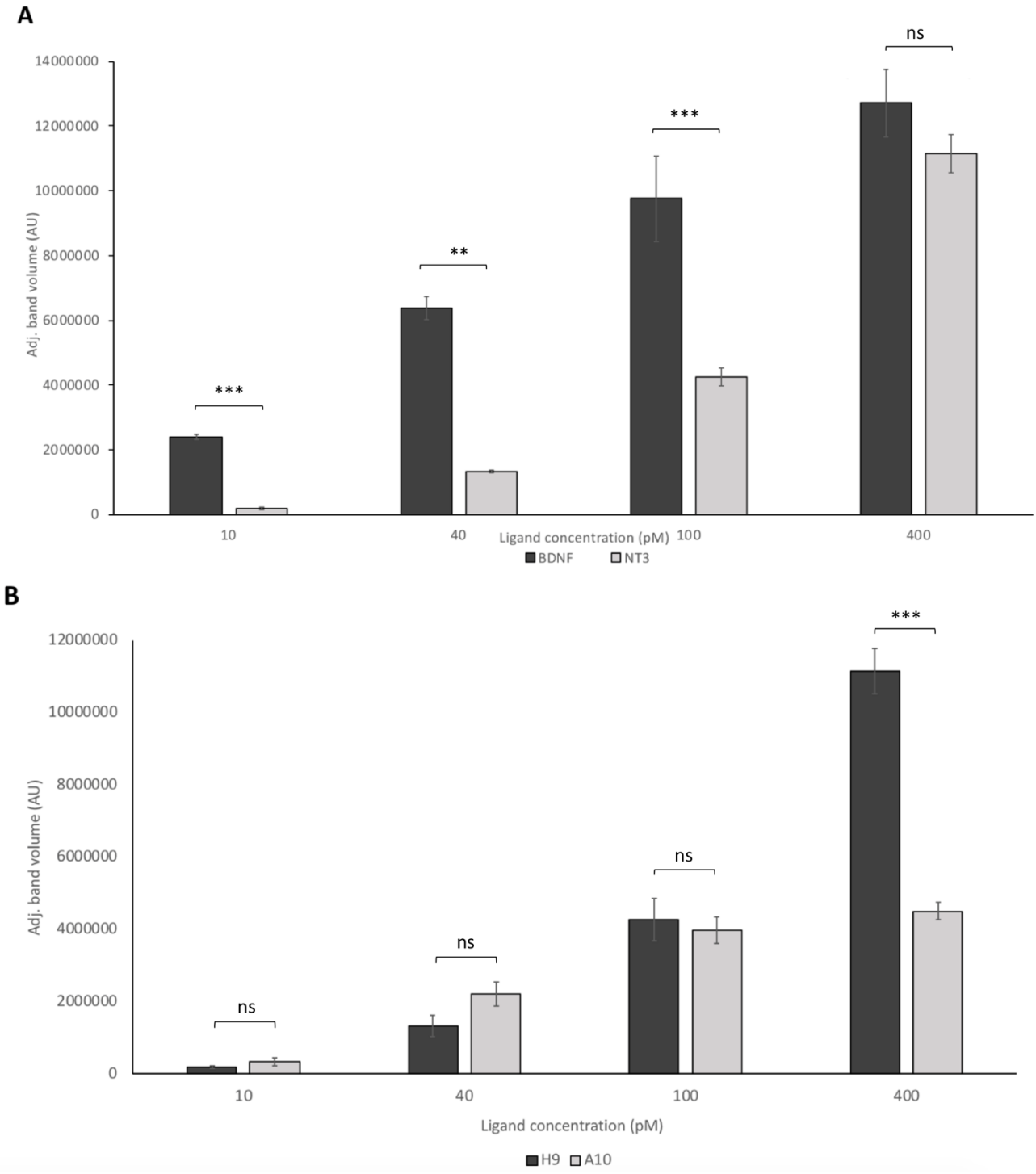

Figure 7.3. Quantification of Trk activation by NT3 and BDNF in H9 and A10 neurons.

Densitometric analysis of the BDNF and NT3 dose responses in H9 neurons (A) and comparison of the NT3 dose-responses between H9 and A10 neurons (B). The error bars refer to SEM and significance indicated with asterisks: ***$p < 0.001$, **$p < 0.01$ and ns = $p > 0.05$. For H9, 10 pM BDNF n = 6, 40 pM BDNF n = 6, 100 pM BDNF n = 9, 400 pM BDNF n = 4, 10 pM NT3 n = 7, 40 pM NT3 n = 7, 100 pM NT3 n = 10, 400 pM NT3 n = 4. For A10, 10 pM NT3 n = 12, 40 pM NT3 n = 11, 100 pM NT3 n = 20, 400 pM NT3 n = 8.

7.2.2. Time-dependent activation of Trk receptors

It has been previously observed that prolonged (24 hour) exposure of H9 neurons to high concentrations of BDNF (2 nM) leads to an almost complete loss of the P-Trk signal (Merkouris et al. 2018). Likewise, prolonged exposure to NT3 in A10 neurons also led to an almost complete loss of the P-Trk signal (Figure 7.4A) and the TrkC receptor itself was barely detectable after 24 hours (Figure 7.4B). The observation that both TrkB and TrkC were subjected to this ligand-induced loss of signal, both with regard to phosphorylation and receptor raised the question of whether the receptors were down regulated by their respective ligands by separate pathways, or if they were co-down regulated, for example if they would associate as receptor clusters.

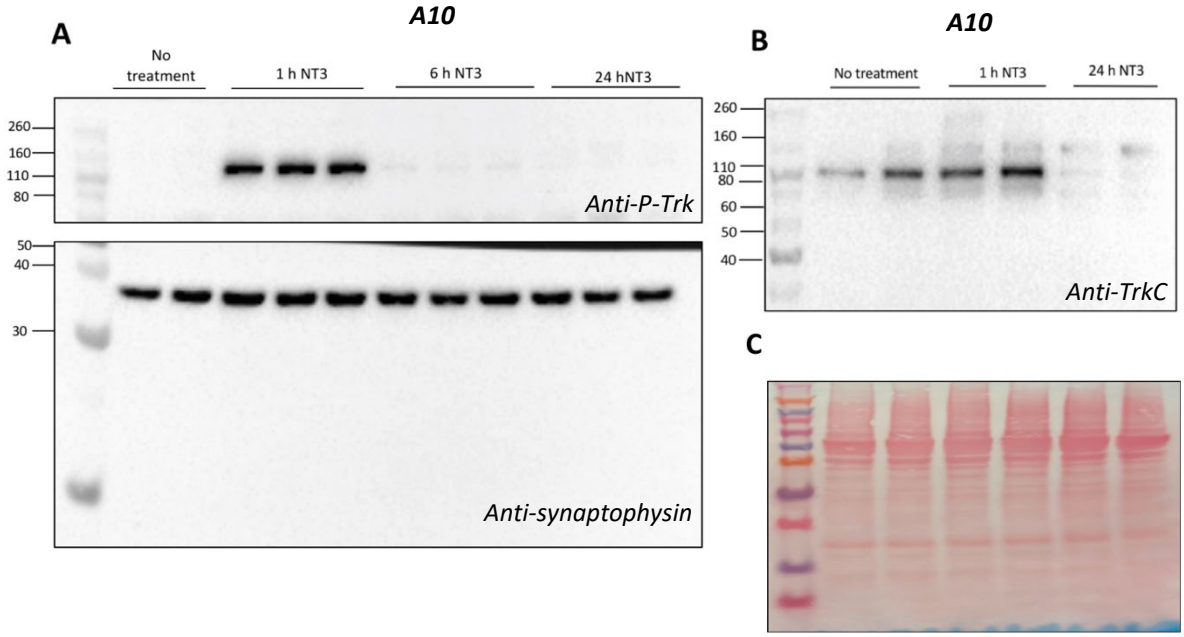

Figure 7.4. Loss of TrkC phosphorylation following prolonged exposure of A10 neurons to NT3.

A10 neurons were exposed to 400 pM NT3 and lysed at the times indicated. The lysates were separated by SDS gel electrophoresis and incubated with anti-P-Trk (upper panel) and anti-synaptophysin (lower panel). Note the dramatic loss of P-Trk signal as early as 6 h after NT3 treatment (A) and the almost complete loss of TrkC protein signal after 24 hours (B). Lysates in (B) were not treated with DTT. (C). shows a Ponceau stain corresponding to (B).

In line with previous results (Merkouris et al. 2018 and unpublished), the re-addition of BDNF after 24 hours at the same concentration (2 nM) failed to rescue the P-Trk signal, suggesting that TrkB may no longer be exposed at the cell surface in a ligand-activatable form (Figure 7.5A). In line with this, probing these lysates with anti-TrkB revealed that TrkB was indeed barely detectable after 24 hours (Figure 7.5B). This finding was exploited to test the possibility that TrkC may be co-downregulated with TrkB. As essentially all neurons co-express TrkB and TrkC (see Chapters 3 and 4) it is conceivable that the downregulation of TrkB may trigger that of TrkC, for example if both receptors were to reside in the same patch of cell membrane. To test this possibility, H9 neurons were treated with BDNF for 24 hours and subsequently exposed to NT3 for 1 hour. Analysis of the cell lysates probed with anti-P-Trk clearly revealed the presence of a NT3-induced signal, indicating that the loss of ligand-activatable TrkB does not impact the ability of TrkC to be activated by NT3 (Figure 7.5A). A further experiment addressing protein, as opposed to P-Trk levels confirmed the marked down regulation of TrkB protein after 24 hours (Figure 7.5B and C) whilst TrkC was still detectable, albeit at somewhat lower levels (Figure 7.5C).

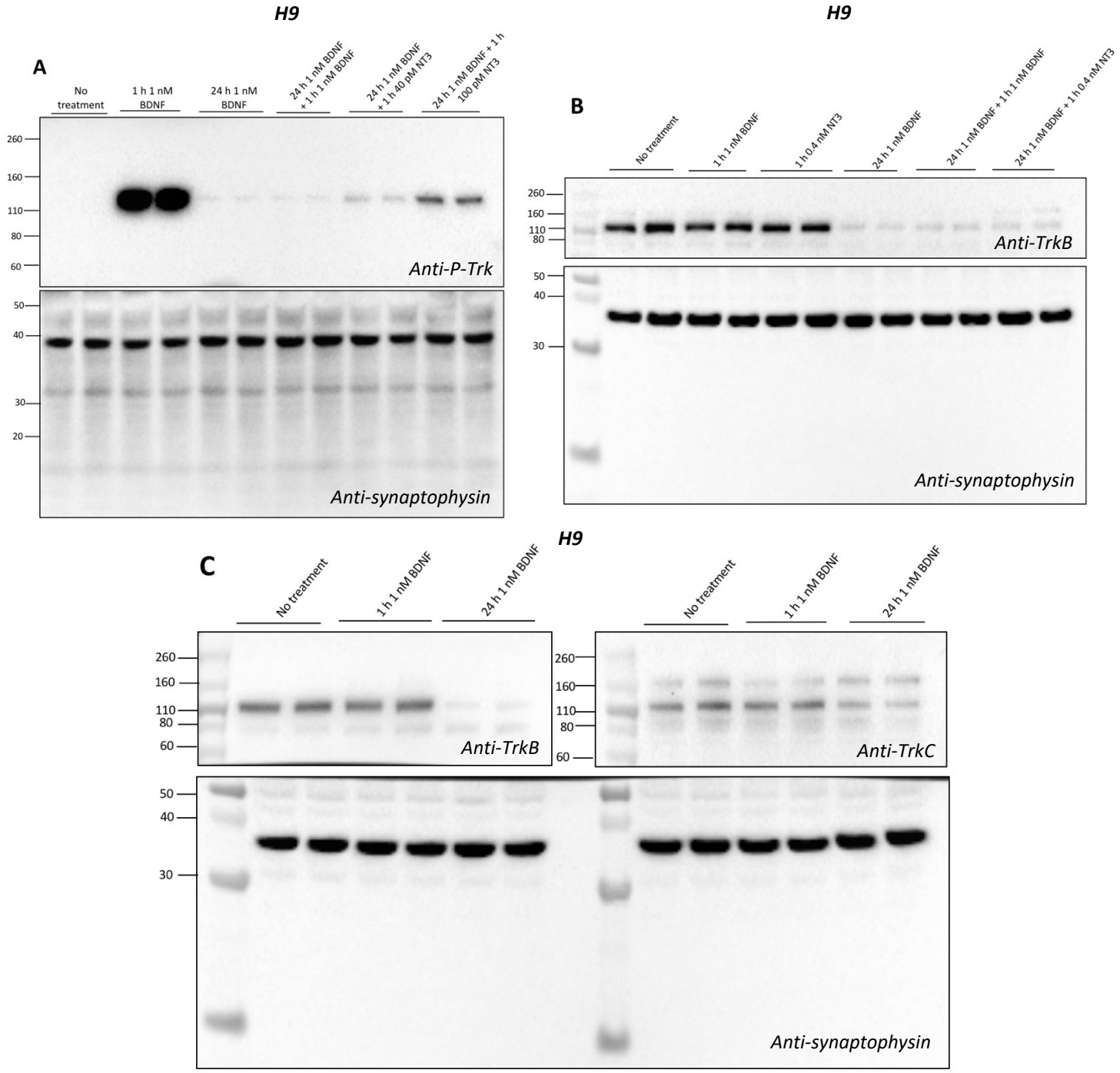

Figure 7.5. Loss of TrkB phosphorylation following prolonged exposure of H9 neurons to high concentrations of BDNF and rescue of a Trk phosphorylation signal by NT3.

H9 neurons were treated as indicated and the lysates separated by SDS gel electrophoresis. Following transfer, the membranes were processed as indicated above. Note that whilst the re-addition of 1 nM BDNF (A) fails to reactivate TrkB, the signal generated by NT3 is unaffected by the BDNF pre-treatment. (B) and (C) TrkB protein is barely detectable after 24 h exposure to 1 nM BDNF whilst TrkC remains detectable. Lysates in (B). and (C). were not treated with DTT. These results were reproduced in 3 independent differentiations.

Given the growing interest in activating Trk pathways to restore deteriorating neuronal function in humans (see General Introduction), the hypothesis was then tested if the loss of P-Trk signal following prolonged exposure of the neurons to saturating concentrations of BDNF (Figure 7.5A) might be concentration-dependent. To this end, neurons were exposed to lower BDNF concentrations, 40 pM instead of 1 nM, and BDNF re-added at the same low concentration 24 hours later. Whilst the initial signal elicited by 40 pM BDNF had disappeared after 24 h (Figure 7.6) the re-addition of BDNF at the same 40 pM was sufficient to restore a clearly detectable P-Trk signal.

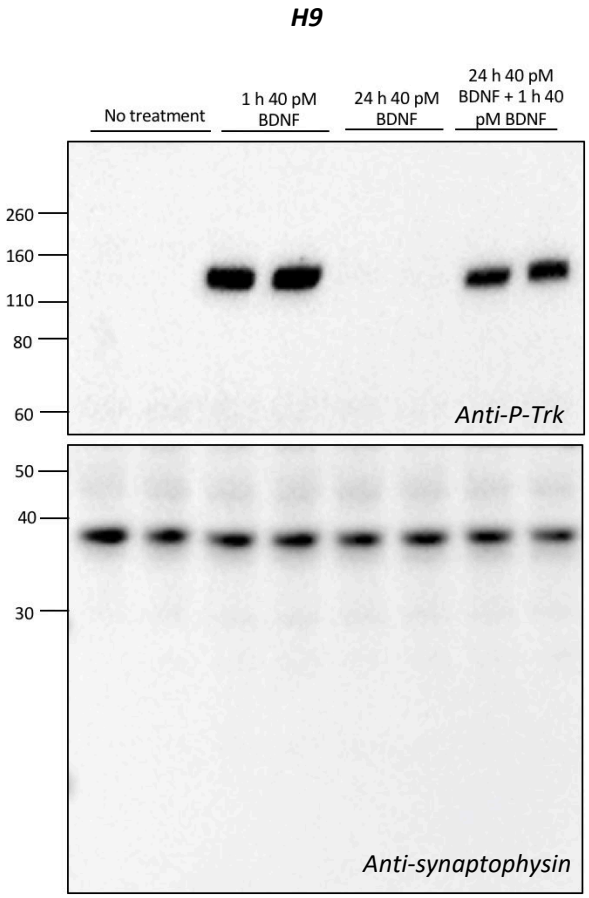

Figure 7.6. Phosphorylation of TrkB following prolonged exposure of H9 neurons to low concentrations of BDNF can be recovered upon re-exposure to BDNF.

H9 neurons were treated with BDNF as above and the lysates separated by SDS gel electrophoresis. The membrane was cut in half and probed with anti-P-Trk (upper panel) and anti-synaptophysin (lower panel). Note that when lower concentrations of BDNF are used, reactivation of TrkB is possible after 24 hours.

7.3. Short discussion

The main conclusion of the results presented in this Chapter is that when expressed in human neurons, TrkC (see Figure 7.1 and General discussion), can be activated at much lower concentrations of NT3 in A10 than is the case when TrkC is expressed in CHO cells (see Chapter 3, Figure 3.8A), with EC_{50}s of about 40 versus 400 pM. The similarity of the NT3 dose-responses between H9 and A10 neurons until 0.1 nM NT3 suggests that TrkC activation also occurs at similarly low NT3 concentrations when TrkC is co-expressed with TrkB, as is the case with H9 neurons (Figure 7.3B).

In A10 neurons, the P-Trk signal saturates at 0.1 nM, suggesting that TrkC phosphorylation cannot be increased by NT3 any further. In H9 neurons, phosphorylation continues to increase as with increasing NT3 concentrations, most likely because of the ability of NT3 to also activate TrkB at high NT3 concentrations. These results also show that TrkB activation by NT3 in human neurons requires higher concentrations than is the case when TrkB is expressed in CHO cells (see Chapter 3, Figure 3.8B). It thus appears that the selectivity of TrkB increases when the receptor is expressed in a neuronal context whilst the affinity of TrkC for NT3 increases. At present there are no molecular explanations accounting for these findings that are likely to be relevant with regard to receptor selectivity and affinity in the developing brain (see General discussion). It is conceivable that specific components expressed in neurons, but not for example CHO cells, might associate with Trk receptors and increase ligand affinity and specificity. For example, the co-expression of p75 with Trk receptors has been reported to increase the binding affinity of NGF for TrkA (Hempstead et al. 1991) and the selectivity of TrkB for BDNF compared with NT3 as well as NT4 (Bibel et al. 1999b). In addition, the localisation of receptors in neuronal processes may be part of the explanation. Indeed, the TrkC and TrkB immunofluorescence images (see Chapter 3 and Chapter 4, Figure 3.7 and Figure 4.3 respectively) indicate that the majority of the receptors are localised in neuronal processes. Thus, bulk measurements of Trk phosphorylation likely reflect biochemical events taking place in neuronal processes rather than in cell bodies. It is thus conceivable that neuronal processes contain molecules such as those associated with the cytoskeleton that may be underrepresented when only cell bodies are examined with regard to Trk receptor activation as is the case when Trk receptors are expressed in vectors such as CHO cells.

Even though TrkB and TrkC show the same distribution in neurons and their processes (see above), they do not seem to be tightly associated in a molecular complex, at least not the degree that the downregulation of one receptor leads to the downregulation of the other. In particular, whilst the P-TrkB signal was lost following prolonged exposure to BDNF, TrkC could

still be phosphorylated by NT3 (Figure 7.5A). Despite this, the levels of TrkC do appear to be lower after long exposure to BDNF (Figure 7.5C). There is no clear explanation for this finding whereby such changes did not measurably impact the ability of TrkC to be phosphorylated by its ligand. It is conceivable that prolonged exposure to saturating BDNF concentrations may progressively trigger internalisation pathways that may act on both TrkB and TrkC leading to the internalisation and degradation of both receptors. Prolonged activation of TrkB by high concentrations of BDNF may result in an overactivation of this degradation pathway thus resulting in the progressive co-internalisation of a proportion of TrkC. Likewise, the loss of the P-Trk signal following prolonged exposure to NT3 (Figure 7.4A), follows the same temporal pattern as the loss of P-Trk signal after prolonged (24 hour) exposures to BDNF (Figure 7.5) (Merkouris et al. 2018). Mechanisms involved in the downregulation of TrkB have been extensively investigated and are thought to involve ubiquitination and proteasome degradation (for review, see Sánchez-Sánchez and Arévalo 2017). In addition, calpain-mediated cleavage of TrkB has been proposed to play a role as degradation of the receptor was found to be prevented by calpain inhibitors (Jerónimo-Santos et al. 2014). These authors mapped a juxta membrane calpain cleavage site in TrkB that is neither present in TrkA nor in TrkC, suggesting that mechanisms other than calpain-mediated cleavage may account for the decrease of TrkC signal following prolonged exposures of the neurons to NT3 (Figure 7.4B). This loss of TrkC signal further validates the notion that it is really TrkC that is involved in NT3 signalling.

The question of the loss of Trk activation following prolonged exposures to Trk activators is important in the context of potential therapies involving the activation of these pathways using for example Trk receptor agonists such as ZEB85 (Merkouris et al. 2018). Given this context, it is interesting to note that the previously reported loss of TrkB phosphorylation following exposure to saturating concentrations of BDNF (Merkouris et al. 2018, see also Figure 7.5A) was *not* observed when lower (40 pM) concentrations of BDNF were used that did allow Trk receptor re-activation after 24 hours using the same 40 pM concentration (Figure 7.6).

The main new findings of this chapter are that TrkC can be activated at very low concentrations of NT3, as low as 40 pM, and that this is likely also the case in neurons co-expressing TrkB as is the case in most neurons in the human brain. Remarkably and unexpectedly, TrkB activation by BDNF in H9 requires higher concentrations, with EC50s of about 200 and 40 pM for BDNF and NT3 (see General discussion for the implications of these findings in the context of *in vivo* assembly of neuronal circuits) (Merkouris et al. 2018).

Chapter 8 - Transcriptional changes downstream of TrkC activation by NT3 and comparison with TrkB activation

8.1. Short Introduction

The availability of the A10 neurons opened the possibility to determine the transcriptional changes downstream of TrkC activation by NT3 and comparisons to be made with those caused by TrkB activation (Merkouris et al. 2018). This previous study with H9 neurons compared 3 different TrkB ligands and all were found to cause very similar transcriptional changes (Merkouris et al. 2018). As Trk signalling elicited by NT3 in the absence of TrkB activation could not be studied thus far, the main objective was to determine gene transcription changes caused by NT3 addition to A10 neurons. Importantly, the absence of TrkB in A10 neurons allowed saturating (2 nM) NT3 concentrations to be used as was also the case in the previous study of TrkB activation by BDNF (Merkouris et al. 2018). This approach, allows maximal gene expression changes to be studied whereas lower, presumably more physiological concentrations may induce changes too subtle and transient to be detected .

8.2. Results

8.2.1. Preparation of samples for RNA sequencing

RNA was extracted from DIV 30 A10 neurons following NT3 addition for 2 and 24 hours. In parallel experiments, DIV 30 H9 neurons were also used and RNA extracted following BDNF addition for 2 and 24 hours. Phase contrast images of the H9 and A10 neurons used for the RNA extraction and subsequent RNA sequencing are illustrated in Figure 8.1.

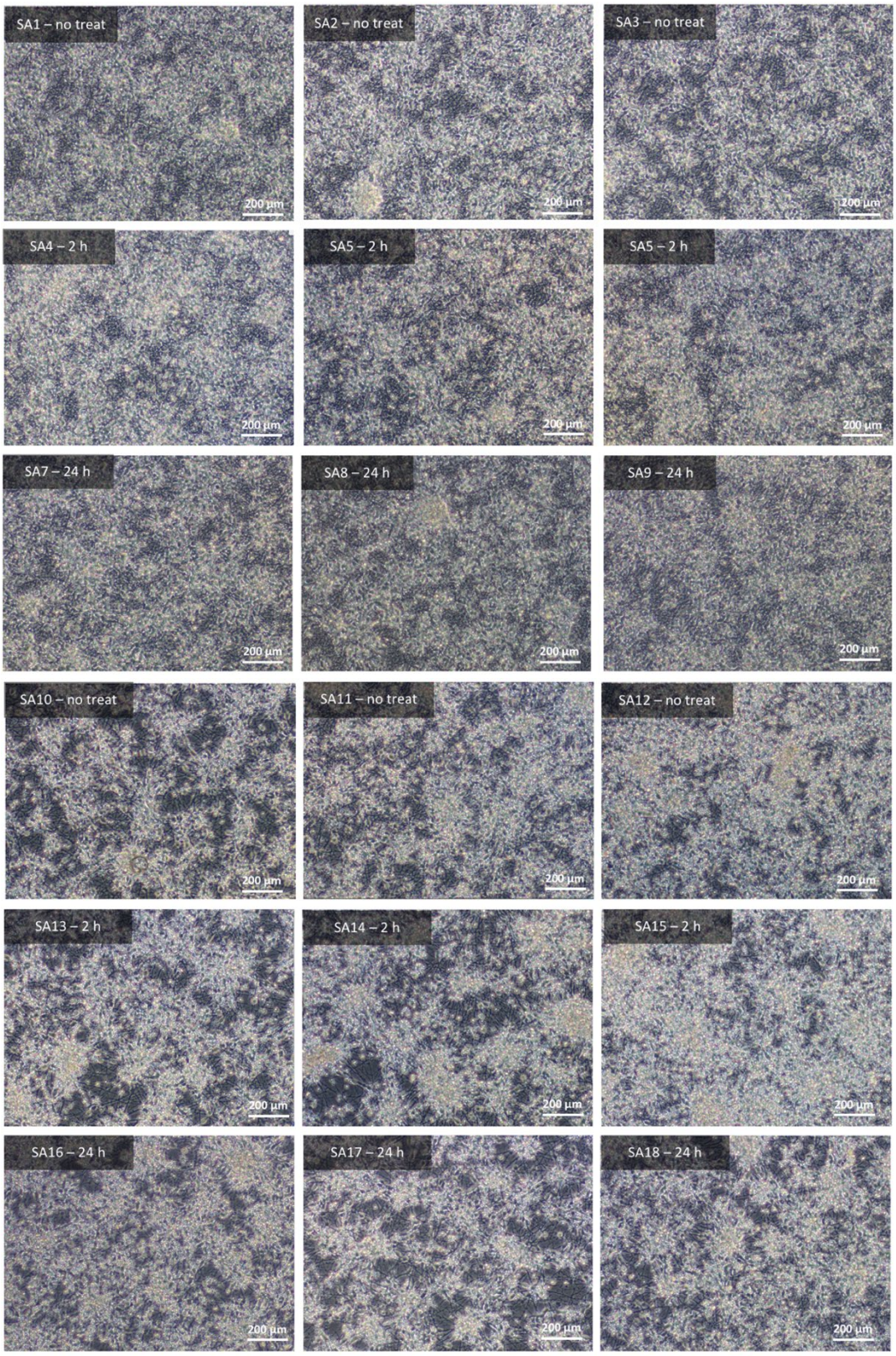

Figure 8.1. Images of the cultures used for RNAseq experiments.

Phase contrast images (20 X magnification) of DIV 30 H9 and A10 neurons at the time of RNA extraction and subsequent RNA sequencing. Samples SA1-SA9 were H9 neurons, and samples SA10-SA18 were A10 neurons. All neurons had the desired morphology. Ligand treatment times are indicated on the images and all ligands were added at a concentration of 2 nM. Each treatment was performed in triplicate.

Following extraction, RNA was quantified and checked for quality by running a small volume on an acrylamide gel and determining the ratio between the 28S and 18S ribosomal subunits (Figure 8.2B). The result was expressed as an RNA Integrity Score (RINe score) and used to determine the overall quality of the input RNA. All samples exceeded the minimum recommended score for RNA sequencing of 7 and were deemed suitable for RNA sequencing (Figure 8.2A).

Following RNA sequencing (see Material and Methods) the files were trimmed and processed and a PCA analysis performed as an indication of whether or not the triplicates would cluster together. Except for sample (SA1 – H9 no treatment) that was then left out from the subsequent analysis, clustering was deemed acceptable (Figure 8.3). Due to this no-treatment outlier, the results obtained with H9 neurons were found to be too variable between triplicates, including in the expression of key neuronal markers. This critical assessment led to the inclusion of the previous data set in the comparison, given that these data showed tight clustering of the triplicates in the corresponding PCA analysis and had been validated by the concomitant use of 3 different TrkB activators (Merkouris et al. 2018).

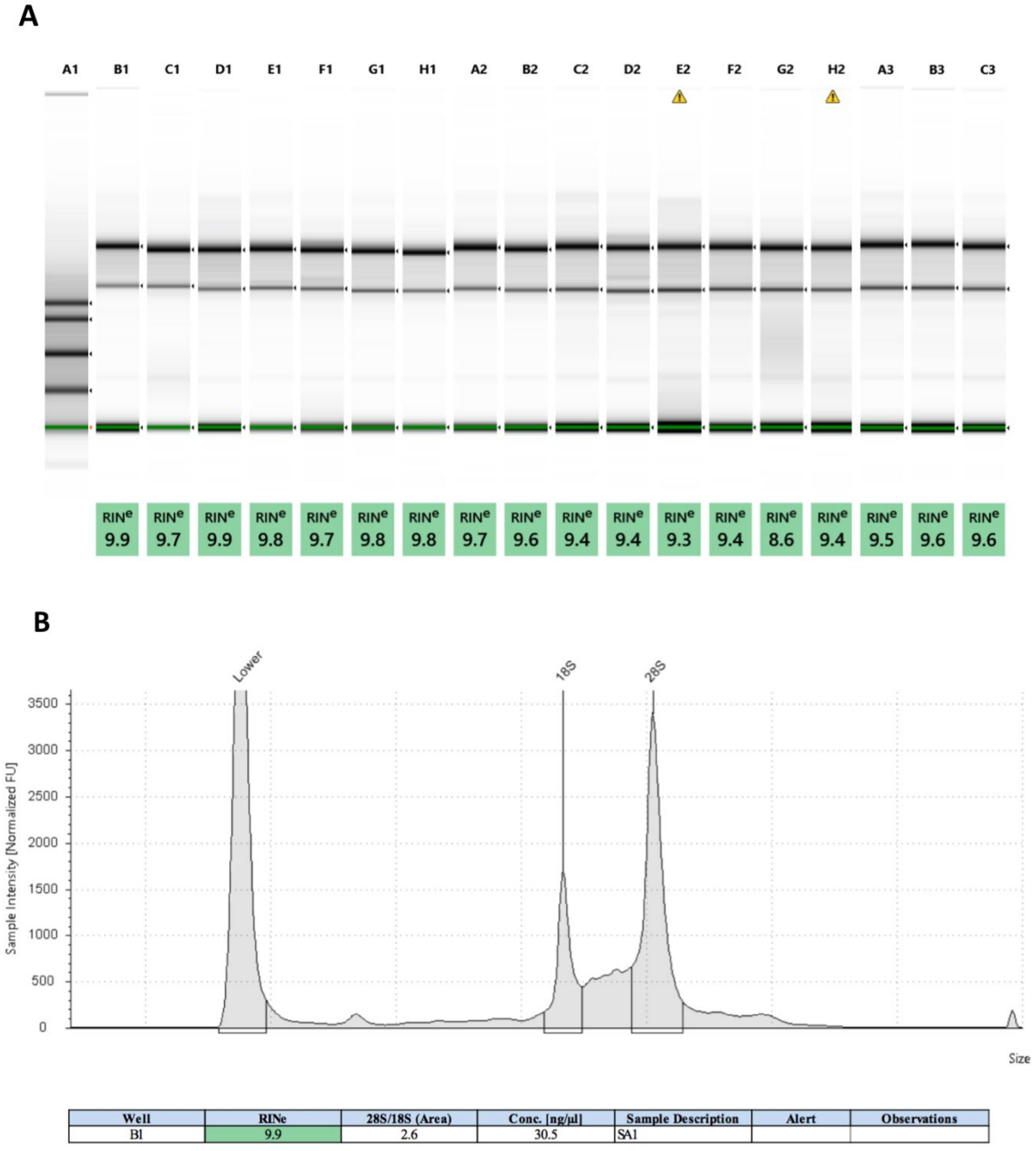

Figure 8.2. Tapestation analysis of RNA samples.

A small volume of RNA was run on an acrylamide gel and quality and quantity assessed using a Tapestation (Agilent). Each RNA sample was analysed by Agilent software and assigned a quality score (RINe) based on the ratio between the 28S and 18S ribosomal subunits. The software analysed the bands shown on the gel (A). Two clear peaks at 28S and 16S indicated minimal contamination and overall good quality RNA samples. An example of this is shown for a sample with a RINe score of 9.9 (B).

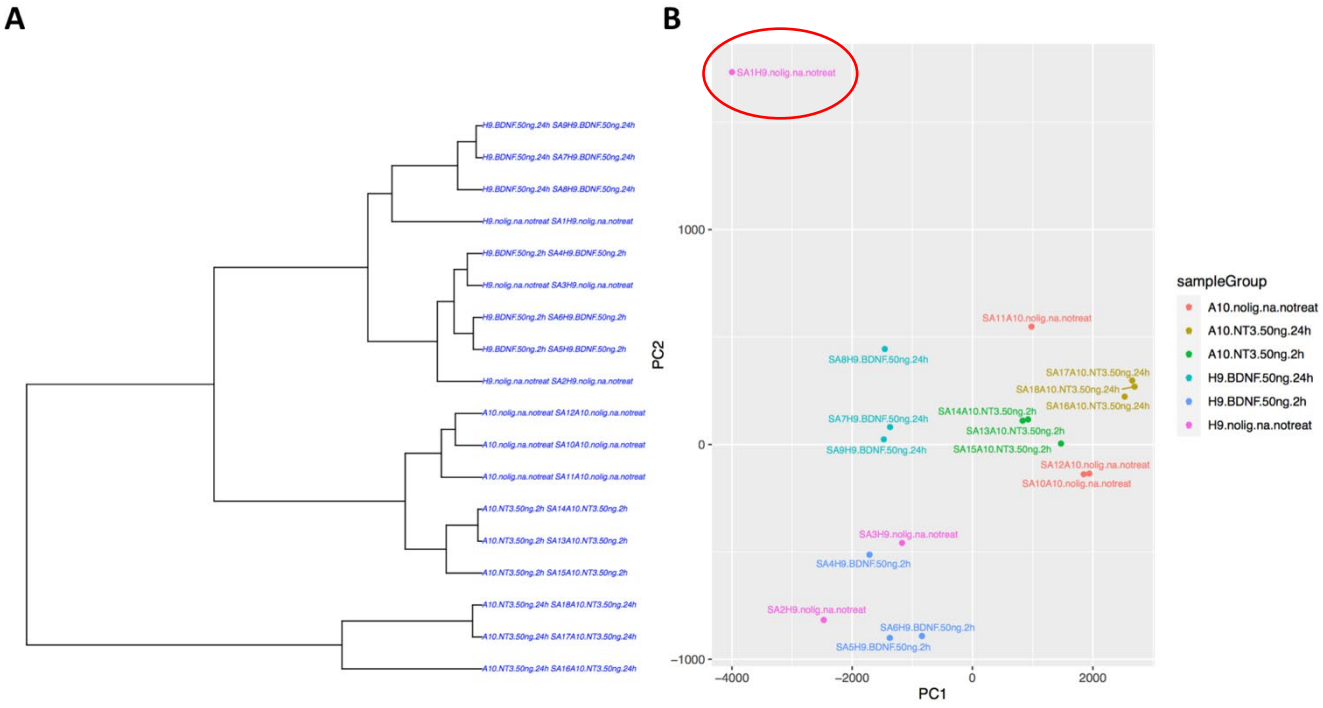

Figure 8.3. Principal Component Analysis (PCA) on all RNAseq samples.

PCA shows gene expression between different controls and treated samples. Each dot represents a treatment i.e. a single well and triplicates are designated the same colour (B). PCA indicates clustering of triplicates of the same treatment except sample 'SA1 H9 no treatment'. Visualisation of triplicate clustering, and lack thereof (B, red oval) and the similarities between each treatment in terms of gene expression is also shown (A).

8.2.2. Comparison of gene expression between untreated H9 and A10 neurons

As expected, only background levels of *NTRK1* (TrkA) and *NGFR* (p75) were detected in A10 neurons, in line with the previous RNAseq analysis performed with H9 neurons. By contrast, *NTRK2* (TrkB) mRNA was still readily detectable in A10 neurons. This was expected as it was not the *NTRK2* promoter that was targeted by the guide RNAs (see Chapter 5), a near impossible task given the multitude of promoters and splice variants described for human *NTRK2* (Luberg et al. 2010b). The strategy chosen was instead to target the *NTRK2* initiation codon and as detailed in Chapter 6, none of the 3 TrkB ligands examined generated a P-Trk signal (Figure 6.4). Furthermore, TrkB protein was hardly detectable in neuronal lysates, with the weak signal possibly the result of cross-reactivity with TrkC (see also Chapter 6, Figure 6.3A). These results indicate that successful translation initiation of activatable TrkB could not be achieved at significant levels with the *NTRK2* mRNA present in these neurons.

In line with the previous study with H9 neurons (Merkouris et al. 2018), a large number of expected neuronal markers were found to be expressed at significant levels, including DARPP-32 (*PPP1R1B*), CTIP2 (*BCL11B*), FOXP1 (*FOXP1*), FOXP2 (*FOXP2*), GAD65 (*GAD2*), GAD67 (*GAD1*) and the dopamine receptor D2 (*DRD2*). Importantly, the untreated H9 and A10 cells were found to be strikingly similar in terms of global gene expression, in spite of the time elapsed between the 2 different sets of experiments (4 years), the involvement of different experimentators and the unavoidable variability in cell culture reagents. In the absence of exposure to either BDNF or NT3, amongst the genes expressed at significant levels in both A10 and H9 neurons, namely 14,824 genes, only 695 and 589 were found to be preferentially expressed in A10 neurons and H9 neurons respectively (Figure 8.4). This means that H9 and A10 neurons shared expression of over 95% of genes.

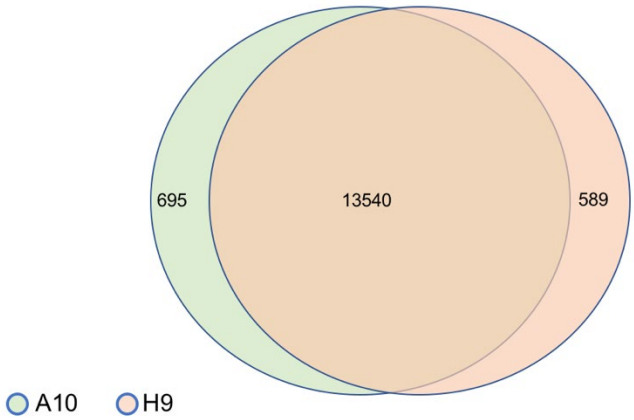

Figure 8.4. Genes expressed by untreated H9 and A10 neurons.

Venn diagram illustrating the number of genes that are shared and differentially expressed between untreated A10 and H9 cultures of neurons. The genes presented in this illustration have been selected based on absolute fold change > 2 and padj < 0.01 by the limma voom algorithm of the Bioconductor R package. Genes differentially expressed in A10 neurons (695) are shown in the green circle and genes differentially expressed in H9 neurons are shown in the orange circle (589). Genes shared between H9 and A10 are indicated in the overlapping section (13540).

As discussed in the context of neurotrophin receptor expression (see General Discussion), these results suggest that under the culture conditions used, the differentiation of hESCs into neurons follows a robust programme that unfolds without detectable interference caused by unavoidable variations between experiments, including small, but unavoidable variations in the composition of the cell culture medium and substrate including Matrigel. Beyond the use of different targeted clones (see Chapter 6), these results also argue for a lack of significant off-target effects of the CRISPR/Cas9 treatment potentially impacting the interpretation of the comparisons between the changes caused by the addition of NT3 to A10 neurons compared with BDNF and H9 neurons.

8.2.3. Transcriptional changes caused by the addition of NT3 to A10 neurons

A10 neurons were treated with NT3 and the transcription changes illustrated using volcano plots at 2 (Figure 8.5A) and 24 hours (Figure 8.5B).

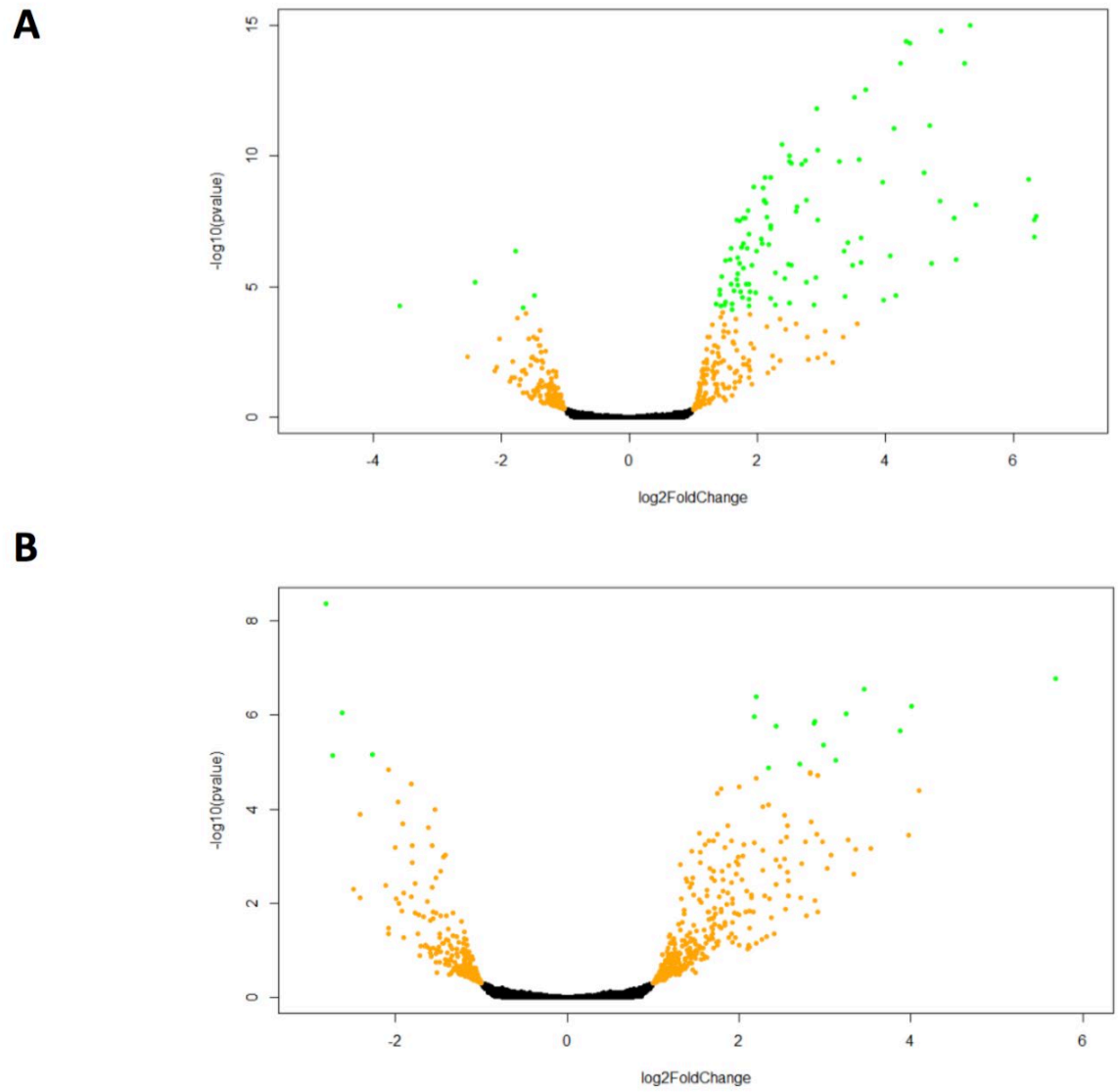

Figure 8.5. NT3-induced changes in gene expression of A10 neurons.

NT3-induced changes in gene expression of A10 neurons at 2 (A) and 24 hours (B). Each dot represents a gene. Black dots mark the genes with padj value > 0.01 and |log2foldchange| < 1. Orange colour marks the genes with padj value > 0.01 and |log2foldchange| > 1. Green colour marks the genes differentially expressed between the 2 conditions with padj < 0.01 and |log2foldchange| > 1. A clickable version of these data allowing identification of each gene as well as a full list of all genes with counts and fold changes will be deposited upon publication of the results.

To ease the overview of the results as well as the comparison with BDNF treatment (see below), the fold changes were plotted and ranked in decreasing order according to their log2 fold change for the 50 genes showing the largest changes observed 2 and 24 hours after the addition of NT3. This analysis revealed that 2 hours after the addition of NT3, a large proportion of the changes observed relate to genes involved in synaptic plasticity and regulated by neuronal activity (Figure 8.6A, red bars). For most genes, increased expression was transient with some such as *JUNB* and *FOSB* for example being even expressed at lower levels after 24 hours compared with neurons not exposed to NT3 (Figure 8.6B).

Figure 8.6. Genes most regulated by NT3 at 2 hours and 24 hours based on log2 fold changes).

Genes up-regulated or down-regulated by NT3 at 2 hours (A) and 24 hours (B) were ranked by log2 fold changes with padj < 0.01 whereby results with one or more zero raw counts in any of the triplicates were removed from the analysis. Red bars indicate genes belonging to a core set of synaptic plasticity genes regulated by neuronal activity (see for example Pruunsild et al. 2017).

A comparison with the previous RNAseq data generated with H9 neurons and also treated with saturating concentrations of ligand (2 nM BDNF treatment for 2 hours) revealed striking parallels, including a number genes related to synaptic plasticity (Figure 8.7A). Compared with the results obtained with NT3 addition, the changes in mRNA levels were found to be more long lasting with BDNF (Figure 8.7B), possibly reflecting the higher levels of TrkB expression compared with TrkC. As is apparent from the results detailed in Chapter 7, the higher levels of TrkB expression are also reflected in a considerably stronger P-Trk signal following the addition of BDNF to H9 neurons, compared with NT3 and A10 neurons.

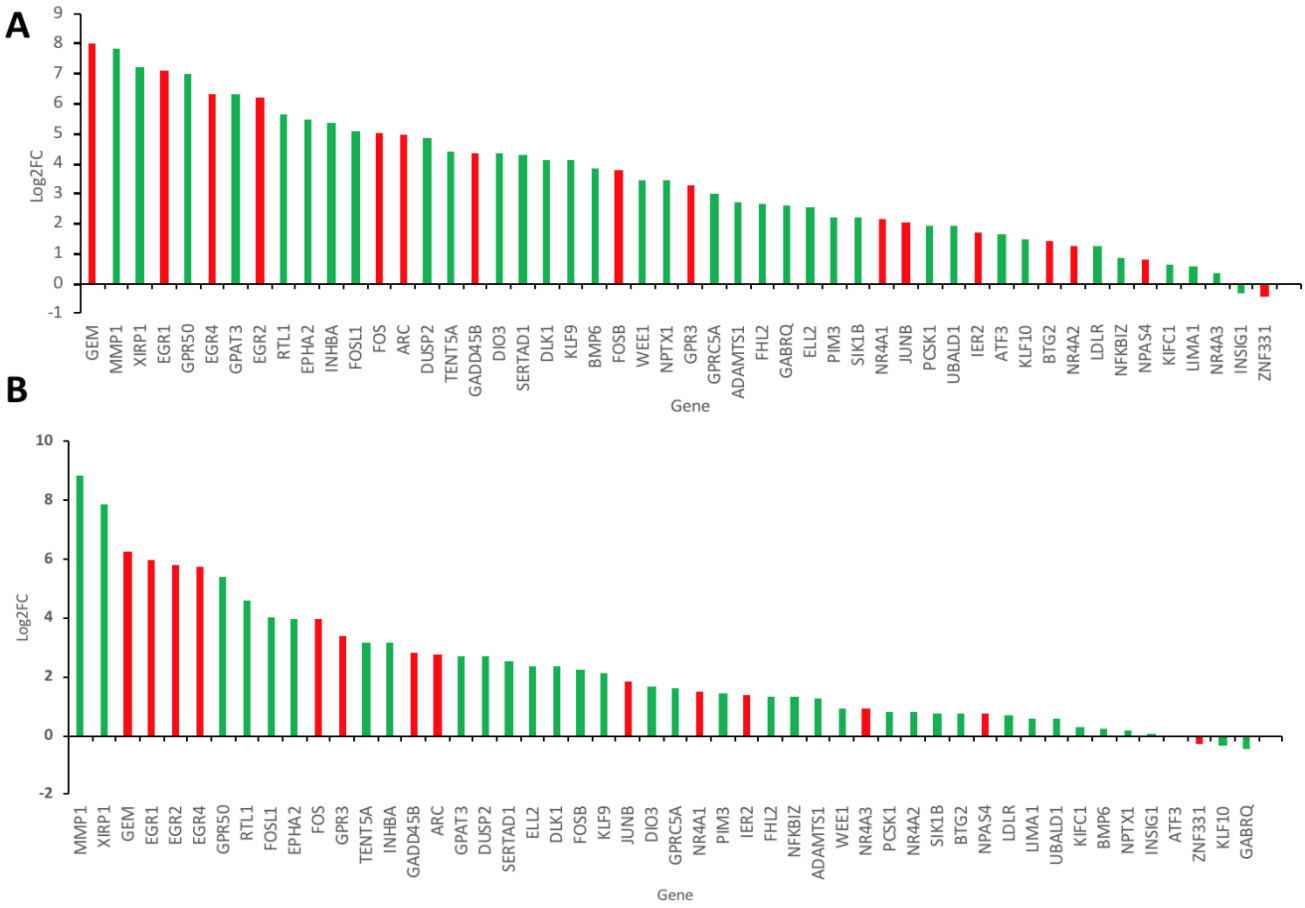

Figure 8.7. Genes most regulated by BDNF at 2 hours and 24 hours based on log2 fold changes.

Genes upregulated or downregulated by BDNF at 2 hours (A) and 24 hours (B) were ranked by fold changes using the same criteria as for A10 cells following NT3 treatment. Red bars also indicate genes regulated by neuronal activity in prolonged cultures of hiPSC-derived neurons (Pruunsild et al. 2017). Non-significant fold changes at 2 hours were noted for: *NFKBIZ, NPAS4, KIFC1, LIMA1, NR4A3* and *INSIG1* (Padj < 0.01) and at 24 hours (B), were noted for*: PCSK1, NR4A2, SIK1B, BTG2, NPAS4, LDLR, LIMA1, UBALD1, KIFC1, BMP6, NPTX1, INSIG1, ATF3, ZNF331, KLF10* and *GABRQ.*

The overall conclusion of these experiments is that most of the changes caused by the addition of NT3 are similar to what has been previously seen with BDNF in TrkB-expressing H9 neurons (Merkouris et al. 2018). In addition, many of the changes are related to genes involved in synaptic plasticity and are known to be regulated by neuronal activity. Some of the genes seemingly differently regulated by BDNF and NT3 were further investigated by RT-qPCR (Figure 8.8), including the activity-dependent, human-specific gene *ZNF331*. This is a zinc finger motif gene with no mouse orthologue rapidly induced in hiPSCs as a result of increased synaptic activity and neuronal depolarisation (Pruunsild et al. 2017). The genes in Figure 8.8 were selected as they appeared to be more up-regulated by NT3 than by BDNF. However, these additional investigations revealed that this apparent differential regulation of gene expression by BDNF in H9, and by NT3 in A10 neurons was simply due to their transient character and could not be confirmed reproducibly using RT-qPCR (Figure 8.8). Presumably, small differences between experimental conditions with regard to the timing of ligand addition and RNA extraction could explain this discrepancy as some of these genes react to ligand additions within minutes.

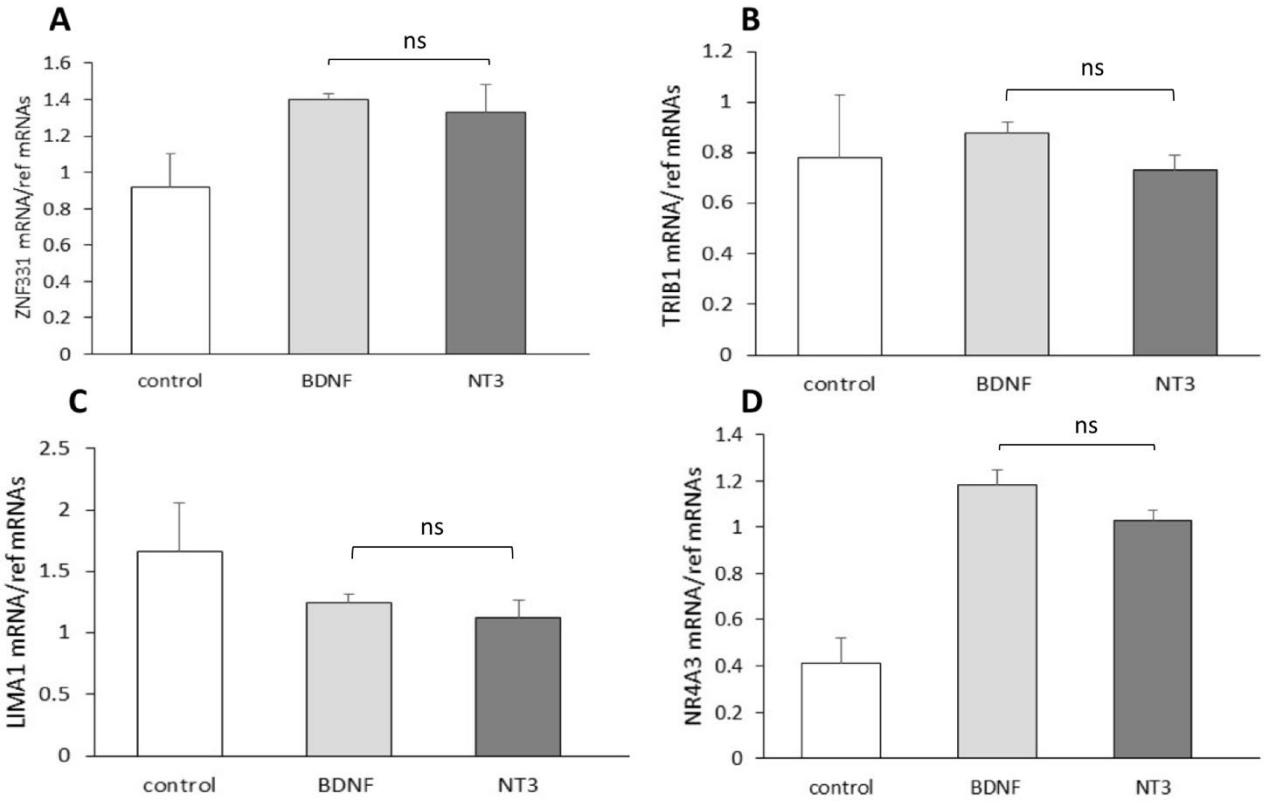

Figure 8.8. RT-qPCR of genes thought to be differentially regulated between BDNF-mediated TrkB phosphorylation and NT3-mediated TrkC phosphorylation.

RT-qPCR performed on RNA derived from H9 neurons after 100 pM ligand treatment. As this is hypothesised to be the concentration of NT3 that selectively activates TrkC the aim was to see a 'TrkC signature' in wild-type H9 neurons. The differential gene expression between NT3 and BDNF from the RNAseq experiment could not be reproduced when RT-qPCR was performed. Genes tested- A: *ZNF331*, B: *TRIB1*, C: *LIMA1*, D: *NR4A3*. The error bars refer to SEM and significance indicated with asterisks: ***p < 0.001, **p < 0.01 and ns = p >0.05. For all treatments n = 3.

These additional results thus further underline the overlap between genes regulated downstream of TrkB and TrkC activation. As such, temporal differences were to be expected given the much higher levels of P-Trk following TrkB activation compared with TrkC activation by NT3.

8.2.4. Validation of the induction of the synaptic plasticity marker *ARC* following Trk activation

The immediate early gene *ARC* (protein designated Arc/Arg3.1) was selected for further investigations as it has been thoroughly studied in the context of synaptic plasticity and TrkB activation by BDNF (for recent review, see Zhang and Bramham 2021). A well-characterised Arc monoclonal antibody was then used to probe membranes of lysates separated by SDS gel electrophoresis of H9 and A10 neurons treated for 1 hour with BDNF and NT3 respectively. Compared with basal Arc levels before addition of BDNF or NT3, Arc levels were found to be quite low and then markedly increased by the addition of either BDNF or NT3 (Figure 8.9A).

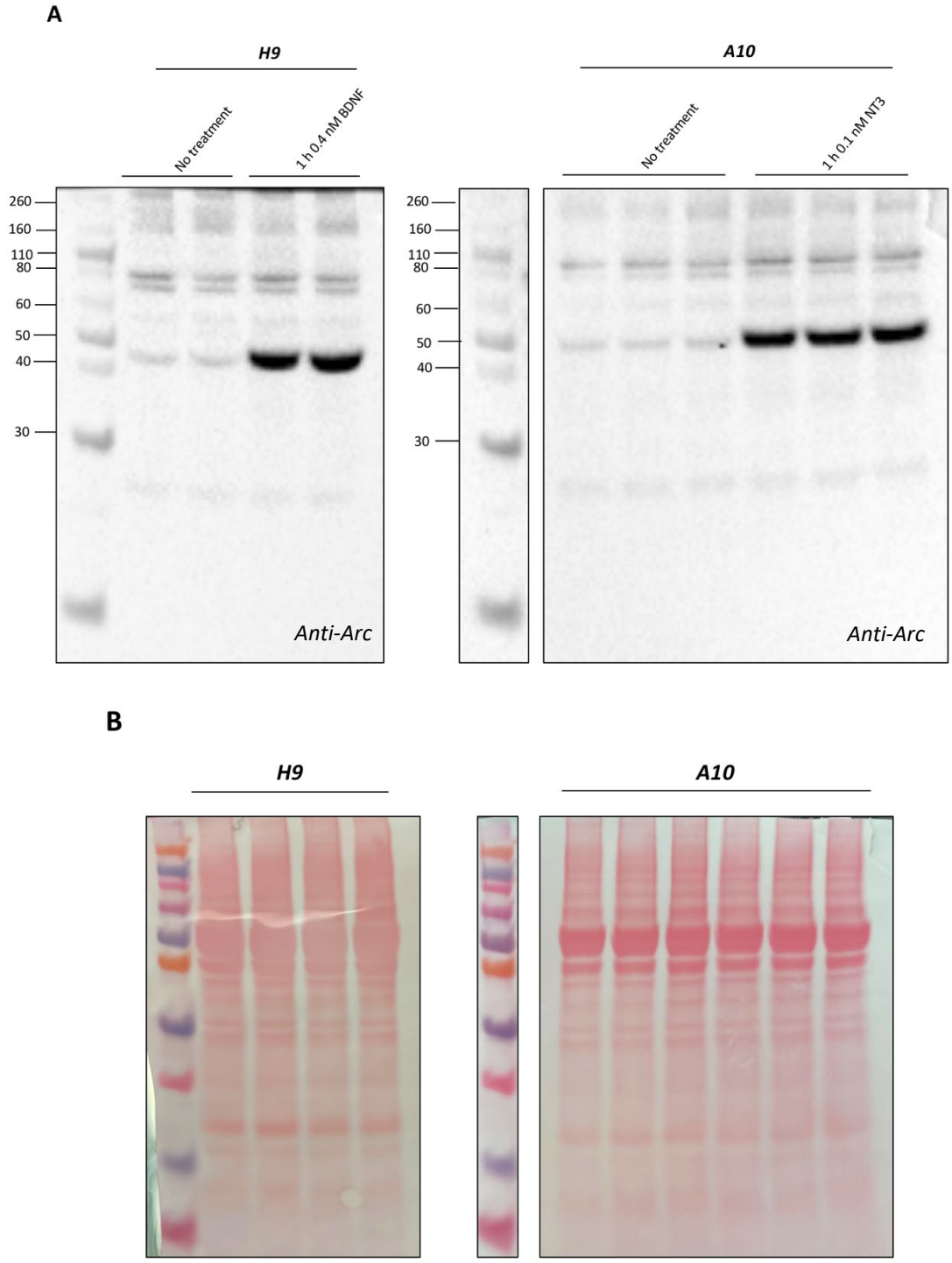

Figure 8.9. Arc is induced by both TrkB and TrkC activation.

Lysates of H9 (left panel) or A10 (right panel) neurons (as indicated) were separated by SDS gel electrophoresis and probed with an anti-Arc antibody (A). The denaturation step by DTT was omitted. Note that crucially, NT3 and BDNF induce the expression of Arc protein. Loading control synaptophysin was not performed in this case due to the similar molecular weights of synaptophysin and Arc protein whereby the Ponceau stains for both blots are shown (B).

8.3. Short discussion

Compared with molecular events downstream of TrkB and its activation by BDNF, very little is known about the role and mode of action of NT3 is the CNS (see General Introduction). Indeed, BDNF and TrkB have been dominating the neurotrophin signalling field in the CNS for some time due to the implications of this ligand-receptor pair in the physiopathology of the CNS. In addition, TrkC signalling is inherently difficult to study owing to the co-expression of TrkB and TrkC by most CNS neurons, the higher levels of expression of TrkB compared with TrkC and the ability of NT3 to activate TrkB.

The generation of cells lacking ligand-activatable forms of TrkB made it possible to gain insights into signalling events caused by NT3 induced Trk phosphorylation and to compare these results with those previously obtained using the same cellular system downstream of TrkB activation. By comparison with previous studies examining gene expression changes downstream of TrkB activation (Traub et al. 2017) or following increased activity in neuronal cultures derived from iPSCs (Pruunsild et al. 2007) the number as well as the magnitude of changes reported here are noticeably higher. A likely explanation is the homogeneity of the cultures, including the findings that all cultured neurons derived from H9 and A10 hESCs expressed TrkB and TrkC receptors.

The few potential differences in gene expression between NT3-TrkC signalling and BDNF-TrkB signalling could not be reproduced using RT-qPCR (Figure 8.8). This was not surprising, given that changes in mRNA expression can be quite transient with for example $p > 0.01$ for *LIMA1* and *NR4A3* mRNA after 2 hours of BDNF treatment. Therefore, the overall conclusion is that TrkC activation triggers very similar events compared with TrkB activation, with the potential of these events to be indistinguishable if better control of the exact timing of ligand addition and RNA extraction could be achieved. As noted, the higher levels of TrkB compared with TrkC are also bound to impact the respective kinetics of gene activation as many of the changes observed are the result of transcriptional cascades. A comparatively large number of changes involved genes related to synaptic plasticity, suggesting that *in vivo*, NT3 may trigger the same processes as BDNF with regard to the modulation of gene expression. As this interpretation raises the question of the biological significance of this dual signalling system, it is important to note that the *availability* of NT3 and BDNF is regulated very differently. As mentioned in the General Introduction, the genes encoding *BDNF* and *NTF3* are organised very differently whereby *BDNF* expression is primarily regulated by neuronal activity. This is not the case for *NTF3* with hormones such as thyroxine playing a dominant role.

Chapter 9 - General discussion

9.1. Overview

The results detailed in the previous chapters indicate that the neurons differentiated from cultured hESCs express the NT3 receptor TrkC, in addition to the BDNF receptor TrkB. To prevent TrkB activation by NT3, hESC clones lacking ligand-activatable forms of TrkB were generated and used to monitor transcriptional changes downstream of Trk activation by NT3. The justification for this "mass analysis" approach, i.e. the extraction of RNA from all cells treated or untreated with NT3, was the observation that essentially all cultured neurons expressed TrkC. The notion that TrkC expression is also functionally relevant in a very large proportion of the neurons was supported by the magnitude of changes in gene expression, in excess of 7-fold for over 50 genes 2 hours after NT3 addition. Amongst this large number of pronounced changes, several genes were identified that are known to be regulated by neuronal activity and involved in synaptic plasticity. Most of these changes overlap with those previously reported downstream of TrkB activation (Merkouris et al. 2018), further emphasising ligand availability, as opposed to events downstream of receptor activation, as the key feature of a signalling system based the secretion of both NT3 and BDNF. Indeed, the most novel observation emerging from these studies with human neurons was that NT3 triggered a Trk phosphorylation response at lower concentrations than those of BDNF required to activate TrkB. The following paragraph discusses some key characteristics of the *in vitro* system used here as well as the functional implications of these *in vitro* observations to the physiology of the developing brain.

9.2. Co-expression of TrkB and TrkC in the CNS

The co-expression of TrkB and TrkC in the CNS has been documented in the rodent CNS and double *in situ* hybridisation experiments with probes for these receptors and it was concluded that fewer than 15% of the neurons may express only one receptor (Kokaia et al. 1995). Comparative *in situ* hybridisation experiments using adjacent brain sections revealed strikingly similar patterns of expression throughout the rat brain (Numan and Seroogy 1999). Similar experiments in the adult pre-frontal cortex have indicated a similar situation in the human brain (Weickert et al. 2005). Importantly, these studies also reported a reduction of the levels of both TrkB and TrkC in several layers of the pre-frontal cortex of patients diagnosed with schizophrenia (Weickert et al. 2005). In a rat model of schizophrenia, activation of TrkB and TrkC by the agonist LM22B-10 has been recently reported to improve the behavioural phenotype (Tigaret et al. 2021). The notion that most CNS neurons express both TrkB and TrkC in humans is also supported by the results of RNAseq experiments published in the Allen Brain Atlas (Figure 9.1).

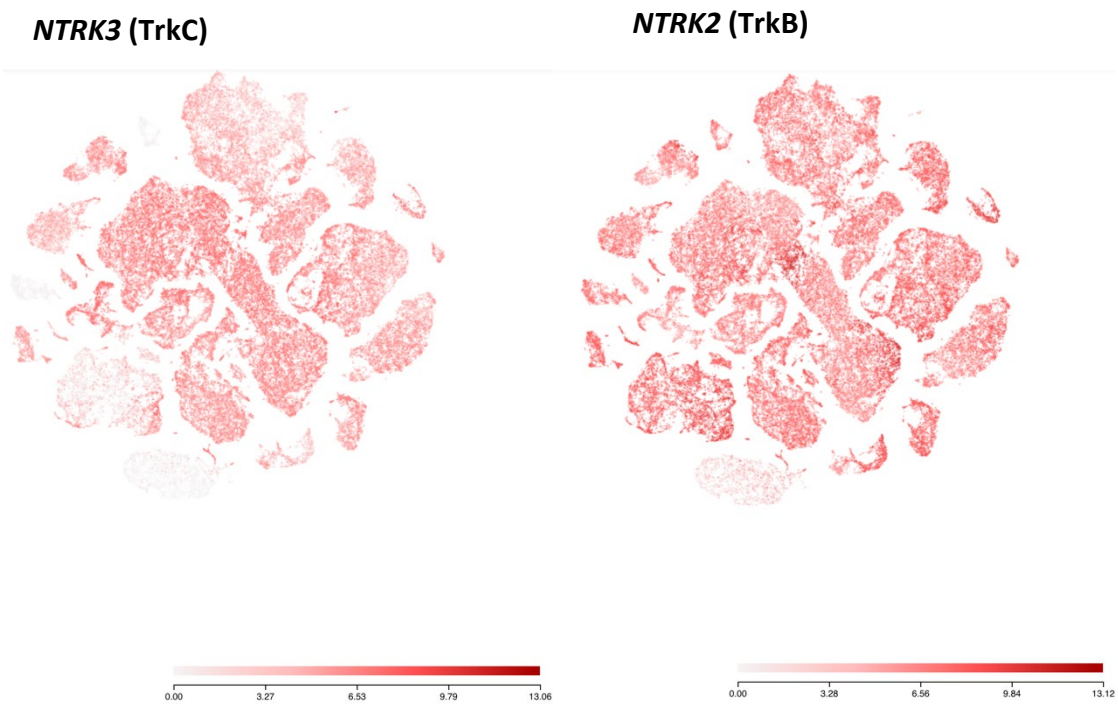

Figure 9.1. RNAseq data showing expression of *NTRK3* and *NTRK2* mRNA in the human brain.

RNAseq data showing visualisation of *NTRK3* and *NTRK2* mRNA expression in the human brain. These RNAseq data also indicate lower levels of expression of *NTRK3* compared with *NTRK2* as well as a lack of *NTRK1* and *NGFR* expression in most of the human brain. Link to data: *https://celltypes.brainmap.org/rnaseq/human_m1_10x?selectedVisualization=Scatter+Plot&colorByFeature=Gene+Expression&colorByFeatureValue=NTRK2*

These results further document the relevance of the cellular system used here with regard to the co-expression of TrkB and TrkC and the lack of expression of p75 and TrkA. As the protocol used to differentiate hESCs was not designed to generate neurons exhibiting these specific characteristics of neurotrophin receptor expression, this pattern is a particularly fortunate feature, presumably reflecting major developmental trajectories unfolding under the tissue culture conditions used. Unlike many other protocols leading to the generation of neurons from hESCs or iPSCs, including earlier versions of the protocol (Telezhkin et al. 2016a), no Trk agonists were used at any stage and TrkB and TrkC expressions are not detectable before about 2 weeks whereby this progressive expression of TrkB and TrkC is not accompanied by detectable expression of TrkA or p75, in line with the RNAseq data based on adult human CNS neurons discussed and cited in the above.

9.3. Trk activation by NT3 in the developing nervous system

9.3.1. PNS

The ability of NT3 to also activate TrkB has been a major problem in the field ever since the identification of TrkB as a BDNF receptor (see Introduction). Early binding studies performed with neurons dissociated from embryonic sensory neurons indicated the presence of large numbers of specific, high-affinity binding sites specific for NT3, but the molecular nature of these binding sites could not be established (Rodriguez-Tebar et al. 1992). The interpretation of these findings was further complicated by the observation that the neurotrophin receptor p75, expressed by most developing PNS neurons forms high affinity binding sites for NT3 (Dechant et al. 1993). The question of whether NT3 can also activate TrkB *in vivo*, in addition to TrkC, has been the topic of many studies with mouse mutants carrying Trk receptor deletions whereby no general conclusions could be reached. Whether or not NT3 can activate TrkB during development seems to depend on the stage of embryonic development and the PNS populations studied (Davies et al. 1995; Stenqvist et al. 2005).

9.3.2. CNS

In the CNS, single mouse mutants lacking either TrkB or TrkC did not show the dramatic phenotype readily observable in the PNS and characterised by the loss of entire sub-populations of neurons, accounting for the early post-natal death of the mutant animals. The observations made in the CNS led instead to the conclusion that TrkB and TrkC signalling might be somewhat redundant (Davies 1994; Minichiello and Klein 1996; Huang and Reichardt 2001). By contrast, more recent experiments involving restricted TrkC deletions as well as the marking of cells carrying the gene deletion clearly revealed the importance of the activation of TrkC by NT3 during post-natal development of the CNS (Joo et al. 2014). In particular, the deletion of TrkC in small numbers of cerebellar Purkinje cells revealed the relevance of NT3/TrkC signalling in the CNS. Specifically, the dendrites of neurons lacking TrkC failed to successfully compete with neighbouring dendrites expressing normal levels of TrkC to colonise the available space in the molecular layer of the cerebellar cortex (Joo et al. 2014). This observation is particularly relevant in the context of BDNF/TrkB versus NT3/TrkC signalling as cerebellar granule cells, the most abundant cell type of the brain (Nakashima et al. 2015) and the source of the input onto the dendrites of Purkinje cells, express both *Bdnf* and *Ntf3* (Hofer et al. 1990; Lindholm et al. 1993). Furthermore, the same study also shows that this competition between the dendrites of Purkinje cells is NT3-dependent as the deletion of NT3 in all granule cells prevents the effect of the sparse deletion of TrkC in Purkinje cells. These results thus revealed a crucial role for NT3/TrkC signalling in the assembly of a CNS

circuit also expressing BDNF and TrkB and provide a functional framework to appreciate the significance of the transcriptional changes caused by TrkB and TrkC activation, including genes regulated by neuronal activity. Most importantly, the new finding that NT3 activates TrkC at lower concentrations than is the case for BDNF activation of TrkB helps explain the activation of TrkC by NT3 in the presence of BDNF.

More generally, the notion of competition for limiting amounts of available growth factors is established in the peripheral nervous system and is at the core of the explanation for naturally occurring cell death during development and its regulation by neurotrophic factors (Barde 1989). However, it has been difficult to extrapolate this notion to the CNS, largely because most gene targeting experiments deleted the neurotrophins or their Trk receptors in all neurons. A notable exception was the deletion of BDNF from just a few neurons in the cerebral cortex (English et al. 2012). Unlike the deletion in all neurons, the sparse deletion of BDNF impaired the dendritic arborisation of these neurons, compared with their wild-type neighbours (English et al. 2012). Together with the sparse deletion of TrkC (Joo et al. 2014), these results further substantiate the notion that the neurotrophin-Trk signalling system is likely to operate at sub-saturating concentrations *in vivo*.

9.4. Unique features of the NT3/TrkC signalling system

By comparison with the other molecular components of the neurotrophin/tyrosine kinase receptor signalling system, both NT3 and TrkC have unique characteristics. On one hand, NT3 is the most promiscuous ligand as it can bind to and activate the kinase domain of the 3 known Trk receptors in mammals. On the other hand, TrkC is uniquely selective and NT3 its only neurotrophin ligand. These surprising characteristics may explain why comparatively little is known about TrkC-mediating signalling in the CNS whereby the most significant complicating factor is the co-expression of TrkB and TrkC by most CNS neurons. An additional feature of TrkC not shared with TrkA and TrkB is its binding affinity for the pre-synaptic protein phosphatase σ (PTPσ). This particular ligand-receptor pair has been demonstrated to have "synaptogenic" properties resulting in the formation of glutamatergic synapses (Takahashi et al. 2011), whereby NT3 potentiates the association between PTPσ and TrkC (Ammendrup-Johnsen et al. 2015). In addition, the TrkC extracellular domain involved PTPσ binding was shown to be distinct from the NT3 binding domain (Takahashi et al. 2011). These previous results further emphasise the role of TrkC in mechanisms involved in the assembly of the nervous system and highlight the need to better understand the role of TrkC activation with regard to regulation of gene expression. In this context, it is noteworthy that several of the genes whose expression is up-regulated following TrkC activation are known to be involved in synaptic plasticity. These include a number of genes regulated by neuronal activity including *NPAS4*, a basic-helix-loop-helix transcription factor belonging to the family of inducible immediate early genes (IEGs) activated within minutes of stimulation to regulate the formation of inhibitory synapses (for review, see Fu et al. 2020). As the major pathway regulating gene expression by neuronal activity involves the cyclic AMP response element (CRE)-binding protein (CREB) (for review, see Shaywitz and Greenberg 1999) just as is also the case downstream of Trk activation, this convergence at the level of changes in gene expression is not surprising. What remains to be seen is whether Trk activation alters the excitability of the neuronal network formed by cultured neurons whereby is not clear if functional synapses have already formed in significant numbers in the relatively young cultures used in this study (neurons are used between DIV 27 and 33). For example, the Pruunsild et al. 2017 study reported a small number (slightly in excess of 100) of relatively small changes in cultures that were maintained for 100 days and depolarised with 4 aminopyridine.

9.5. Trk activation and transcriptional changes

Throughout the project, the activation of TrkB and TrkC by their corresponding ligands was monitored using kinase domain activation as a read out and antibodies specifically recognising phosphorylated tyrosine residues located in what is known as the activation loop of tyrosine kinase receptors (Cunningham et al. 1997; MacDonald et al. 2000). The sequence targeted by the antibodies reporting the tyrosine phosphorylation of this activation loop is identical for the 3 Trk receptors (see Chapter 5, Short Introduction). As a result, the specific identity of activated Trk receptors, in this case TrkB and TrkC cannot be distinguished using these antibodies. Despite this, with regard to the monitoring of Trk receptor activation, one of the questions at the core of the project, these antibodies are invaluable tools. In addition, the 3 Trk receptors can be phosphorylated on tyrosine residues activated by other cell surface receptors, including G protein coupled receptors (for review, see Lee et al. 2002). These mechanisms involve the phosphorylation of tyrosine residues outside the activation loop and are mediated by small tyrosine kinases of the Src family activated by cell surface receptors such as adenosine or epidermal growth factor receptors (Lee and Chao 2001; Puehringer et al. 2013). This means that the phosphorylation of tyrosine residues of Trk receptors does not necessarily mean activation of the kinase domains of the receptors. Whether or not such mechanisms may play a role in the recent discovery that all antidepressants cause TrkB phosphorylation is not entirely clear as the study did not use antibodies targeting the kinase activation loop (Casarotto et al. 2021).

The comparison of the transcriptional changes caused by the addition of either BDNF to H9 neurons or of NT3 to A10 neurons indicate striking similarities (see Chapter 8). Notably, a number of genes known to be increased by neuronal activity and to play a role in synaptic plasticity are induced by the addition of BDNF and NT3. These include a number of DNA binding proteins and transcription factors known as immediate early genes as well one of the most studied gene products in the context of synaptic plasticity and TrkB activation by BDNF, namely Arc, also designated Arg3.1 (Bramham et al. 2008; Nikolaienko et al. 2018; Zhang and Bramham 2021).

Small differences between the pattern and especially the fold-changes downstream of BDNF and NT3 addition should be interpreted with caution as the changes were analysed at single time points (see Chapter 8 for further details). As the parallels between the transcriptional changes induced by increasing the excitability of the cultures and the activation of

neurotrophin receptors are striking, it would be interesting to investigate whether or not the addition of neurotrophins modulates the excitability of the cultures. Neurotrophins including NT3 have been shown to cause increased neurotransmitter release (Lohof et al. 1993; He et al. 2000) and it is conceivable that such mechanisms may play a role. As such, the parallels between changes in gene transcription induced by increased activity following neuronal depolarisation and Trk receptor activation are not surprising given that the pathways converge on DNA binding elements such as the cAMP response element-binding protein (CREB) that is phosphorylated following the activation of both pathways (for review, see Shaywitz and Greenberg 1999). Calcium imaging of the cultures before and after neurotrophin addition may help answering such questions whereby changes in neuronal activity typically lead to smaller and fewer transcriptional changes compared with those reported here (see for example Pruunsild et al. 2017).

9.6. Outlook

While the neurotrophin field has been increasingly dominated by BDNF because of its established relevance to the physiopathology of the CNS, especially with the discovery of mutations and polymorphisms in the *BDNF* and *NTRK2* genes, the work detailed in the above related to NT3 signalling indicates that NT3 and TrkC are likely to be as relevant to CNS function as BDNF and TrkB. The parallels between these signalling systems are striking whereby these investigations were only made possible following the realisation that post-mitotic neurons can be reproducibly generated from hESCs in unlimited numbers. In addition, with the core characteristics of receptor expression being strikingly similar to those in the human brain: Co-expression of TrkB and TrkC coupled with lack of detectable expression of p75 and TrkA. In the future, it will be interesting to understand the nature of the molecular cascades leading to the generation of cultured neurons with such relevant properties. Investigations of these kinds may lead to the discovery of core programmes of differentiation of human CNS neurons leading to specific patterns of receptor expression, under conditions where the expression of these receptors is not used to direct the differentiation of these neurons.

References

Ammendrup-Johnsen, I., Naito, Y., Craig, A. M. and Takahashi, H. (2015). Neurotrophin-3 Enhances the Synaptic Organizing Function of TrkC-Protein Tyrosine Phosphatase sigma in Rat Hippocampal Neurons. *J Neurosci* 35(36), pp. 12425-12431. 10.1523/JNEUROSCI.1330-15.2015.

Arber, C., Precious, S. V., Cambray, S., Risner-Janiczek, J. R., Kelly, C., Noakes, Z., Fjodorova, M. *et al.* (2015). Activin A directs striatal projection neuron differentiation of human pluripotent stem cells. *Development* 142(7), pp. 1375-1386. 10.1242/dev.117093.

Ateaque, S. and Barde, Y. A. (2021). A new molecular target for antidepressants. *Cell Res* 31(5), pp. 489-490. 10.1038/s41422-021-00500-1.

Banfield, M. J., Naylor, R. L., Robertson, A. G., Allen, S. J., Dawbarn, D. and Brady, R. L. (2001). Specificity in Trk receptor:neurotrophin interactions: the crystal structure of TrkB-d5 in complex with neurotrophin-4/5. *Structure* 9(12), pp. 1191-1199. 10.1016/s0969-2126(01)00681-5.

Barbacid, M. (1994). The Trk family of neurotrophin receptors. *J Neurobiol* 25(11), pp. 1386-1403. 10.1002/neu.480251107.

Barde, Y. A. (1989). Trophic factors and neuronal survival. *Neuron* 2(6), pp. 1525-1534. 10.1016/0896-6273(89)90040-8.

Barde, Y. A., Edgar, D. and Thoenen, H. (1982). Purification of a new neurotrophic factor from mammalian brain. *Embo j* 1(5), pp. 549-553.

Barker, P. A., Mantyh, P., Arendt-Nielsen, L., Viktrup, L. and Tive, L. (2020). Nerve Growth Factor Signaling and Its Contribution to Pain. *J Pain Res* 13(pp. 1223-1241. 10.2147/JPR.S247472.

Bergner, A., Oganessyan, V., Muta, T., Iwanaga, S., Typke, D., Huber, R. and Bode, W. (1996). Crystal structure of a coagulogen, the clotting protein from horseshoe crab: a structural homologue of nerve growth factor. *EMBO J* 15(24), pp. 6789-6797.

Bibel, M. and Barde, Y. A. (2000). Neurotrophins: key regulators of cell fate and cell shape in the vertebrate nervous system. *Genes Dev* 14(23), pp. 2919-2937. 10.1101/gad.841400.

Bibel, M., Hoppe, E. and Barde, Y.-A. (1999a). Biochemical and functional interactions between the neurotrophin receptors trk and p75NTR. *The EMBO Journal* 18(3), pp. 616-622. https://doi.org/10.1093/emboj/18.3.616.

Bibel, M., Hoppe, E. and Barde, Y. A. (1999b). Biochemical and functional interactions between the neurotrophin receptors trk and p75NTR. *EMBO J* 18(3), pp. 616-622. 10.1093/emboj/18.3.616.

Bochukova, E. G., Lawler, K., Croizier, S., Keogh, J. M., Patel, N., Strohbehn, G., Lo, K. K. *et al.* (2018). A Transcriptomic Signature of the Hypothalamic Response to Fasting and BDNF Deficiency in Prader-Willi Syndrome. *Cell Rep* 22(13), pp. 3401-3408. 10.1016/j.celrep.2018.03.018.

Boltaev, U., Meyer, Y., Tolibzoda, F., Jacques, T., Gassaway, M., Xu, Q., Wagner, F. *et al.* (2017). Multiplex quantitative assays indicate a need for reevaluating reported small-molecule TrkB agonists. *Sci Signal* 10(493), pp. 10.1126/scisignal.aal1670.

Bothwell, M. (2014). NGF, BDNF, NT3, and NT4. *Handb Exp Pharmacol* 220(pp. 3-15. 10.1007/978-3-642-45106-5_1.

Bramham, C. R., Worley, P. F., Moore, M. J. and Guzowski, J. F. (2008). The immediate early gene arc/arg3.1: regulation, mechanisms, and function. *J Neurosci* 28(46), pp. 11760-11767. 10.1523/JNEUROSCI.3864-08.2008.

Bruntraeger, M., Byrne, M., Long, K. and Bassett, A. R. (2019). Editing the genome of human induced pluripotent stem cells using CRISPR/Cas9 ribonucleoprotein complexes.*CRISPR Gene Editing*. Humana Press, New York, NY, pp. 153-183.

Bueker, E. D. (1948). Implantation of tumors in the hind limb field of the embryonic chick and the developmental response of the lumbosacral nervous system. *Anat Rec* 102(3), pp. 369-389. 10.1002/ar.1091020309.

Casarotto, P. C., Girych, M., Fred, S. M., Kovaleva, V., Moliner, R., Enkavi, G., Biojone, C. *et al.* (2021). Antidepressant drugs act by directly binding to TRKB neurotrophin receptors. *Cell* 184(5), pp. 1299-1313 e1219. 10.1016/j.cell.2021.01.034.

Castren, E. and Kojima, M. (2017). Brain-derived neurotrophic factor in mood disorders and antidepressant treatments. *Neurobiol Dis* 97(Pt B), pp. 119-126. 10.1016/j.nbd.2016.07.010.

Chambers, S. M., Fasano, C. A., Papapetrou, E. P., Tomishima, M., Sadelain, M. and Studer, L. (2009). Highly efficient neural conversion of human ES and iPS cells by dual inhibition of SMAD signaling. *Nat Biotechnol* 27(3), pp. 275-280. 10.1038/nbt.1529.

Cohen, S. (1960). PURIFICATION OF A NERVE-GROWTH PROMOTING PROTEIN FROM THE MOUSE SALIVARY GLAND AND ITS NEURO-CYTOTOXIC ANTISERUM. *Proc Natl Acad Sci U S A* 46(3), pp. 302-311. 10.1073/pnas.46.3.302.

Cohen, S. and Levi-Montalcini, R. (1957). Purification and properties of a nerve growth-promoting factor isolated from mouse sarcoma 180. *Cancer Res* 17(1), pp. 15-20.

Crowley, C., Spencer, S. D., Nishimura, M. C., Chen, K. S., Pitts-Meek, S., Armanini, M. P., Ling, L. H. *et al.* (1994). Mice lacking nerve growth factor display perinatal loss of sensory and sympathetic neurons yet develop basal forebrain cholinergic neurons. *Cell* 76(6), pp. 1001-1011. 10.1016/0092-8674(94)90378-6.

Cunningham, M. E., Stephens, R. M., Kaplan, D. R. and Greene, L. A. (1997). Autophosphorylation of activation loop tyrosines regulates signaling by the TRK nerve growth factor receptor. *J Biol Chem* 272(16), pp. 10957-10967. 10.1074/jbc.272.16.10957.

Davies, A. M. (1994). The role of neurotrophins in the developing nervous system. *J Neurobiol* 25(11), pp. 1334-1348. 10.1002/neu.480251103.

Davies, A. M., Minichiello, L. and Klein, R. (1995). Developmental changes in NT3 signalling via TrkA and TrkB in embryonic neurons. *Embo j* 14(18), pp. 4482-4489.

Dechant, G., Rodriguez-Tebar, A., Kolbeck, R. and Barde, Y. A. (1993). Specific high-affinity receptors for neurotrophin-3 on sympathetic neurons. *J Neurosci* 13(6), pp. 2610-2616.

Doudna, J. A. and Charpentier, E. (2014). Genome editing. The new frontier of genome engineering with CRISPR-Cas9. *Science* 346(6213), pp. 1258096. 10.1126/science.1258096.

Egan, M. F., Kojima, M., Callicott, J. H., Goldberg, T. E., Kolachana, B. S., Bertolino, A., Zaitsev, E. *et al.* (2003). The BDNF val66met polymorphism affects activity-dependent secretion of BDNF and human memory and hippocampal function. *Cell* 112(2), pp. 257-269. 10.1016/s0092-8674(03)00035-7.

Einarsdottir, E., Carlsson, A., Minde, J., Toolanen, G., Svensson, O., Solders, G., Holmgren, G. *et al.* (2004). A mutation in the nerve growth factor beta gene (NGFB) causes loss of pain perception. *Hum Mol Genet* 13(8), pp. 799-805. 10.1093/hmg/ddh096.

Eisenberg, D. P., Ianni, A. M., Wei, S. M., Kohn, P. D., Kolachana, B., Apud, J., Weinberger, D. R. *et al.* (2013). Hippocampal dysfunction in schizophrenia: association with brain-derived neurotrophic factor genotype. *Mol Psychiatry* 18(6), pp. 631. 10.1038/mp.2013.53.

English, C. N., Vigers, A. J. and Jones, K. R. (2012). Genetic evidence that brain-derived neurotrophic factor mediates competitive interactions between individual cortical neurons. *Proc Natl Acad Sci U S A* 109(47), pp. 19456-19461. 10.1073/pnas.1206492109.

Ernfors, P., Henschen, A., Olson, L. and Persson, H. (1989). Expression of nerve growth factor receptor mRNA is developmentally regulated and increased after axotomy in rat spinal cord motoneurons. *Neuron* 2(6), pp. 1605-1613. 10.1016/0896-6273(89)90049-4.

Ernfors, P., Ibáñez, C. F., Ebendal, T., Olson, L. and Persson, H. (1990). Molecular cloning and neurotrophic activities of a protein with structural similarities to nerve growth factor: developmental and topographical expression in the brain. *Proc Natl Acad Sci U S A* 87(14), pp. 5454-5458. 10.1073/pnas.87.14.5454.

Ernfors, P., Lee, K. F. and Jaenisch, R. (1994a). Mice lacking brain-derived neurotrophic factor develop with sensory deficits. *Nature* 368(6467), pp. 147-150. 10.1038/368147a0.

Ernfors, P., Lee, K. F., Kucera, J. and Jaenisch, R. (1994b). Lack of neurotrophin-3 leads to deficiencies in the peripheral nervous system and loss of limb proprioceptive afferents. *Cell* 77(4), pp. 503-512. 10.1016/0092-8674(94)90213-5.

Ernfors, P., Van De Water, T., Loring, J. and Jaenisch, R. (1995). Complementary roles of BDNF and NT-3 in vestibular and auditory development. *Neuron* 14(6), pp. 1153-1164. 10.1016/0896-6273(95)90263-5.

Farinas, I., Jones, K. R., Backus, C., Wang, X. Y. and Reichardt, L. F. (1994). Severe sensory and sympathetic deficits in mice lacking neurotrophin-3. *Nature* 369(6482), pp. 658-661. 10.1038/369658a0.

Franco, M. L., Nadezhdin, K. D., Goncharuk, S. A., Mineev, K. S., Arseniev, A. S. and Vilar, M. (2020). Structural basis of the transmembrane domain dimerization and rotation in the activation mechanism of the TRKA receptor by nerve growth factor. *J Biol Chem* 295(1), pp. 275-286. 10.1074/jbc.RA119.011312.

Fu, J., Guo, O., Zhen, Z. and Zhen, J. (2020). Essential Functions of the Transcription Factor Npas4 in Neural Circuit Development, Plasticity, and Diseases. *Front Neurosci* 14(pp. 603373. 10.3389/fnins.2020.603373.

Glass, D. J., Nye, S. H., Hantzopoulos, P., Macchi, M. J., Squinto, S. P., Goldfarb, M. and Yancopoulos, G. D. (1991). TrkB mediates BDNF/NT-3-dependent survival and proliferation

in fibroblasts lacking the low affinity NGF receptor. *Cell* 66(2), pp. 405-413. 10.1016/0092-8674(91)90629-d.

Gorski, J. A., Balogh, S. A., Wehner, J. M. and Jones, K. R. (2003). Learning deficits in forebrain-restricted brain-derived neurotrophic factor mutant mice. *Neuroscience* 121(2), pp. 341-354.

Greene, L. A. and Tischler, A. S. (1976). Establishment of a noradrenergic clonal line of rat adrenal pheochromocytoma cells which respond to nerve growth factor. *Proc Natl Acad Sci U S A* 73(7), pp. 2424-2428. 10.1073/pnas.73.7.2424.

Hallbook, F., Ibanez, C. F. and Persson, H. (1991). Evolutionary studies of the nerve growth factor family reveal a novel member abundantly expressed in Xenopus ovary. *Neuron* 6(5), pp. 845-858. 10.1016/0896-6273(91)90180-8.

Hamburger, V. (1934). The effects of wing bud extirpation on the development of the central nervous system in chick embryos. *Journal of Experimental Zoology* 68(pp. 449-494.

Hamburger, V. (1993). The history of the discovery of the nerve growth factor. *J Neurobiol* 24(7), pp. 893-897. 10.1002/neu.480240702.

Han, F., Guan, X., Guo, W. and Lu, B. (2019). Therapeutic potential of a TrkB agonistic antibody for ischemic brain injury. *Neurobiol Dis* 127(pp. 570-581. 10.1016/j.nbd.2019.04.009.

He, X., Yang, F., Xie, Z. and Lu, B. (2000). Intracellular Ca(2+) and Ca(2+)/calmodulin-dependent kinase II mediate acute potentiation of neurotransmitter release by neurotrophin-3. *J Cell Biol* 149(4), pp. 783-792. 10.1083/jcb.149.4.783.

Hempstead, B. L., Martin-Zanca, D., Kaplan, D. R., Parada, L. F. and Chao, M. V. (1991). High-affinity NGF binding requires coexpression of the trk proto-oncogene and the low-affinity NGF receptor. *Nature* 350(6320), pp. 678-683. 10.1038/350678a0.

Hernandez-Echeagaray, E. (2020). Neurotrophin-3 modulates synaptic transmission. *Vitam Horm* 114(pp. 71-89. 10.1016/bs.vh.2020.04.008.

Hofer, M., Pagliusi, S. R., Hohn, A., Leibrock, J. and Barde, Y. A. (1990). Regional distribution of brain-derived neurotrophic factor mRNA in the adult mouse brain. *EMBO J* 9(8), pp. 2459-2464.

Hofer, M. M. and Barde, Y. A. (1988). Brain-derived neurotrophic factor prevents neuronal death in vivo. *Nature* 331(6153), pp. 261-262. 10.1038/331261a0.

Hohn, A., Leibrock, J., Bailey, K. and Barde, Y. A. (1990). Identification and characterization of a novel member of the nerve growth factor/brain-derived neurotrophic factor family. *Nature* 344(6264), pp. 339-341. 10.1038/344339a0.

Honea, R. A., Cruchaga, C., Perea, R. D., Saykin, A. J., Burns, J. M., Weinberger, D. R., Goate, A. M. *et al.* (2013). Characterizing the role of brain derived neurotrophic factor genetic variation in Alzheimer's disease neurodegeneration. *PLoS One* 8(9), pp. e76001. 10.1371/journal.pone.0076001.

Huang, E. J. and Reichardt, L. F. (2001). Neurotrophins: roles in neuronal development and function. *Annu Rev Neurosci* 24(pp. 677-736. 10.1146/annurev.neuro.24.1.677.

Indo, Y., Tsuruta, M., Hayashida, Y., Karim, M. A., Ohta, K., Kawano, T., Mitsubuchi, H. *et al.* (1996). Mutations in the TRKA/NGF receptor gene in patients with congenital insensitivity to pain with anhidrosis. *Nat Genet* 13(4), pp. 485-488. 10.1038/ng0896-485.

Ip, N. Y., Ibáñez, C. F., Nye, S. H., McClain, J., Jones, P. F., Gies, D. R., Belluscio, L. *et al.* (1992). Mammalian neurotrophin-4: structure, chromosomal localization, tissue distribution, and receptor specificity. *Proc Natl Acad Sci U S A* 89(7), pp. 3060-3064. 10.1073/pnas.89.7.3060.

Jerónimo-Santos, A., Vaz, S. H., Parreira, S., Rapaz-Lérias, S., Caetano, A. P., Buée-Scherrer, V., Castrén, E. *et al.* (2014). Dysregulation of TrkB Receptors and BDNF Function by Amyloid-β Peptide is Mediated by Calpain. *Cerebral Cortex* 25(9), pp. 3107-3121. 10.1093/cercor/bhu105.

Johnson, D., Lanahan, A., Buck, C. R., Sehgal, A., Morgan, C., Mercer, E., Bothwell, M. *et al.* (1986). Expression and structure of the human NGF receptor. *Cell* 47(4), pp. 545-554. 10.1016/0092-8674(86)90619-7.

Jones, B. D. M., Farooqui, S., Kloiber, S., Husain, M. O., Mulsant, B. H. and Husain, M. I. (2021). Targeting Metabolic Dysfunction for the Treatment of Mood Disorders: Review of the Evidence. *Life (Basel)* 11(8), pp. 10.3390/life11080819.

Jones, K. R., Fariñas, I., Backus, C. and Reichardt, L. F. (1994). Targeted disruption of the BDNF gene perturbs brain and sensory neuron development but not motor neuron development. *Cell* 76(6), pp. 989-999. 10.1016/0092-8674(94)90377-8.

Jones, K. R. and Reichardt, L. F. (1990). Molecular cloning of a human gene that is a member of the nerve growth factor family. *Proc Natl Acad Sci U S A* 87(20), pp. 8060-8064. 10.1073/pnas.87.20.8060.

Joo, W., Hippenmeyer, S. and Luo, L. (2014). Neurodevelopment. Dendrite morphogenesis depends on relative levels of NT-3/TrkC signaling. *Science* 346(6209), pp. 626-629. 10.1126/science.1258996.

Kaisho, Y., Yoshimura, K. and Nakahama, K. (1990). Cloning and expression of a cDNA encoding a novel human neurotrophic factor. *FEBS Lett* 266(1-2), pp. 187-191. 10.1016/0014-5793(90)81536-w.

Kaplan, D. R., Martin-Zanca, D. and Parada, L. F. (1991). Tyrosine phosphorylation and tyrosine kinase activity of the trk proto-oncogene product induced by NGF. *Nature* 350(6314), pp. 158-160. 10.1038/350158a0.

Katoh-Semba, R., Takeuchi, I. K., Inaguma, Y., Ito, H. and Kato, K. (1999). Brain-derived neurotrophic factor, nerve growth and neurotrophin-3 selected regions of the rat brain following kainic acid-induced seizure activity. *Neurosci Res* 35(1), pp. 19-29. 10.1016/s0168-0102(99)00059-0.

Klein, R., Jing, S. Q., Nanduri, V., O'Rourke, E. and Barbacid, M. (1991a). The trk proto-oncogene encodes a receptor for nerve growth factor. *Cell* 65(1), pp. 189-197. 10.1016/0092-8674(91)90419-y.

Klein, R., Lamballe, F., Bryant, S. and Barbacid, M. (1992). The trkB tyrosine protein kinase is a receptor for neurotrophin-4. *Neuron* 8(5), pp. 947-956. 10.1016/0896-6273(92)90209-v.

Klein, R., Nanduri, V., Jing, S. A., Lamballe, F., Tapley, P., Bryant, S., Cordon-Cardo, C. *et al.* (1991b). The trkB tyrosine protein kinase is a receptor for brain-derived neurotrophic factor and neurotrophin-3. *Cell* 66(2), pp. 395-403. 10.1016/0092-8674(91)90628-c.

Klein, R., Parada, L. F., Coulier, F. and Barbacid, M. (1989). trkB, a novel tyrosine protein kinase receptor expressed during mouse neural development. *Embo j* 8(12), pp. 3701-3709.

Klein, R., Silos-Santiago, I., Smeyne, R. J., Lira, S. A., Brambilla, R., Bryant, S., Zhang, L. *et al.* (1994). Disruption of the neurotrophin-3 receptor gene trkC eliminates la muscle afferents and results in abnormal movements. *Nature* 368(6468), pp. 249-251. 10.1038/368249a0.

Klein, R., Smeyne, R. J., Wurst, W., Long, L. K., Auerbach, B. A., Joyner, A. L. and Barbacid, M. (1993). Targeted disruption of the trkB neurotrophin receptor gene results in nervous system lesions and neonatal death. *Cell* 75(1), pp. 113-122.

Kokaia, Z., Metsis, M., Kokaia, M., Elmer, E. and Lindvall, O. (1995). Co-expression of TrkB and TrkC receptors in CNS neurones suggests regulation by multiple neurotrophins. *Neuroreport* 6(5), pp. 769-772. 10.1097/00001756-199503270-00016.

Korte, M., Carroll, P., Wolf, E., Brem, G., Thoenen, H. and Bonhoeffer, T. (1995). Hippocampal long-term potentiation is impaired in mice lacking brain-derived neurotrophic factor. *Proc Natl Acad Sci U S A* 92(19), pp. 8856-8860. 10.1073/pnas.92.19.8856.

Kuruvilla, R., Zweifel, L. S., Glebova, N. O., Lonze, B. E., Valdez, G., Ye, H. and Ginty, D. D. (2004). A neurotrophin signaling cascade coordinates sympathetic neuron development through differential control of TrkA trafficking and retrograde signaling. *Cell* 118(2), pp. 243-255. 10.1016/j.cell.2004.06.021.

Lamballe, F., Klein, R. and Barbacid, M. (1991). trkC, a new member of the trk family of tyrosine protein kinases, is a receptor for neurotrophin-3. *Cell* 66(5), pp. 967-979. 10.1016/0092-8674(91)90442-2.

Leake, P. A., Akil, O. and Lang, H. (2020). Neurotrophin gene therapy to promote survival of spiral ganglion neurons after deafness. *Hear Res* 394(pp. 107955. 10.1016/j.heares.2020.107955.

Lee, F. S. and Chao, M. V. (2001). Activation of Trk neurotrophin receptors in the absence of neurotrophins. *Proc Natl Acad Sci U S A* 98(6), pp. 3555-3560. 10.1073/pnas.061020198.

Lee, F. S., Rajagopal, R. and Chao, M. V. (2002). Distinctive features of Trk neurotrophin receptor transactivation by G protein-coupled receptors. *Cytokine & Growth Factor Reviews* 13(1), pp. 11-17. https://doi.org/10.1016/S1359-6101(01)00024-7.

Lee, R., Kermani, P., Teng, K. K. and Hempstead, B. L. (2001). Regulation of cell survival by secreted proneurotrophins. *Science* 294(5548), pp. 1945-1948. 10.1126/science.1065057.

Leibrock, J., Lottspeich, F., Hohn, A., Hofer, M., Hengerer, B., Masiakowski, P., Thoenen, H. *et al.* (1989). Molecular cloning and expression of brain-derived neurotrophic factor. *Nature* 341(6238), pp. 149-152. 10.1038/341149a0.

Levi-Montalcini, R. and Booker, B. (1960). DESTRUCTION OF THE SYMPATHETIC GANGLIA IN MAMMALS BY AN ANTISERUM TO A NERVE-GROWTH PROTEIN. *Proc Natl Acad Sci U S A* 46(3), pp. 384-391. 10.1073/pnas.46.3.384.

Levi-Montalcini, R. and Hamburger, V. (1951). Selective growth stimulating effects of mouse sarcoma on the sensory and sympathetic nervous system of the chick embryo. *J Exp Zool* 116(2), pp. 321-361. 10.1002/jez.1401160206.

Li, G. and Hidalgo, A. (2021). The Toll Route to Structural Brain Plasticity. *Front Physiol* 12(pp. 679766. 10.3389/fphys.2021.679766.

Liepinsh, E., Ilag, L. L., Otting, G. and Ibáñez, C. F. (1997). NMR structure of the death domain of the p75 neurotrophin receptor. *Embo j* 16(16), pp. 4999-5005. 10.1093/emboj/16.16.4999.

Lindholm, D., Castren, E., Tsoulfas, P., Kolbeck, R., Berzaghi Mda, P., Leingartner, A., Heisenberg, C. P. *et al.* (1993). Neurotrophin-3 induced by tri-iodothyronine in cerebellar granule cells promotes Purkinje cell differentiation. *J Cell Biol* 122(2), pp. 443-450. 10.1083/jcb.122.2.443.

Lindsay, R. M., Thoenen, H. and Barde, Y. A. (1985). Placode and neural crest-derived sensory neurons are responsive at early developmental stages to brain-derived neurotrophic factor. *Dev Biol* 112(2), pp. 319-328. 10.1016/0012-1606(85)90402-6.

Liu, X., Ernfors, P., Wu, H. and Jaenisch, R. (1995). Sensory but not motor neuron deficits in mice lacking NT4 and BDNF. *Nature* 375(6528), pp. 238-241. 10.1038/375238a0.

Locksley, R. M., Killeen, N. and Lenardo, M. J. (2001). The TNF and TNF receptor superfamilies: integrating mammalian biology. *Cell* 104(4), pp. 487-501. 10.1016/s0092-8674(01)00237-9.

Lohof, A. M., Ip, N. Y. and Poo, M. M. (1993). Potentiation of developing neuromuscular synapses by the neurotrophins NT-3 and BDNF. *Nature* 363(6427), pp. 350-353. 10.1038/363350a0.

Luberg, K., Wong, J., Weickert, C. S. and Timmusk, T. (2010a). Human TrkB gene: novel alternative transcripts, protein isoforms and expression pattern in the prefrontal cerebral cortex during postnatal development. *Journal of Neurochemistry* 113(4), pp. 952-964. https://doi.org/10.1111/j.1471-4159.2010.06662.x.

Luberg, K., Wong, J., Weickert, C. S. and Timmusk, T. (2010b). Human TrkB gene: novel alternative transcripts, protein isoforms and expression pattern in the prefrontal cerebral cortex during postnatal development. *J Neurochem* 113(4), pp. 952-964. 10.1111/j.1471-4159.2010.06662.x.

MacDonald, J. I., Gryz, E. A., Kubu, C. J., Verdi, J. M. and Meakin, S. O. (2000). Direct binding of the signaling adapter protein Grb2 to the activation loop tyrosines on the nerve growth factor receptor tyrosine kinase, TrkA. *J Biol Chem* 275(24), pp. 18225-18233. 10.1074/jbc.M001862200.

Maher, P. A. (1988). Nerve growth factor induces protein-tyrosine phosphorylation. *Proc Natl Acad Sci U S A* 85(18), pp. 6788-6791. 10.1073/pnas.85.18.6788.

Maisonpierre, P. C., Belluscio, L., Squinto, S., Ip, N. Y., Furth, M. E., Lindsay, R. M. and Yancopoulos, G. D. (1990). Neurotrophin-3: a neurotrophic factor related to NGF and BDNF. *Science* 247(4949 Pt 1), pp. 1446-1451. 10.1126/science.2321006.

Malik, S. C., Sozmen, E. G., Baeza-Raja, B., Le Moan, N., Akassoglou, K. and Schachtrup, C. (2021). In vivo functions of p75(NTR): challenges and opportunities for an emerging therapeutic target. *Trends Pharmacol Sci* 42(9), pp. 772-788. 10.1016/j.tips.2021.06.006.

Mariga, A., Mitre, M. and Chao, M. V. (2017). Consequences of brain-derived neurotrophic factor withdrawal in CNS neurons and implications in disease. *Neurobiol Dis* 97(Pt B), pp. 73-79. 10.1016/j.nbd.2016.03.009.

Martin-Zanca, D., Barbacid, M. and Parada, L. F. (1990). Expression of the trk proto-oncogene is restricted to the sensory cranial and spinal ganglia of neural crest origin in mouse development. *Genes Dev* 4(5), pp. 683-694. 10.1101/gad.4.5.683.

Martin-Zanca, D., Hughes, S. H. and Barbacid, M. (1986). A human oncogene formed by the fusion of truncated tropomyosin and protein tyrosine kinase sequences. *Nature* 319(6056), pp. 743-748. 10.1038/319743a0.

McDonald, N. Q., Lapatto, R., Murray-Rust, J., Gunning, J., Wlodawer, A. and Blundell, T. L. (1991). New protein fold revealed by a 2.3-A resolution crystal structure of nerve growth factor. *Nature* 354(6352), pp. 411-414. 10.1038/354411a0.

Menard, M., Costechareyre, C., Coelho-Aguiar, J. M., Jarrosson-Wuilleme, L., Rama, N., Blachier, J., Kindbeiter, K. *et al.* (2018). The dependence receptor TrkC regulates the number of sensory neurons during DRG development. *Dev Biol* 442(2), pp. 249-261. 10.1016/j.ydbio.2018.07.022.

Meng, Y., Heybrock, S., Neculai, D. and Saftig, P. (2020). Cholesterol Handling in Lysosomes and Beyond. *Trends in Cell Biology* 30(6), pp. 452-466. https://doi.org/10.1016/j.tcb.2020.02.007.

Merkouris, S., Barde, Y. A., Binley, K. E., Allen, N. D., Stepanov, A. V., Wu, N. C., Grande, G. *et al.* (2018). Fully human agonist antibodies to TrkB using autocrine cell-based selection from a combinatorial antibody library. *Proc Natl Acad Sci U S A* 115(30), pp. E7023-e7032. 10.1073/pnas.1806660115.

Minichiello, L., Calella, A. M., Medina, D. L., Bonhoeffer, T., Klein, R. and Korte, M. (2002). Mechanism of TrkB-mediated hippocampal long-term potentiation. *Neuron* 36(1), pp. 121-137. 10.1016/s0896-6273(02)00942-x.

Minichiello, L. and Klein, R. (1996). TrkB and TrkC neurotrophin receptors cooperate in promoting survival of hippocampal and cerebellar granule neurons. *Genes Dev* 10(22), pp. 2849-2858. 10.1101/gad.10.22.2849.

Mitre, M., Mariga, A. and Chao, M. V. (2017). Neurotrophin signalling: novel insights into mechanisms and pathophysiology. *Clin Sci (Lond)* 131(1), pp. 13-23. 10.1042/CS20160044.

Nakashima, K., Umeshima, H. and Kengaku, M. (2015). Cerebellar granule cells are predominantly generated by terminal symmetric divisions of granule cell precursors. *Dev Dyn* 244(6), pp. 748-758. 10.1002/dvdy.24276.

Nickel, W. (2010). Pathways of unconventional protein secretion. *Curr Opin Biotechnol* 21(5), pp. 621-626. 10.1016/j.copbio.2010.06.004.

Nikolaienko, O., Patil, S., Eriksen, M. S. and Bramham, C. R. (2018). Arc protein: a flexible hub for synaptic plasticity and cognition. *Semin Cell Dev Biol* 77(pp. 33-42. 10.1016/j.semcdb.2017.09.006.

Nikoletopoulou, V., Lickert, H., Frade, J. M., Rencurel, C., Giallonardo, P., Zhang, L., Bibel, M. *et al.* (2010). Neurotrophin receptors TrkA and TrkC cause neuronal death whereas TrkB does not. *Nature* 467(7311), pp. 59-63. 10.1038/nature09336.

Numan, S. and Seroogy, K. B. (1999). Expression of trkB and trkC mRNAs by adult midbrain dopamine neurons: a double-label in situ hybridization study. *J Comp Neurol* 403(3), pp. 295-308. 10.1002/(sici)1096-9861(19990118)403:3<295::aid-cne2>3.0.co;2-l.

Park, H. and Poo, M. M. (2013). Neurotrophin regulation of neural circuit development and function. *Nat Rev Neurosci* 14(1), pp. 7-23. 10.1038/nrn3379.

Pfrieger, F. W. and Ungerer, N. (2011). Cholesterol metabolism in neurons and astrocytes. *Prog Lipid Res* 50(4), pp. 357-371. 10.1016/j.plipres.2011.06.002.

Pruunsild, P., Bengtson, C. P. and Bading, H. (2017). Networks of Cultured iPSC-Derived Neurons Reveal the Human Synaptic Activity-Regulated Adaptive Gene Program. *Cell Rep* 18(1), pp. 122-135. 10.1016/j.celrep.2016.12.018.

Pruunsild, P., Kazantseva, A., Aid, T., Palm, K. and Timmusk, T. (2007). Dissecting the human BDNF locus: bidirectional transcription, complex splicing, and multiple promoters. *Genomics* 90(3), pp. 397-406. 10.1016/j.ygeno.2007.05.004.

Puehringer, D., Orel, N., Luningschror, P., Subramanian, N., Herrmann, T., Chao, M. V. and Sendtner, M. (2013). EGF transactivation of Trk receptors regulates the migration of newborn cortical neurons. *Nat Neurosci* 16(4), pp. 407-415. 10.1038/nn.3333.

Radeke, M. J., Misko, T. P., Hsu, C., Herzenberg, L. A. and Shooter, E. M. (1987). Gene transfer and molecular cloning of the rat nerve growth factor receptor. *Nature* 325(6105), pp. 593-597. 10.1038/325593a0.

Rauskolb, S., Zagrebelsky, M., Dreznjak, A., Deogracias, R., Matsumoto, T., Wiese, S., Erne, B. *et al.* (2010). Global deprivation of brain-derived neurotrophic factor in the CNS reveals an area-specific requirement for dendritic growth. *J Neurosci* 30(5), pp. 1739-1749. 10.1523/JNEUROSCI.5100-09.2010.

Rodriguez-Tébar, A., Dechant, G. and Barde, Y. A. (1990). Binding of brain-derived neurotrophic factor to the nerve growth factor receptor. *Neuron* 4(4), pp. 487-492. 10.1016/0896-6273(90)90107-q.

Rodriguez-Tebar, A., Dechant, G., Gotz, R. and Barde, Y. A. (1992). Binding of neurotrophin-3 to its neuronal receptors and interactions with nerve growth factor and brain-derived neurotrophic factor. *EMBO J* 11(3), pp. 917-922.

Rosenthal, A., Goeddel, D. V., Nguyen, T., Lewis, M., Shih, A., Laramee, G. R., Nikolics, K. *et al.* (1990). Primary structure and biological activity of a novel human neurotrophic factor. *Neuron* 4(5), pp. 767-773. 10.1016/0896-6273(90)90203-r.

Sánchez-Sánchez, J. and Arévalo, J. C. (2017). A Review on Ubiquitination of Neurotrophin Receptors: Facts and Perspectives. *Int J Mol Sci* 18(3), pp. 10.3390/ijms18030630.

Schwab, M. E., Otten, U., Agid, Y. and Thoenen, H. (1979). Nerve growth factor (NGF) in the rat CNS: absence of specific retrograde axonal transport and tyrosine hydroxylase induction in locus coeruleus and substantia nigra. *Brain Res* 168(3), pp. 473-483. 10.1016/0006-8993(79)90303-2.

Shaywitz, A. J. and Greenberg, M. E. (1999). CREB: A Stimulus-Induced Transcription Factor Activated by A Diverse Array of Extracellular Signals. *Annual Review of Biochemistry* 68(1), pp. 821-861. 10.1146/annurev.biochem.68.1.821.

Shen, J. and Maruyama, I. N. (2012). Brain-derived neurotrophic factor receptor TrkB exists as a preformed dimer in living cells. *J Mol Signal* 7(1), pp. 2. 10.1186/1750-2187-7-2.

Shen, J., Sun, D., Shao, J., Chen, Y., Pang, K., Guo, W. and Lu, B. (2019). Extracellular Juxtamembrane Motif Critical for TrkB Preformed Dimer and Activation. *Cells* 8(8), pp. 10.3390/cells8080932.

Shorey, M. L. (1909). The effect of the destruction of peripheral areas on the differentiation of the neuroblasts. . *Journal of Experimental Zoology* 7(1), pp. 25-63.

Sonoyama, T., Stadler, L. K. J., Zhu, M., Keogh, J. M., Henning, E., Hisama, F., Kirwan, P. *et al.* (2020). Human BDNF/TrkB variants impair hippocampal synaptogenesis and associate with neurobehavioural abnormalities. *Sci Rep* 10(1), pp. 9028. 10.1038/s41598-020-65531-x.

Soppet, D., Escandon, E., Maragos, J., Middlemas, D. S., Reid, S. W., Blair, J., Burton, L. E. *et al.* (1991). The neurotrophic factors brain-derived neurotrophic factor and neurotrophin-3 are ligands for the trkB tyrosine kinase receptor. *Cell* 65(5), pp. 895-903. 10.1016/0092-8674(91)90396-g.

Stenqvist, A., Agerman, K., Marmigere, F., Minichiello, L. and Ernfors, P. (2005). Genetic evidence for selective neurotrophin 3 signalling through TrkC but not TrkB in vivo. *EMBO Rep* 6(10), pp. 973-978. 10.1038/sj.embor.7400512.

Szobota, S., Mathur, P. D., Siegel, S., Black, K., Saragovi, H. U. and Foster, A. C. (2019). BDNF, NT-3 and Trk receptor agonist monoclonal antibodies promote neuron survival, neurite extension, and synapse restoration in rat cochlea ex vivo models relevant for hidden hearing loss. *PLoS One* 14(10), pp. e0224022. 10.1371/journal.pone.0224022.

Takahashi, H., Arstikaitis, P., Prasad, T., Bartlett, T. E., Wang, Y. T., Murphy, T. H. and Craig, A. M. (2011). Postsynaptic TrkC and presynaptic PTPsigma function as a bidirectional excitatory synaptic organizing complex. *Neuron* 69(2), pp. 287-303. 10.1016/j.neuron.2010.12.024.

Tao, X., Finkbeiner, S., Arnold, D. B., Shaywitz, A. J. and Greenberg, M. E. (1998). Ca2+ influx regulates BDNF transcription by a CREB family transcription factor-dependent mechanism. *Neuron* 20(4), pp. 709-726. 10.1016/s0896-6273(00)81010-7.

Tauszig-Delamasure, S., Yu, L. Y., Cabrera, J. R., Bouzas-Rodriguez, J., Mermet-Bouvier, C., Guix, C., Bordeaux, M. C. *et al.* (2007). The TrkC receptor induces apoptosis when the dependence receptor notion meets the neurotrophin paradigm. *Proc Natl Acad Sci U S A* 104(33), pp. 13361-13366. 10.1073/pnas.0701243104.

Telezhkin, V., Schnell, C., Yarova, P., Yung, S., Cope, E., Hughes, A., Thompson, B. A. *et al.* (2016a). Forced cell cycle exit and modulation of GABAA, CREB, and GSK3beta signaling promote functional maturation of induced pluripotent stem cell-derived neurons. *Am J Physiol Cell Physiol* 310(7), pp. C520-541. 10.1152/ajpcell.00166.2015.

Telezhkin, V., Schnell, C., Yarova, P., Yung, S., Cope, E., Hughes, A., Thompson, B. A. *et al.* (2016b). Forced cell cycle exit and modulation of GABAA, CREB, and GSK3β signaling promote functional maturation of induced pluripotent stem cell-derived neurons. *Am J Physiol Cell Physiol* 310(7), pp. C520-541. 10.1152/ajpcell.00166.2015.

Thomson, J. A., Itskovitz-Eldor, J., Shapiro, S. S., Waknitz, M. A., Swiergiel, J. J., Marshall, V. S. and Jones, J. M. (1998). Embryonic stem cell lines derived from human blastocysts. *Science* 282(5391), pp. 1145-1147. 10.1126/science.282.5391.1145.

Tigaret, C. M., Lin, T.-C. E., Morrell, E. R., Sykes, L., Moon, A. L., O'Donovan, M. C., Owen, M. J. *et al.* (2021). Neurotrophin receptor activation rescues cognitive and synaptic abnormalities caused by hemizygosity of the psychiatric risk gene Cacna1c. *Molecular Psychiatry* 26(6), pp. 1748-1760. 10.1038/s41380-020-01001-0.

Traub, S., Stahl, H., Rosenbrock, H., Simon, E., Florin, L., Hospach, L., Hörer, S. *et al.* (2017). Pharmaceutical Characterization of Tropomyosin Receptor Kinase B-Agonistic Antibodies on Human Induced Pluripotent Stem (hiPS) Cell-Derived Neurons. *J Pharmacol Exp Ther* 361(3), pp. 355-365. 10.1124/jpet.117.240184.

Weickert, C. S., Ligons, D. L., Romanczyk, T., Ungaro, G., Hyde, T. M., Herman, M. M., Weinberger, D. R. *et al.* (2005). Reductions in neurotrophin receptor mRNAs in the prefrontal cortex of patients with schizophrenia. *Mol Psychiatry* 10(7), pp. 637-650. 10.1038/sj.mp.4001678.

West, A. E., Pruunsild, P. and Timmusk, T. (2014). Neurotrophins: transcription and translation. *Handb Exp Pharmacol* 220(pp. 67-100. 10.1007/978-3-642-45106-5_4.

Wiesmann, C., Ultsch, M. H., Bass, S. H. and de Vos, A. M. (1999). Crystal structure of nerve growth factor in complex with the ligand-binding domain of the TrkA receptor. *Nature* 401(6749), pp. 184-188. 10.1038/43705.

Wilson, S. I. and Edlund, T. (2001). Neural induction: toward a unifying mechanism. *Nat Neurosci* 4 Suppl(pp. 1161-1168. 10.1038/nn747.

Wise, B. L., Seidel, M. F. and Lane, N. E. (2021). The evolution of nerve growth factor inhibition in clinical medicine. *Nat Rev Rheumatol* 17(1), pp. 34-46. 10.1038/s41584-020-00528-4.

Yazdani, M., Deogracias, R., Guy, J., Poot, R. A., Bird, A. and Barde, Y. A. (2012). Disease modeling using embryonic stem cells: MeCP2 regulates nuclear size and RNA synthesis in neurons. *Stem Cells* 30(10), pp. 2128-2139. 10.1002/stem.1180.

Yuan, W., Ibanez, C. F. and Lin, Z. (2019). Death domain of p75 neurotrophin receptor: a structural perspective on an intracellular signalling hub. *Biol Rev Camb Philos Soc* 94(4), pp. 1282-1293. 10.1111/brv.12502.

Zagrebelsky, M. and Korte, M. (2014). Form follows function: BDNF and its involvement in sculpting the function and structure of synapses. *Neuropharmacology* 76 Pt C(pp. 628-638. 10.1016/j.neuropharm.2013.05.029.

Zhang, H. and Bramham, C. R. (2021). Arc/Arg3.1 function in long-term synaptic plasticity: Emerging mechanisms and unresolved issues. *Eur J Neurosci* 54(8), pp. 6696-6712. 10.1111/ejn.14958.

Zhu, B., Pennack, J. A., McQuilton, P., Forero, M. G., Mizuguchi, K., Sutcliffe, B., Gu, C. J. *et al.* (2008). Drosophila neurotrophins reveal a common mechanism for nervous system formation. *PLoS Biol* 6(11), pp. e284. 10.1371/journal.pbio.0060284.

Zidovetzki, R. and Levitan, I. (2007). Use of cyclodextrins to manipulate plasma membrane cholesterol content: Evidence, misconceptions and control strategies. *Biochimica et*

Biophysica Acta (BBA) - Biomembranes 1768(6), pp. 1311-1324. https://doi.org/10.1016/j.bbamem.2007.03.026.